Development of *In Vivo* Stable Astatine-211 Labeled Scaffold and Its Application in Cancer Radiotheranostics

Laboratory of Molecular Imaging and Radiotherapy,

Graduate School and Faculty of Pharmaceutical Sciences

Chiba University

July, 2024

Yuta Kaizuka

Table of Contents

Introduction

Radiopharmaceuticals are a class of pharmaceutical agents containing radioisotopes (RIs). They are administered to patients by localized, intravascular, or oral administration but are most often given intravenously.[1,2] Currently, a wide range of RIs are employed clinically, including radioactive metals and radioactive halogens. These agents are utilized to diagnose and treat various diseases, including cancer, through the radiation emitted by the RIs. Among these RIs, γ-ray or β^+-particle emitting RIs are used for diagnosis because of the high penetrability of the emitted radiation. On the other hand, β^--particle or α-particle emitting RIs are used for therapy because of their high cytotoxicity.

Two types of diagnostic systems are used for radiopharmaceutical-based diagnosis. If the RIs emit γ-rays, they can be used for Single Photon Computed Tomography (SPECT), and if the RIs emit β^+-particles, they can be used for Positron Emission Tomography (PET) imaging. SPECT images are obtained using γ-cameras to acquire multiple 2-D images from multiple angles, which are then reconstructed using a computer to get a 3-D image. SPECT uses collimators in front of the detectors to block γ-rays from directions other than the pre-determined one, resulting in a significantly lower radiation detection sensitivity.[3] As a result, SPECT provides low-resolution and low-quantitative images compared to PET.[4] However, in general, the half-life of the RIs used in SPECT is longer than that of the RIs used in PET and commercially available, so clinically, the number of SPECT machines is much larger than that of PET machines. On the other hand, in PET images, β^+-particle emitting RIs are used. The β^+-particles produce two annihilation radiations with an energy of 511 keV due to the interaction of positrons and electrons. As these annihilation photons are emitted in diametrically opposite directions, the radiation can be determined without collimators by coincidence detection by γ-cameras installed in the opposite direction. Coincidence detections can also allow radiation attenuation correction, so PET images provide higher resolution and quantitative images than SPECT images. Although the number of PET systems in clinical use is smaller than the number of SPECT systems due to the short half-life of RIs used in PET, these features of PET imaging have resulted in seven times the number of recent publications on PET studies than the number of publications on SPECT studies.[5]

β^-- and α-particles are used in radiotherapy because of their cytotoxic properties. In general, these radiations induce cellular damage through direct mechanisms (e.g., DNA damage and protein damage) and indirect mechanisms (e.g., cellular damage from reactive oxygen species (ROS) generated by radiolysis of water).[6] β^--particles are electrons, which are small particles with one negative charge. The interaction of β^--particles to materials is not strong, and then the path length of β^--particles in the body is long (0.5-5 mm), indicating the linear energy transfer (LET)

is low. In general, β^--particles show cytotoxic effects by inducing single-strand DNA breaks through indirect mechanisms. As the path length of β^--particles is long, they can damage many cells in the vicinity of the RIs.[7] On the other hand, α-particles are nuclei of helium and have two positive charges. Since the interaction of α-particles to materials is very high and then the path length of α-particles is very short (50-100 μm), their LET is approximately 400 times higher than that of β^--particles.[8] Generally, α-particles show cytotoxic effects by inducing double-strand DNA breaks through direct mechanisms. The shorter path length of α particles compared to β^--particles can provide very strong damage only to cells adjacent to the RIs, minimizing damage to healthy cells.[7] These properties of α-particles have led to several recent studies on the development of radiolabeled compounds using α particle-emitting RIs.

To use RI for diagnosis and therapy for diseases, it is necessary to deriver RI to the lesion. If the RIs themselves have inherent targeting abilities (e.g., radium-223 (^{223}Ra) and strontium-89 (^{89}Sr), which have bone-targeting properties, are used for bone metastatic cancers, and iodine-123 (^{123}I), iodin-131 (^{131}I), which are recognized by the sodium iodide symporter (NIS), are used for thyroid cancer), these RIs are administered as is.[9] In the case of radiometals, as some radiometal-chelate complexes accumulate in specific tissues and lesions due to physiological effects, they can be used to diagnose and treat diseases. For instance, ^{99m}Tc-labeled mercaptoacetyltriglycine (^{99m}Tc-MAG3) is utilized to evaluate renal function due to its characteristic rapid accumulation in renal tubular cells and subsequent swift excretion into urine.[10] Additionally, ^{111}In-labeled diethylenetriaminepentaacetic acid (^{111}In-DTPA) is utilized to evaluate cerebrospinal fluid (CSF) space lesions. This is because ^{111}In-DTPA exhibits physiological similarities to CSF and distributes along the CSF flow patterns when administered into the subarachnoid space.[11] Another method of delivering RI to the lesion is to bind the RI to a targeting molecule that accumulates at the lesion site. Various compounds are used as targeting molecules, including small molecules, peptides, antibodies, or antigens that interact with transporters, enzymes, receptors, or nanoparticles. To prepare radiolabeled targeting molecules, RIs are bound directly or indirectly to the targeting molecules. A typical example of a direct method is direct iodination of proteins. In this method, RI-labeled proteins are obtained by binding reactive I^+ generated using an oxidizing agent (such as chloramine-T) to tyrosine residues in the protein.[12] While this method allows for simple and high-yield radioiodine labeling of proteins, the use of oxidizing and reducing agents may risk protein denaturation or disulfide bond cleavage.[13,14] On the other hand, some targeting molecules do not have radiolabeling moieties. In such cases, RI-labeled compounds are prepared by indirect methods. Indirect methods include introducing an RI-labeled agent into the targeting molecule or introducing a chelating agent into the targeting molecule (bifunctional chelating agent: an agent with both a chelating moiety and a protein binding moiety) to label the radiometal. Typical RI-

labeled agents used to prepare RI-labeled compounds are the Bolton-Hunter reagent and N-succinimidyl 3-iodobenzoate.[15] Using these RI-labeled agents, radioiodine-labeled protein can be obtained without oxidative and reductive conditions. A typical bifunctional chelating agent is p-SCN-Bn-DOTA. p-SCN group binds to the targeting molecules via amino group and DOTA moiety complexes with radiometal. DOTA can form stable complexes with a variety of radiometals such as indium-111 (^{111}In), gallium-68 (^{68}Ga), lutetium-177 (^{177}Lu), and actinium-225 (^{225}Ac). Therefore, DOTA is the most used chelating agent in nuclide medicine. In recent years, indirect method has been mainly used for the preparation of radiolabeled compounds, because indirect methods can be introduced various functions, such as the ability to hold RIs stably or to show high stability against enzymatic degradation.

Theranostics refers to the combination of therapy and diagnosis, and when radionuclides are used, it is specifically called radiotheranostics.[16] In the case of radiopharmaceuticals, it is easy to prepare RI-labeled compounds with similar biodistribution of diagnostic and therapeutic RI-labeled compounds by replacing the RIs to be labeled from diagnostic RIs to therapeutic RIs. If the therapeutic RI-labeled compound shows a similar biodistribution as the diagnostic RI-labeled compound, the biodistribution of the therapeutic RI-labeled compounds can be predicted from the biodistribution of diagnostic RI-labeled compounds. In such cases, the diagnostic RI-labeled compound shows accumulation in the target tissues, such as tumors. The therapeutic RI-labeled compound is also expected to accumulate in the target tissue, and the patient can be treated with the therapeutic RI-labeled compound. If the diagnostic RI-labeled compound does not show accumulation in the target tissues, the therapeutic RI-labeled compound is also not expected to accumulate in the target tissue, and the patient changes the treatment method.

Radiotheranostics offers several notable benefits. One such advantage is the provision of evidence-based medicine (EBM). Historically, anticancer agents are administered initially, and the therapeutic response is determined after several months, determining whether treatment with that anticancer agent should be continued. As a result, treatment results are often disappointing. In the case of radiotheranostics, the treatment effect can be predicted before the therapeutic RI-labeled compound is administered, thus providing highly reliable EBM-based treatment. In addition, radiotheranostics not only selects patients expected to respond well to treatment but also enables monitoring of target expression levels through periodic imaging after treatment initiation, allowing for adjustment of therapeutic agent dosage or consideration of alternative therapies. Thus, this treatment strategy contributes to personalized medicine. Moreover, radiotheranostics, with these advantages, is rational from a healthcare economics perspective. Since many countries, including Japan, face an aging population and social security costs are straining national budgets, optimizing medical costs is significantly essential.

In the early days of radiotheranostics, the pair of SPECT diagnosis and therapy using β^--emitting RIs were used for radiotheranostics. Examples include radiotheranostics of thyroid cancer with iodine-123 (^{123}I) and iodine-131 (^{131}I), radiotheranostics of malignant lymphomas with ^{111}In and yttrium-90 (^{90}Y) using RI-labeled antibodies, and even radiotheranostics neuroendocrine tumors with ^{111}In and ^{177}Lu using somatostatin targeting peptide.[17,18] Currently, the pair of PET diagnosis and therapy using β^--emitting RIs has become the mainstay of radiotheranostics because PET can provide higher resolution images than SPECT. For example, radiotheranostics of neuroendocrine tumors with ^{68}Ga and ^{177}Lu using somatostatin targeting peptide and radiotheranostics of prostate cancer with ^{68}Ga and ^{177}Lu using prostate-specific membrane antigen (PSMA)-targeted peptide have been performed.[19,20] Furthermore, in recent years, the high therapeutic efficacy of α-particle emitting RIs has been reported, and it is expected that the pair of PET diagnosis and therapy using α-particle emitting RIs will become the mainstay of radiotheranostics in the near future. Indeed, recently, PSMA-targeted peptides labeled with ^{68}Ga and ^{225}Ac (α-particle emitting RI) combinations have been reported. This study demonstrated significant therapeutic effects with ^{225}Ac-labeled PSMA-targeting agents in patients who showed a tendency for progression with ^{177}Lu-labeled PSMA-targeted agents.[21,22]

As mentioned above, as, it is expected that the pair of PET diagnosis and therapy using α-particle emitting RIs will become the mainstay of radiotheranostics in the near future, the RIs-labeled compounds using β^+- and α-particle emitting RIs are being developed. However, there are several problems in the production of these radiolabeled compounds. One of the most significant problems is the difficulty of producing α-particle emitting RIs. ^{225}Ac is one of the most studied α-emitting nuclides in the world, but the current ^{225}Ac production is insufficient to meet the growing global demand.[23] To address this problem, various production methods are being explored. In Japan, experimental production of ^{225}Ac using charged particles with ^{226}Ra has recently started, but the supply system is still inadequate.[24] Securing the raw material ^{226}Ra for domestic production of ^{225}Ac remains a concern. In addition, in ^{225}Ac-labeled radiopharmaceuticals, releasing daughter nuclides from the chelator due to recoil energy during α-decay is inevitable. These daughter nuclides undergo further decay (Figure 1), and the relatively long-lived daughter nuclide (^{213}Bi) produced in this process redistributes to healthy tissues, potentially causing side effects.[6,25] Since α-particle has high biological effects, α-particle emitting RIs must be reliably delivered to target tissues. Therefore, the instability of ^{225}Ac-labeled compounds is not suitable for producing RI-labeled compounds.

^{211}At is an α-emitting RI that has recently shown promise for therapeutic use.[26,27] With a half-life of 7.2 hours, ^{211}At is suitable for the pharmacokinetics of target molecules with relatively rapid blood clearance, such as small molecules, peptides, and antibody fragments. Furthermore, ^{211}At

provides high therapeutic efficacy as 100% of its decay results in α-particle emission (Figure 1). Unlike ^{225}Ac, ^{211}At does not generate long-lived, cytotoxic radiation-emitting daughter nuclides, thus limiting redistribution and damage to healthy tissues. Additionally, the availability of ^{211}At is superior compared to other therapeutic RIs. The most commonly used nuclear reaction for ^{211}At production is ^{209}Bi(α, 2n)^{211}At, where natural bismuth (^{209}Bi) is irradiated with alpha beams generated by accelerators such as cyclotrons.[28] The raw material ^{209}Bi is 100% naturally abundant, making it low-cost and easily obtainable, and ^{211}At can be produced using cyclotrons, facilitating domestic production. Due to these excellent characteristics, clinical applications of ^{211}At are anticipated, and several clinical studies have begun in Japan.

Table 1 shows the radionuclides in clinical use in Japan. A wide variety of RIs are clinically used, and many are imported. In particular, all radionuclides currently in clinical use are imported. Because of the short half-life of RIs used in radiopharmaceuticals, RIs are usually transported by air. However, air transport is susceptible to delays due to weather conditions, mechanical issues, and changes in international circumstances. Delays in the transport of RIs may result in insufficient radioactivity. Consequently, this may necessitate treatment cancellation or modification, potentially causing a significant burden on both patients and healthcare providers. Therefore, therapeutic RIs that can be manufactured domestically would be very useful. As mentioned above, ^{211}At is a radionuclide that can be produced domestically, and the development of radiotheranostic agents using ^{211}At as a therapeutic RI is considered to be very effective.

^{211}At is an α-emitting RI belonging to the halogen family. Several radiohalogens are used clinically. Fluorine-18 (^{18}F) is a β^+-particle emitting RI used for PET diagnosis. ^{123}I is a γ-ray emitting RI and is used for SPECT diagnosis. ^{131}I emits both γ-ray and β^-particle and is then used for SPECT diagnosis and therapy. In addition, ^{125}I is a γ-ray emitting RI with a long half-life (ca. 60d), making it useful for preclinical studies. Among these RIs, ^{18}F is a promising RI for clinical applications. ^{18}F emits short-range β^+-particles (providing high resolution) at a high emission rate (97%) and has a low proportion of γ-rays and an adequate half-life (110 minutes).[29] Furthermore, ^{18}F can be produced using cyclotrons. These attractive characteristics have led to the development of various ^{18}F-labeled agents, including [^{18}F]-fluorodeoxyglucose ([^{18}F]FDG).[30-32] [^{18}F]FDG is a glucose analog transported into cells via glucose transporters (GLUTs) like glucose. Once internalized, [^{18}F]FDG is phosphorylated by hexokinase. However, due to the absence of a hydroxyl group at the 2-position, [^{18}F]FDG does not undergo further metabolism. Consequently, the phosphorylated [^{18}F]FDG becomes trapped within the cell (metabolic trapping). This property allows [^{18}F]FDG to accumulate selectively in tissues exhibiting high glucose uptake. As a result, [^{18}F]FDG can be utilized to diagnose various types of tumors that demonstrate increased glucose consumption compared to normal tissues. Since the approval of [^{18}F]FDG use in Japan in 2005, ^{18}F

has been routinely produced in domestic cyclotrons. Consequently, ^{18}F is the most readily available PET nuclide in Japan. These properties of ^{18}F are expected to lead to the development of radiotheranostic agents using the pair of ^{18}F and ^{211}At.

Domestic production

Radionuclide	Purpose	Half-life
^{18}F	PET	110 m
^{67}Ga	SPECT	3.3 d
^{111}In	SPECT	2.8 d
^{123}I	SPECT	13 h
^{201}Tl	SPECT	73 h
^{211}At	α-therapy	7 h

Imported

Radionuclide	Purpose	Half-life
^{68}Ga	PET	68 m
^{90}Y	β^--therapy	64 h
$^{99}Mo/^{99m}Tc$	SPECT	66 h/6 h
^{131}I	SPECT /β^--therapy	8 d
^{177}Lu	β^--therapy	6.6 d
^{223}Ra	α-therapy	11.4 d

Table 1. Radionuclides used in Japan

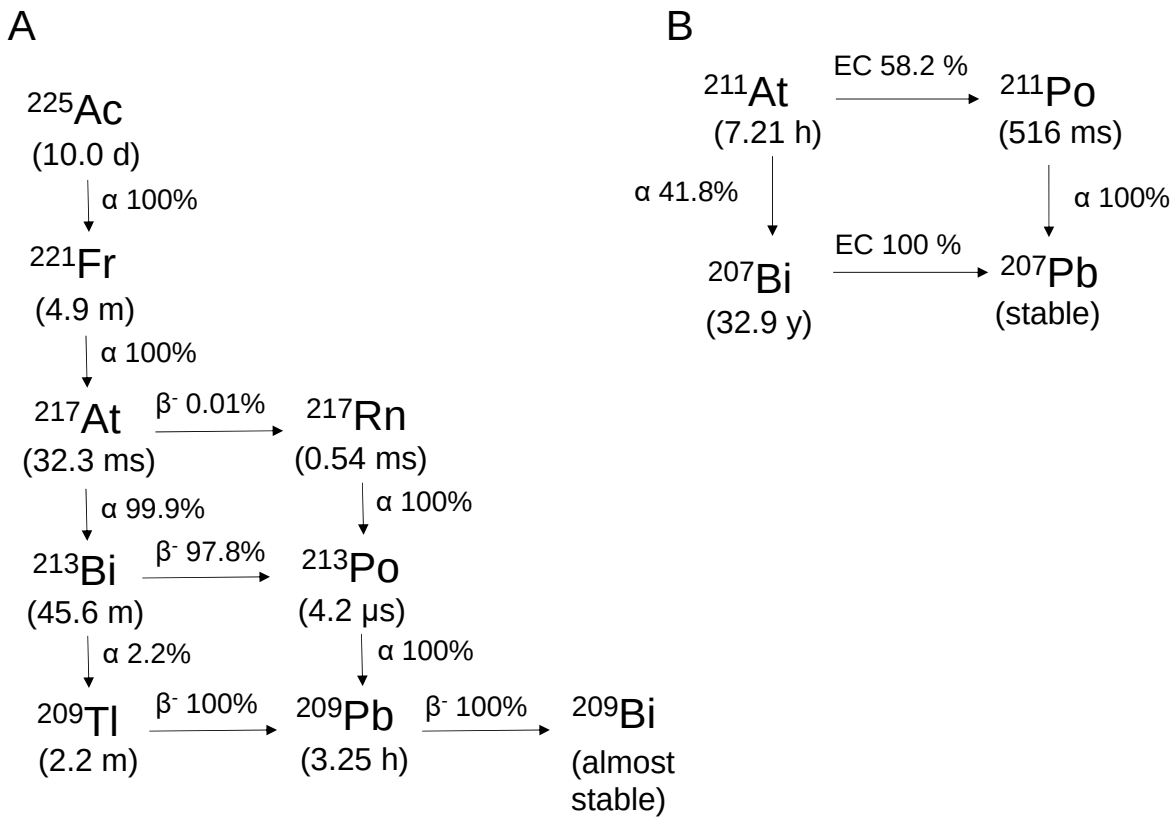

Figure 1. Decay chains of α-emitters

(A) represents the decay chains of ^{225}Ac, and (B) represents the decay chains of ^{211}At

As mentioned above, considering the domestic availability of these RIs, radiotheranostics combining ^{211}At (α-particle therapy) and ^{18}F (PET) is expected to be the most feasible approach in Japan. However, despite ^{18}F and ^{211}At belonging to the halogen group, they exhibit several significantly different characteristics.

One difference is the reactivity of labeling. ^{18}F is produced as [^{18}F]F_2 or $^{18}F^-$, with the latter being preferred for ^{18}F-labeled agents development due to its superior specific activity. $^{18}F^-$ is obtained as an aqueous solution, but its nucleophilicity is significantly reduced due to hydrogen bonding with surrounding water molecules. [33] Therefore, it is necessary to evaporate the water and conduct labeling reactions in non-protic polar solvents. Although the addition of phase-transfer catalysts improves the nucleophilicity of ^{18}F, harsh reaction temperatures are still required. [33,34] In contrast, ^{211}At exhibits high nucleophilicity and electrophilicity, making labeling easy for both aliphatic and aromatic scaffolds. [35]

Another difference is the in vivo stability of their respective radiolabeled agents. This has hindered the utilization of ^{18}F and ^{211}At in radiotheranostics. Generally, the stability of radiohalogen-labeled compounds can be explained by the strength of the carbon-halogen (C-X) bond energy. C-X bond energy tends to weaken with heavier halogens (Table 2), making ^{18}F-labeled compounds the most stable against dehalogenation, while ^{211}At-labeled compounds exhibit lower stability.[27] Furthermore, aliphatic labeling scaffolds have weaker C-X energies than aromatic scaffolds, suggesting that aromatic scaffolds are more suitable for ^{211}At labeling. Indeed, radioiodine, which is a heavy halogen element like ^{211}At, is introduced into benzene derivatives such as iodobenzoate, and these radioiodinated compounds show high stability both in vitro and in vivo. However, ^{211}At-labeled benzene derivatives such as ^{211}At-astatobenzoate showed high stability in vitro but less stability in vivo, where deastatination was observed. [36,37] Free ^{211}At in vivo tends to accumulate in the stomach, thyroid, spleen, and lungs. [27] Several animal studies have reported toxicity associated with free ^{211}At, with observed damage to various organs, particularly the thyroid.[38] Deastatination occurs more rapidly, with small molecules metabolizing faster than antibodies.[39] This poses a significant challenge for ^{211}At with a relatively short half-life because it is suitable for small carriers such as small molecules and peptides that exhibit rapid distribution.

Table 2. Phenyl and alkyl-halogen bond energies (kJ/mol)

The table was cited from François et al.[39]

X	*Phenyl-X*	*Alkyl-X*
F	523	444
Cl	398	339
Br	335	285
I	268	222±12
At	197±20	163±12

To prevent in vivo deastatination, several studies have attempted to develop stable ^{211}At-labeled compounds. Notable examples include boron cage compounds and benzoate-type labeling scaffolds containing guanidinomethyl groups (Figure 3). The high in vivo stability of ^{211}At-labeled boron cage compounds can be explained by the stronger B-At bond than the C-At bond.[40] However, the application of boron cage compounds is limited due to unfavorable kidney and liver retention.[40] Astatobenzylguanidine derivatives show some resistance to deastatination but still exhibit significantly higher accumulation in tissues where free ^{211}At concentrates compared to their radioiodine-labeled counterparts.[41] Currently, no labeling scaffold provides ^{211}At-labeled agents with attractive pharmacokinetics.

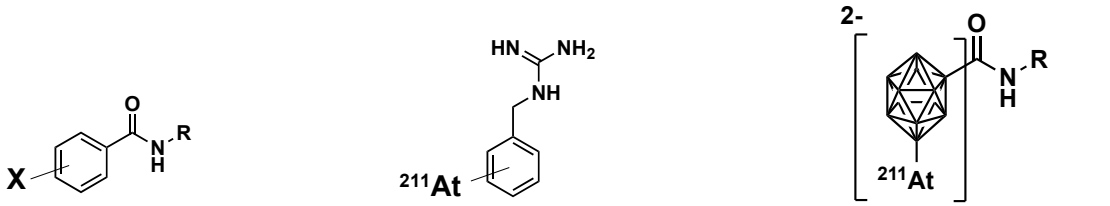

X= I: iodobenzoate
^{211}At: astatobenzoate

Astatobenzylguanidine

Boron cage compound

Figure 3. Structures of iodobenzoate and ^{211}At-labeled derivatives.

To realize radiotheranostics combining domestically producible ^{18}F (PET) and ^{211}At (α-particle therapy), it is essential to develop scaffolds that demonstrate high stability against in vivo dehalogenation and allow labeling of all radiohalogens under acceptable reaction conditions. In particular, developing labeling scaffolds that can stably retain ^{211}At in vivo is highly needed because such scaffolds are extremely limited.

Therefore, I initially decided to develop labeling scaffolds for ^{18}F and ^{211}At radiotheranostics. Alkyl halides typically undergo dehalogenation in vivo through nucleophilic attack by biomolecules such as glutathione or metabolism via cytochrome P450 (CYP).[42] The former dehalogenation mechanism should be overcome by using a bulky scaffold. Thus, this study focused on the neopentyl-type labeling scaffold used for ^{18}F labeling. However, the stability of neopentyl halides against the latter dehalogenation mechanism remains unclear. Therefore, in Chapter 1, I evaluated the stability of ^{211}At-labeled compounds using neopentyl-type labeling groups and derived a labeling scaffold applicable to radiotheranostics combining ^{18}F and ^{211}At.

In Chapter 2, I aimed to develop radiotheranostic agents using the derived neopentyl-type labeling scaffold. This chapter focused on the increased demand for amino acids due to active cellular processes in cancer and selected amino acids as cancer-targeting molecules. I developed ^{18}F and ^{211}At-labeled amino acid derivatives with neopentyl scaffolds and evaluated their usefulness as radiotheranostic agents.

Chapter 1. Development of alkyl-type labeling scaffold for *in vivo* stable ^{211}At-labeled compounds

Introduction

There are 32 known isotopes of astatine, all of which are radioactive, and even the longest-lived of them, ^{210}At, has a half-life of only 8.2 h. Because of these characteristics, no labeled scaffold specific for astatine had been developed. Because astatine is a heavy halogen element like iodine and supposed to have similar chemical properties to iodine, ^{211}At-labeled compounds have been prepared by replacing the radioiodine in radioiodine-labeled compounds with ^{211}At. Since iodobenzoate derivatives such as Bolton-Hunter reagent and N-succinimidyl 3-iodobenzoate have been used for radioiodine labeling agents with high in vivo stability, astatobenzoate derivatives have been widely used to prepare ^{211}At-labeled compounds. However, numerous studies have reported deastatination as a significant issue with astatobenzoate derivatives.[43-45]

While some deastatination mechanisms have been proposed, the precise process remains elusive.[35,46] To enhance the stability of astatobenzoate, the introduction of substituents such as guanidino groups to introduce a positive charge or electron-donating methoxy groups to increase the electron density of the aromatic ring was attempted.[47,48] Nevertheless, these efforts have not fully resolved the *in vivo* stability issues of ^{211}At-labeled compounds. Therefore, developing a new scaffold that provides in vivo stable ^{211}At-labeled compounds remains crucial.

Alkyl halides, particularly alkyl iodides and alkyl astatides, are unstable in vivo. These compounds undergo dehalogenation due to nucleophilic attacks by biomolecules such as glutathione and metabolism by cytochrome P450 (CYP) enzymes.[42] However, from the organic chemistry perspective, acquiring stability against the former dehalogenation mechanism should be possible using a sterically hindered labeling scaffold.

Several studies have reported that steric bulk inhibits CYP-mediated metabolism.[49,50] In drug metabolism mediated by CYPs, since hydrophobic and steric interactions primarily determine substrate binding and orientation, steric hindrance restricts access to the iron-bound oxidizing species at the active site.[51,52] Furthermore, it has been reported that steric hindrance can induce ″metabolic site switching,″ wherein metabolism at alternative sites is favored over dehalogenation.[53]

Considering this, I focused on the bulky neopentyl structure as a potential labeling scaffold for radiohalogens. Neopentyl halides exhibit high stability against nucleophilic attacks due to their

significant steric hindrance.[54] However, the stability of neopentyl halides against CYP-mediated metabolism remains unexplored.

[^{18}F]1-(2,2-dihydroxymethyl-3-fluoropropyl)-2-nitroimidazole ([^{18}F]DiFA) has been reported as a compound with a neopentyl halide.[55] Based on the structure of [^{18}F]DiFA, [^{125}I]BHIN and [^{211}At]BHAN (Figure 4) were designed as model compounds to evaluate the stability of the neopentyl structure against dehalogenation. While [^{18}F]DiFA possesses two hydroxyl groups on its neopentyl structure, these hydroxyl groups may not be essential for the steric hindrance of the neopentyl structure. From the consideration, I also synthesized [^{125}I]EHIN, with one hydroxyl group, and [^{125}I]DEIN, with no hydroxyl group, as derivatives of [^{125}I]BHIN. Opportunities to obtain ^{211}At are limited, so ^{125}I was used in the preliminary study because it is commercially available.

In this study, the stabilities of the ^{125}I-labeled neopentyl derivatives were evaluated, and a promising scaffold that can stably retain radiohalogen *in vivo* was explored. After identifying a promising scaffold through the assessment, I labeled it with ^{211}At and evaluated its stability *in vivo.* I also prepared ^{125}I and ^{211}At labeled compounds using the conventional halogen labeling scaffold benzoate ([^{125}I]MIBAN, [^{211}At]MABAN, Figure 5) and compared their stability with neopentyl halides.

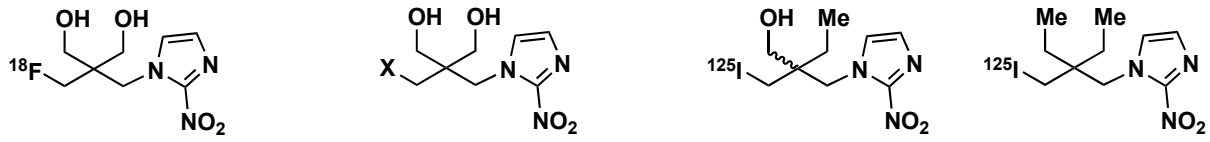

[^{18}F]DiFA X=^{125}I: [^{125}I]BHIN ^{211}At: [^{211}At]BHAN [^{125}I]EHIN [^{125}I]DEIN

Figure 4. Structure of neopentyl halide derivatives

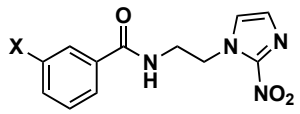

X=^{125}I: [^{125}I]MIBAN
^{211}At: [^{211}At]MABAN

Figure 5. Structure of benzoate derivatives

Results

Synthesis

The non-radioactive [^{127}I]BHIN, [^{127}I]EHIN, and [^{127}I]DEIN were synthesized through the pathways shown in Schemes 1 to 3.

The synthesis of non-radioactive [^{127}I]MIBIN was accomplished through the condensation of previously reported N-(2-aminoethyl)-2-nitroimidazole with meta-iodobenzoic acid (Scheme 4).[56] Additionally, N-[N-(meta-tributylstannylbenzoyl)-2-aminoethyl]-2-nitroimidazole was synthesized as a labeling precursor for [^{125}I]MIBAN and [^{211}At]MABAN by condensing meta-tributylstannylbenzoic acid with N-(2-aminoethyl)-2-nitroimidazole.

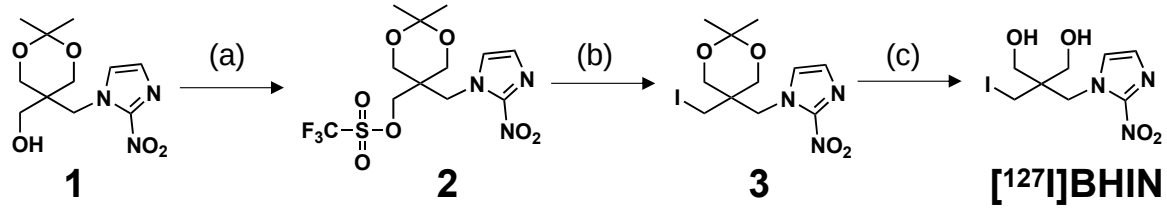

Reagent(s): (a) trifluoromethanesulfonic anhydride, 2,6-lutidine, CH_2Cl_2; (b) sodium iodide, MeCN; (c) p-Toluenesulfonic acid, MeOH.

Scheme 1. Synthesis of [^{127}I]BHIN

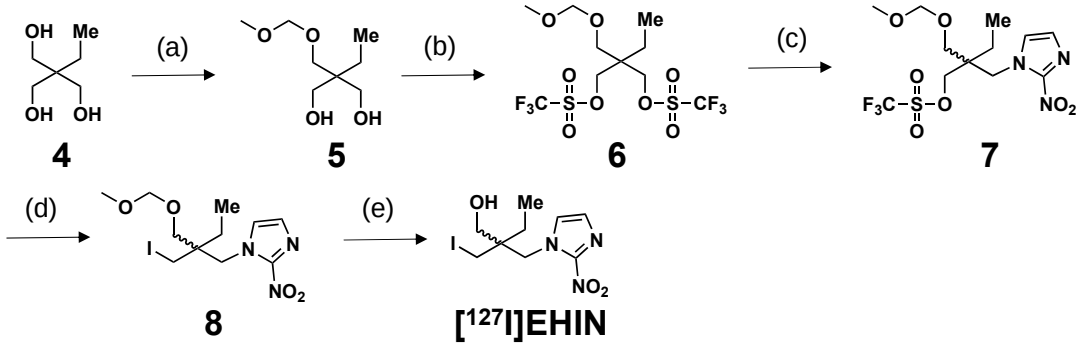

Reagent(s): (a) diisopropylethylamine, 4-dimethylaminopyridine, chloromethyl methyl ether, THF; (b) trifluoromethanesulfonic anhydride, diisopropylethylamine, CH_2Cl_2; (c) 2-nitroimidazole, DIEA, CH_2Cl_2; (d) sodium iodide, MeCN; (e) 1M HCl aq., MeOH.

Scheme 2. Synthesis of [^{127}I]EHIN

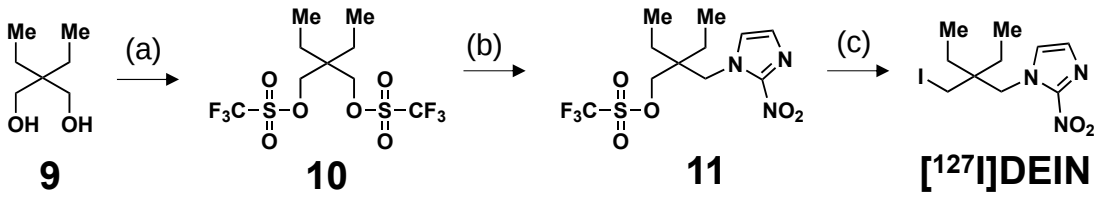

Reagent(s): (a) trifluoromethanesulfonic anhydride, 2,6-lutidine, CH_2Cl_2; (b) 2-nitroimidazole, potassium carbonate, DMF; (c) sodium iodide, MeCN.

Scheme 3. Synthesis of [^{127}I]DEIN

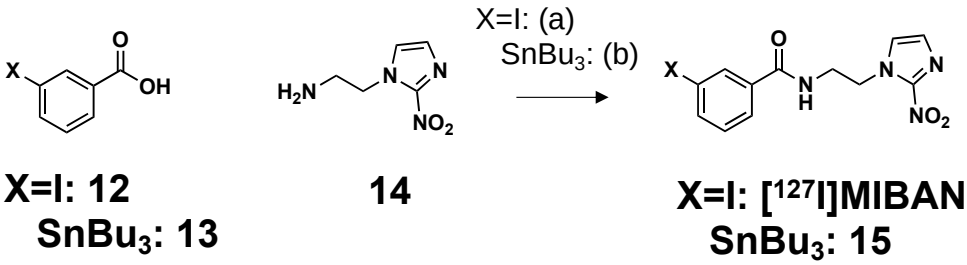

Reagent(s): (a) 1-[bis(dimethylamino)methyliumyl]-1H-1,2,3-triazolo[4,5-b]pyridine-3-oxide hexafluorophosphate (**HATU**), 1-hydroxy-7-azabenzotriazole (**HOAt**), triethylamine, MeCN ; (b)HATU, HOAt, triethylamine, DMF.

Scheme 4. Synthesis of [^{127}I]MIBAN and compound 15

The glucuronide conjugates (GC) of non-radioactive [^{127}I]BHIN and [^{127}I]EHIN ([^{127}I]BHIN-GC and [^{127}I]EHIN-GC) were prepared by reacting [^{127}I]BHIN or [^{127}I]EHIN with uridine 5′ - diphosphoglucuronic acid (UDPGA) in the solution of mouse liver microsomes. After removing the enzyme with ethanol, [^{127}I]BHIN-GC and [^{127}I]EHIN-GC were purified using reverse-phase (RP) HPLC.

^{125}I/^{211}At Labeling

[^{125}I]BHIN, [^{125}I]EHIN, and [^{125}I]DEIN were labeled with ^{125}I through an S_{N2} reaction with [^{125}I]NaI starting from compounds 2, 7, and 11, respectively. For [^{125}I]BHIN and [^{125}I]EHIN, the protective groups were removed after the introduction of ^{125}I. The radiochemical yields were 68.8% (2 steps) for [^{125}I]BHIN, 12.5% (2 steps) for [^{125}I]EHIN, and 17.9% for [^{125}I]DEIN. The ^{125}I labeling of [^{125}I]EHIN exhibited enhanced yield in the presence of organic bases (67.0%, 2 steps).

[^{211}At]BHAN was obtained by introducing ^{211}At through an S_{N2} reaction starting from compound 2, followed by deprotection of the protective groups. The radiochemical yield was 88.6% (2 steps).

[^{125}I]MIBAN and [^{211}At]MABAN were obtained from compound 15 by introducing ^{125}I or ^{211}At through an electrophilic reaction. The radiochemical yields were 94.2% and 39.2%, respectively.

The purity of all labeled compounds was over 95%. The production of all ^{125}I-labeled compounds was confirmed by matching the retention times in RP-HPLC with those of their ^{127}I-labeled counterparts (Figure 6). Since astatine has no stable isotopes, the production of [^{211}At]BHAN and [^{211}At]MABAN was confirmed by matching the retention times in RP-HPLC with those of the non-radioactive [^{127}I]BHIN and [^{127}I]MIBAN, respectively.

The glucuronide conjugates of [^{125}I]BHIN and [^{125}I]EHIN ([^{125}I]BHIN-GC and [^{125}I]EHIN-GC) were synthesized by reacting [^{125}I]BHIN or [^{125}I]EHIN with UDPGA in the solution of mouse liver microsomes, followed by purification using RP-HPLC.

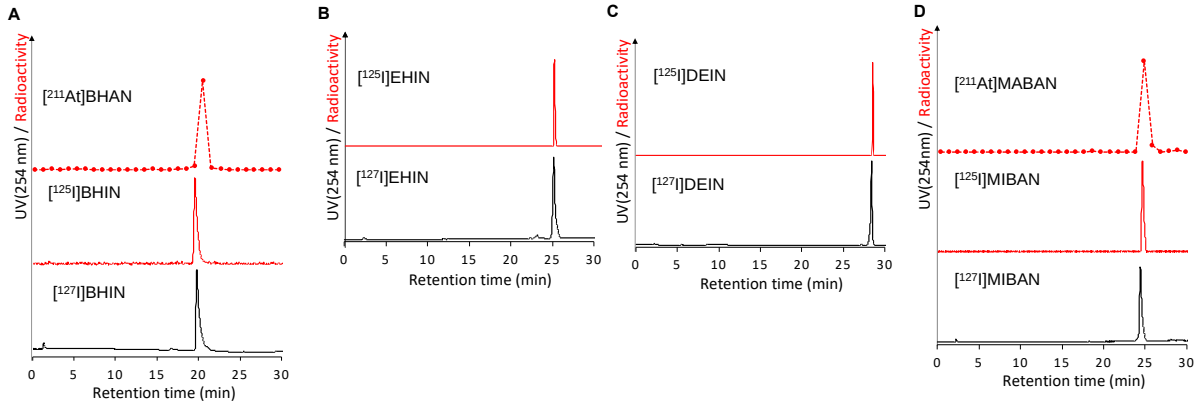

Figure 6. RP-HPLC radiochromatograms of [^{125}I]BHIN and [^{211}At]BHAN (A), [^{125}I]EHIN (B), [^{125}I]DEIN (C), and [^{125}I]MIBAN and [^{211}At]BHAN (D)

In vitro assessment

Stability against nucleophilic attack

The stability of neopentyl derivatives in GSH solution (10 mM) is shown in Table 3. [^{125}I]BHIN, [^{125}I]EHIN, [^{125}I]DEIN, and [^{211}At]BHAN all remained intact at over 95% after 24 hours of incubation in the GSH solution.

Table 3. Stability of neopentyl derivatives in GSH solution.

Time (h)	% Control			
	[^{125}I]BHIN	[^{125}I] EHIN	[^{125}I]DEIN	[^{211}At]BHAN
1	98.4 ± 0.2	99.9 ± 0.2	98.3 ± 0.2	Not determined
3	98.5 ± 0.2	99.1 ± 0.5	98.0 ± 0.1	Not determined
6	98.2 ± 0.3	98.5 ± 0.1	97.3 ± 0.7	Not determined
24	96.6 ± 1.0	96.4 ± 0.3	95.1 ± 0.7	98.8 ± 1.7

*Results are reported as mean ± SD (n=3).

Stability against CYP metabolism

The stability of neopentyl derivatives in CYP-activated microsome solutions is shown in Table 4. When using liver microsomes derived from mice, [^{125}I]BHIN remained stable and intact even after 30 minutes of incubation (Figure 7). However, the proportion of intact [^{125}I]EHIN and [^{125}I]DEIN decreased, and the proportion of the void volume peak increased. Using hydrophilic interaction liquid chromatography (HILIC)-HPLC, which is suitable for the analysis of highly water-soluble substances, each of the void peaks was reanalyzed, and the retention times of these peaks were found to correspond to those of the [^{125}I]NaI peak (Figure 8). When human liver microsomes were used instead of mouse liver microsomes at similar final CYP concentrations (0.233 mM for mice and 0.257 mM for humans), [^{125}I]EHIN remained intact after incubation, but [^{125}I]DEIN showed a significant decrease in radioactivity in the void volume. [^{125}I]BHIN, [^{125}I]BHIN-GC, and [^{125}I]EHIN-GC recorded a single radioactivity peak with retention times similar to those of the intact fractions. [^{211}At]BHAN also remained unchanged after incubation with human and mouse liver microsomes.

Table 4. Stability against CYP metabolism.

	% Intact fractions (% void volume fractions)	
	Mouse liver microsomes	Human liver microsomes
[^{125}I]BHIN	> 99.8 (<0.2)	> 99.8 (<0.2)
[^{125}I]EHIN	72.0 ± 2.0 (23.5±3.7)	>99.8 (<0.2)
[^{125}I]DEIN	2.2 ± 0.1 (52.6 ± 10.0)	1.5 ± 0.3 (16.5 ± 0.5)
[^{125}I]BHIN-GC	> 99.8 (< 0.2)	> 99.8 (< 0.2)
[^{125}I]EHIN-GC	> 99.8 (< 0.2)	> 99.8 (< 0.2)
[^{211}At]BHAN	96.9 ± 0.8*	96.9 ± 2.9*

Area % of the fraction not retained by RP-HPLC is shown in brackets.

*Determined by RP-TLC analysis.

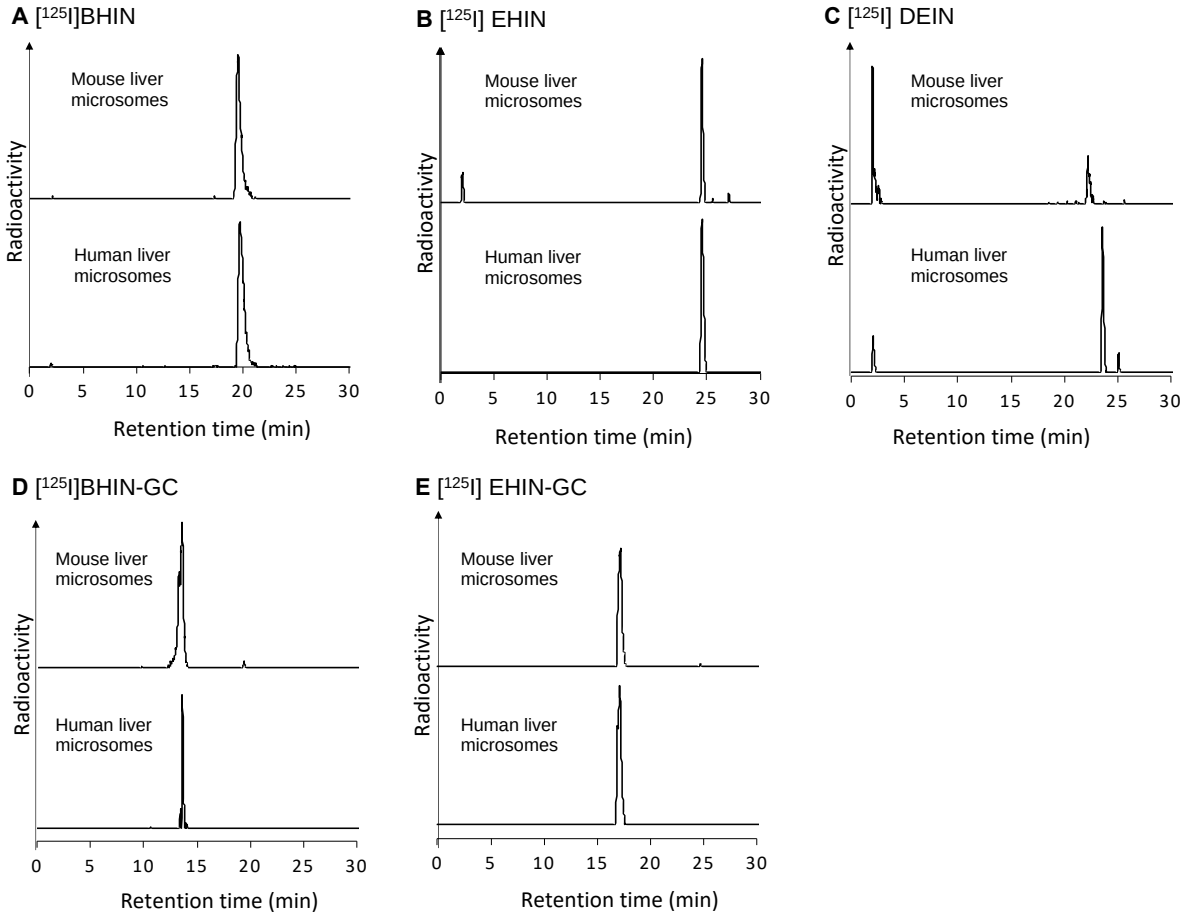

Figure 7. RP-HPLC charts of ^{125}I-labeled neopentyl derivatives ((A): [^{125}I]BHIN, (B): [^{125}I]EHIN, (C): [^{125}I]DEIN, (D): [^{125}I]BHIN-GC, (E): [^{125}I]EHIN-GC) after incubation in CYP-activated mouse- and human-derived microsome solutions.

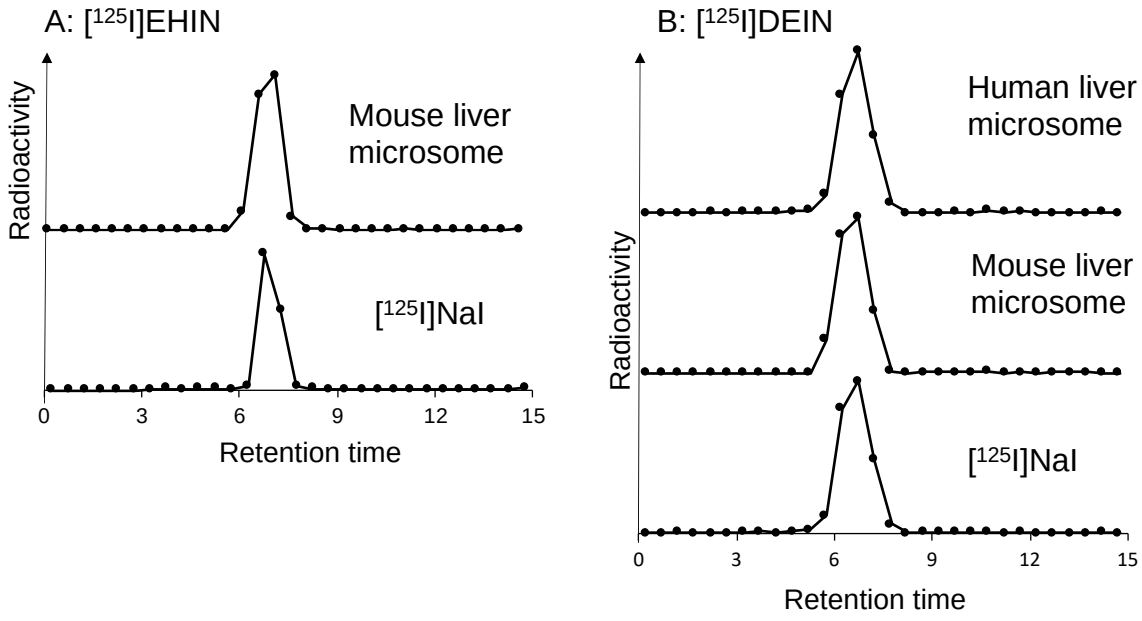

Figure 8. HILIC-HPLC reanalysis of metabolites eluted in the void volume of RP-HPLC following stability testing using microsomes.

Glucuronidation test

[^{125}I]BHIN, [^{125}I]EHIN, and [^{211}At]BHAN were incubated for 30 minutes in a solution containing mouse-derived or human-derived liver microsomes and UDPGA. These microsomes contain uridine 5'-diphosphate glucuronosyltransferase (UGT), which is responsible for glucuronidation. When using mouse-derived microsomes, peaks with shorter retention times (indicating increased hydrophilicity) were detected for [^{125}I]BHIN and [^{125}I]EHIN compared to the intact compounds (Figure 9). Similarly, [^{211}At]BHAN produced metabolites with higher Rf values (indicating increased hydrophilicity) after incubation with mouse-derived microsomes. Similar tests using non-radioactive iodine and extensive mass spectrometry and ^{1}H-NMR results identified these metabolites as the respective glucuronide conjugates ([^{125}I]BHIN-GC, [^{125}I]EHIN-GC and [^{211}At]BHAN-GC) (Figure 10).

On the other hand, when using human-derived liver microsomes, [^{125}I]EHIN was slightly converted to its glucuronide conjugate, but [^{125}I]BHIN was hardly converted. However, when the incubation time was extended to 6 hours, [^{125}I]BHIN was also converted to its glucuronide conjugate. [^{211}At]BHAN underwent glucuronidation similarly to [^{125}I]BHIN, with a comparable formation rate.

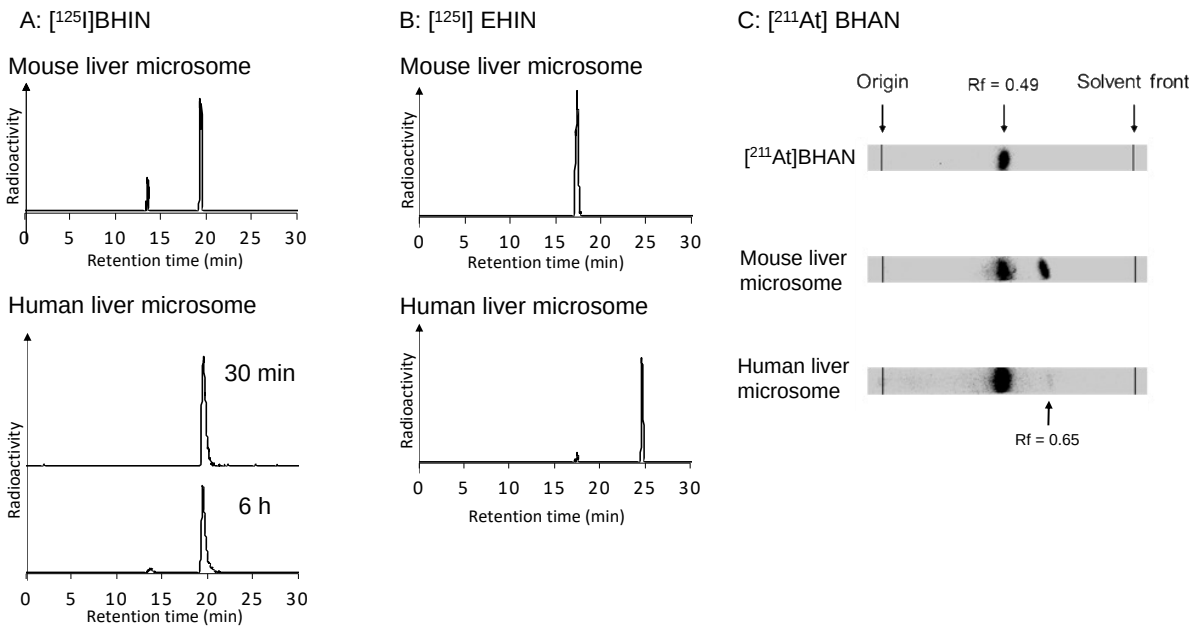

Figure 9. *In vitro* glucuronidation of [^{125}I]BHIN, [^{125}I]EHIN and [^{211}At]BHAN. (A) shows the RP-HPLC chromatograms obtained following glucuronidation assays of [^{125}I]BHIN using mouse- and human-derived liver microsomes. (B) shows the RP-HPLC chromatograms obtained following glucuronidation assays of [^{125}I]EHIN using mouse- and human-derived liver microsomes. (C) shows the RP-TLC of [^{211}At]BHAN standard and the RP-TLC obtained following glucuronidation assays of [^{211}At]BHAN using mouse- and human-derived liver microsomes.

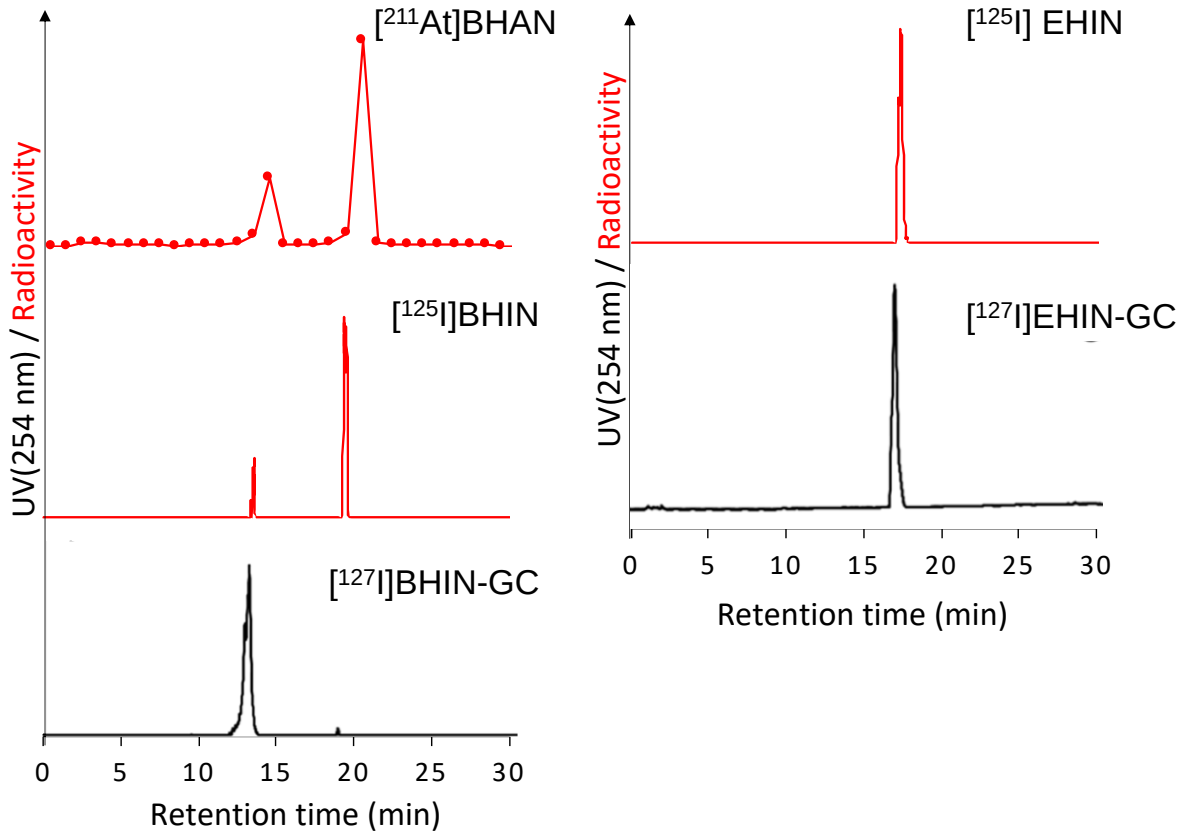

Figure 10. Comparison of retention times with nonradioactive glucuronide conjugates. The figure shows the RP-HPLC chromatograms obtained from glucuronidation assays using mouse liver microsomes. The red line represents the chromatogram of the radiolabeled samples ([^{211}At]BHAN, [^{125}I]BHIN, and [^{125}I]EHIN) after the glucuronidation assay, while the black line depicts the chromatogram of the non-radioactive glucuronide conjugates ([^{125}I]BHIN-GC, and [^{125}I]EHIN-GC).

Biodistributions

The time-dependent biodistribution after administration of [^{125}I]BHIN, [^{125}I]EHIN, [^{125}I]DEIN, [^{125}I]MIBAN, [^{211}At]BHAN, and [^{211}At]MABAN to normal mice are shown in Table 5-10. The ^{125}I-labeled neopentyl derivatives ([^{125}I]BHIN, [^{125}I]EHIN, [^{125}I]DEIN) exhibited rapid blood clearance (Figure 11). Among these derivatives, [^{125}I]DEIN showed the highest accumulation in the stomach at 6 hours post-administration and in the neck (including the thyroid) at 24 hours post-administration. In contrast, [^{125}I]BHIN showed the lowest accumulation in these tissues. All ^{125}I-labeled neopentyl derivatives were primarily excreted in the urine. The accumulation of [^{211}At]BHAN in the stomach and spleen was low (Figure 12). [^{211}At]BHAN exhibited similar pharmacokinetics to [^{125}I]BHIN, with no significant differences except for the radioactivity in the kidneys at 1-hour post-administration. On the other hand, [^{125}I]MIBAN and [^{211}At]MIBAN showed different pharmacokinetics, with significant differences observed in many organs. In the group administered [^{211}At]MIBAN, high radioactivity was observed in the stomach, neck (including the thyroid), and spleen, showing significantly higher accumulation compared to [^{125}I]BHIN, [^{125}I]MIBAN, and [^{211}At]BHAN.

Table 5. Biodistribution of [^{125}I]BHIN

	10 min	1 h	3 h	6 h	24 h
Blood	1.77 ± 0.20$^{‖,\#}$	0.18 ± 0.07$^{‡,\#}$	0.11 ± 0.01$^{‡,§,\#}$	0.21 ± 0.15$^{‡,\#}$	0.03 ± 0.01$^{\#}$
Liver	3.99 ± 2.26$^{‡,§,‖}$	0.60 ± 0.05$^{‡,‖}$	0.37 ± 0.14$^{‡,‖}$	0.29 ± 0.24$^{‡,‖}$	0.03 ± 0.00$^{‡,‖}$
Spleen	1.09 ± 0.17$^{\#}$	0.15 ± 0.03$^{\#}$	0.08 ± 0.02$^{\#}$	0.10 ± 0.05$^{\#}$	0.02 ± 0.01$^{\#}$
Kidney	9.88 ± 1.48$^{‡,‖,\#}$	1.90 ± 0.81¶	0.40 ± 0.12$^{‡,§,\#}$	0.77 ± 0.86	0.04 ± 0.02$^{‡,‖,\#}$
Pancreas	1.46 ± 0.12 $^{§,‖}$	0.24 ± 0.08$^{\#}$	0.12 ± 0.03$^{‡,\#}$	0.20 ± 0.10	0.04 ± 0.02$^{\#}$
Stomach†	0.60 ± 0.05$^{‡,\#}$	0.38 ± 0.05$^{\#}$	0.65 ± 0.09$^{‡,\#}$	1.15 ± 0.31$^{‡,\#}$	0.24 ± 0.07$^{\#}$
Intestine†	9.64 ± 4.84$^{‡,§,‖}$	12.34 ± 1.97$^{‡,§,‖}$	7.90 ± 2.11$^{‡,§,‖}$	7.46 ± 1.89$^{‡,§,‖}$	0.48 ± 0.21$^{‡,§,‖}$
Muscle	1.13 ± 0.11$^{‖,\#}$	0.29 ± 0.25$^{\#}$	0.18 ± 0.15$^{\#}$	0.17 ± 0.16$^{\#}$	0.02 ± 0.01$^{\#}$
Neck†	1.26 ± 0.47$^{\#}$	0.17 ± 0.06$^{\#}$	0.33 ± 0.03$^{\#}$	0.73 ± 0.21$^{‡,§,\#}$	2.76 ± 1.19‡,§
Urine†				65.94 ± 11.80	81.10 ± 6.17
Feces†				0.17 ± 0.15	8.79 ± 3.54

*Tissue radioactivity is expressed as %ID/g for each group (n=5); results are reported as mean ± SD. †Expressed as %ID. $^{‡,§,‖,¶,\#}$Statistical significances were determined by Tukey's test; $p < 0.05$ compared with [^{125}I]DEIN (‡), [^{125}I]EHIN (§), [^{125}I]MIBAN ($^{‖}$), [^{211}At]BHAN (¶) and [^{211}At]MABAN ($^{\#}$).

Table 6. Biodistribution of [^{125}I]EHIN

	10 min	1 h	3 h	6 h	24 h
Blood	1.45 ± 0.24	0.38 ± 0.07‡	0.38 ± 0.10‡,§	0.35 ± 0.07‡	0.05 ± 0.03
Liver	8.29 ± 0.73 §	1.79 ± 0.86$^{‖}$	1.19 ± 0.41$^{‖}$	0.60 ± 0.22$^{‡,‖}$	0.11 ± 0.02$^{‖}$
Spleen	1.33 ± 0.23	0.23 ± 0.04	0.23 ± 0.05	0.16 ± 0.02	0.04 ± 0.02
Kidney	11.43 ± 2.01$^{‡,‖}$	1.82 ± 0.63	0.75 ± 0.12‡,§	0.61 ± 0.36	0.11 ± 0.02$^{‖}$
Pancreas	2.15 ± 0.16$^{‡,§,‖}$	0.34 ± 0.12	0.27 ± 0.05	0.21 ± 0.05	0.06 ± 0.03
Stomach†	1.21 ± 0.22‡	2.71 ± 1.17	1.49 ± 0.60	1.19 ± 0.42‡	0.44 ± 0.39
Intestine†	18.97 ± 5.83 §	27.15 ± 5.15 $^{§,‖}$	25.06 ± 3.45 $^{§,‖}$	12.03 ± 3.97$^{‡,‖}$	0.90 ± 0.97
Muscle	1.36 ± 0.25$^{‖}$	0.17 ± 0.06	0.11 ± 0.03	0.09 ± 0.02	0.02 ± 0.02
Neck †	2.17 ± 0.80	0.86 ± 0.19	1.26 ± 0.21	2.62 ± 0.70 §	5.78 ± 1.70$^{‡,§,‖}$
Urine †				56.47 ± 4.84	61.18 ± 9.85
Feces†				6.56 ± 2.58	15.06 ± 6.49

*Tissue radioactivity is expressed as %ID/g for each group (n=5); results are reported as mean ± SD. †Expressed as %ID. $^{‡,§,‖}$Statistical significances were determined by Tukey's test; $p < 0.05$ compared with [^{125}I]DEIN (‡), [^{125}I]BHIN (§) and [^{125}I]MIBAN ($^{‖}$).

Table 7. Biodistribution of [^{125}I]DEIN

	10 min	1 h	3 h	6 h	24 h
Blood	1.44 ± 0.20	1.06 ± 0.32$^{‡,§,‖}$	0.87 ± 0.17$^{‡,§,‖}$	0.89 ± 0.18$^{‡,§,‖}$	0.08 ± 0.01
Liver	7.68 ± 1.40§	3.30 ± 1.07§	2.32 ± 1.30§	1.56 ± 0.58$^{‡,§,‖}$	0.22 ± 0.04$^{§,‖}$
Spleen	0.99 ± 0.14	0.59 ± 0.15	0.42 ± 0.07	0.46 ± 0.24	0.15 ± 0.19
Kidney	6.26 ± 0.86‡,§	2.58 ± 0.77	1.23 ± 0.06$^{‡,§,‖}$	1.01 ± 0.24	0.18 ± 0.02$^{§,‖}$
Pancreas	1.43 ± 0.07‡	0.66 ± 0.18	0.46 ± 0.11$^{§,‖}$	0.76 ± 0.68	0.06 ± 0.01
Stomach†	2.05 ± 0.28$^{‡,§,‖}$	5.22 ± 1.79	3.51 ± 1.56§	5.19 ± 1.95$^{‡,§,‖}$	0.25 ± 0.07
Intestine†	21.15 ± 2.67§	30.68 ± 5.57$^{§,‖}$	28.57 ± 3.86$^{§,‖}$	25.34 ± 2.27$^{‡,§,‖}$	0.53 ± 0.08
Muscle	1.06 ± 0.17$^{‖}$	0.41 ± 0.16	0.23 ± 0.04	0.21 ± 0.04	0.05 ± 0.01
Neck†	1.12 ± 0.09	0.94 ± 0.83	1.03 ± 1.42	4.14 ± 1.86$^{§,‖}$	10.60 ± 2.28$^{‡,§,‖}$
Urine†				26.55 ± 4.23	52.60 ± 2.41
Feces†				0.56 ± 0.78	13.19 ± 3.97

*Tissue radioactivity is expressed as %ID/g for each group (n=5); results are reported as mean ± SD. †Expressed as %ID. $^{‡,§,‖}$Statistical significances were determined by Tukey's test; $p < 0.05$ compared with [^{125}I]EHIN (‡), [^{125}I]BHIN (§), and [^{125}I]MIBAN ($^{‖}$).

Table 8. Biodistribution of [^{125}I]MIBAN

	10 min	1 h	3 h	6 h	24 h
Blood	1.19 ± 0.08$^{‖,¶,#}$	0.38 ± 0.02$^{‡,#}$	0.22 ± 0.03$^{‡,#}$	0.19 ± 0.05$^{‡,#}$	0.05 ± 0.01$^{#}$
Liver	8.36 ± 1.19$^{‖,¶,#}$	3.66 ± 0.83$^{‖,¶}$	2.33 ± 0.19$^{§,‖,¶,#}$	2.46 ± 0.24$^{‡,§,‖,¶,#}$	0.80 ± 0.16$^{‡,§,‖,¶,#}$
Spleen	1.14 ± 0.18$^{#}$	0.27 ± 0.06$^{#}$	0.13 ± 0.02$^{#}$	0.14 ± 0.05$^{#}$	0.04 ± 0.02$^{#}$
Kidney	4.50 ± 0.35$^{§,‖,¶}$	1.88 ± 0.24¶	0.65 ± 0.07$^{‡,¶,#}$	0.51 ± 0.08	0.32 ± 0.08$^{‡,§,‖,¶,#}$
Pancreas	1.44 ± 0.08$^{§,#}$	0.36 ± 0.07$^{#}$	0.18 ± 0.02$^{‡,#}$	0.36 ± 0.43	0.08 ± 0.01$^{#}$
Stomach†	1.04 ± 0.25$^{‡,#}$	1.24 ± 0.14$^{#}$	1.44 ± 0.14$^{#}$	0.74 ± 0.18$^{‡,#}$	0.17 ± 0.12$^{#}$
Intestine†	25.47 ± 5.01$^{‖,¶,#}$	46.97 ± 1.71$^{‡,§,‖,¶,#}$	39.86 ± 7.65$^{‡,§,‖,¶,#}$	38.77 ± 6.82$^{‡,§,‖,¶,#}$	0.81 ± 0.31
Muscle	2.34 ± 0.14‡,§,¶	0.36 ± 0.24$^{#}$	0.13 ± 0.02$^{#}$	0.10 ± 0.03$^{#}$	0.05 ± 0.01$^{#}$
Neck†	2.15 ± 0.56¶	0.61 ± 0.10$^{#}$	0.69 ± 0.12$^{#}$	1.00 ± 0.27$^{‡,#}$	1.60 ± 0.36$^{‡,§,#}$
Urine†				27.61 ± 1.84	35.02 ± 3.92
Feces†				7.80 ± 10.09	46.91 ± 0.33

*Tissue radioactivity is expressed as %ID/g for each group (n=5); results are reported as mean ± SD. †Expressed as %ID.$^{‡,§,‖,¶,#}$Statistical significances were determined by Tukey's test; $p < 0.05$ compared with [^{125}I]DEIN (‡), [^{125}I]EHIN (§), [^{125}I]BHIN ($^{‖}$), [^{211}At]BHAN (¶) and [^{211}At]MABAN ($^{#}$).

Table 9. Biodistribution of [^{211}At]BHAN

	10 min	1 h	3 h	6 h	24 h
Blood	1.93 ± 0.33§	0.20 ± 0.08$^{‖}$	0.18 ± 0.05$^{‖}$	0.13 ± 0.01$^{‖}$	0.07 ± 0.05$^{‖}$
Liver	3.21 ± 0.29§	0.22 ± 0.05$^{§,‖}$	0.22 ± 0.15§	0.20 ± 0.05§	0.01 ± 0.00$^{§,‖}$
Spleen	1.32 ± 0.46$^{‖}$	0.42 ± 0.08$^{‖}$	0.39 ± 0.14$^{‖}$	0.61 ± 0.11$^{‖}$	0.16 ± 0.05$^{‖}$
Kidney	9.10 ± 3.10$^{§,‖}$	0.48 ± 0.16$^{‡,§,‖}$	0.21 ± 0.05$^{§,‖}$	0.29 ± 0.08$^{‖}$	0.04 ± 0.01$^{§,‖}$
Pancreas	1.62 ± 0.40$^{‖}$	0.35 ± 0.10$^{‖}$	0.31 ± 0.15$^{‖}$	0.38 ± 0.10	0.11 ± 0.03$^{‖}$
Stomach†	0.88 ± 0.13$^{‖}$	0.98 ± 0.34$^{‖}$	1.15 ± 0.28$^{‖}$	1.24 ± 0.69$^{‖}$	0.78 ± 0.24$^{‖}$
Intestine†	10.26 ± 2.22§	10.93 ± 3.21§	9.13 ± 1.36§	10.30 ± 3.81§	0.73 ± 0.20
Muscle	1.22 ± 0.24$^{§,‖}$	0.28 ± 0.09$^{‖}$	0.18 ± 0.03$^{‖}$	0.26 ± 0.07	0.09 ± 0.02$^{‖}$
Neck†	0.47 ± 0.10$^{§,‖}$	0.12 ± 0.02$^{‖}$	0.21 ± 0.08$^{‖}$	0.24 ± 0.12$^{‖}$	0.07 ± 0.06$^{‖}$

*Tissue radioactivity is expressed as %ID/g for each group (n=4); results are reported as mean ± SD. †Expressed as %ID. $^{‡,§,‖}$Statistical significances were determined by Tukey's test; $p < 0.05$ compared with [^{125}I]BHIN (‡), [^{125}I]MIBAN (§) and [^{211}At]MABAN ($^{‖}$).

Table 10. Biodistribution of [^{211}At]MABAN

	10 min	1 h	3 h	6 h	24 h
Blood	2.73 ± 0.42‡,§	1.95 ± 0.37$^{‡,§,‖}$	1.49 ± 0.09$^{‡,§,‖}$	0.93 ± 0.20$^{‡,§,‖}$	0.33 ± 0.12$^{‡,§,‖}$
Liver	2.11 ± 0.44§	2.13 ± 0.86§	1.08 ± 0.07§	0.75 ± 0.22§	0.26 ± 0.08‡,§
Spleen	5.48 ± 0.60$^{‡,§,‖}$	10.19 ± 4.05$^{‡,§,‖}$	7.66 ± 1.71$^{‡,§,‖}$	3.92 ± 0.74$^{‡,§,‖}$	1.67 ± 0.43$^{‡,§,‖}$
Kidney	4.21 ± 0.73$^{‡,‖}$	3.02 ± 0.60$^{‖}$	2.12 ± 0.24$^{‡,§,‖}$	1.35 ± 0.35$^{‖}$	0.50 ± 0.13$^{‡,§,‖}$
Pancreas	2.74 ± 0.37$^{‡,§,‖}$	2.25 ± 0.53$^{‡,§,‖}$	1.29 ± 0.20$^{‡,§,‖}$	0.81 ± 0.20	0.92 ± 0.40$^{‡,§,‖}$
Stomach†	5.37 ± 0.65$^{‡,§,‖}$	11.50 ± 6.96$^{‡,§,‖}$	22.92 ± 1.99$^{‡,§,‖}$	12.65 ± 1.69$^{‡,§,‖}$	2.72 ± 0.80$^{‡,§,‖}$
Intestine†	6.55 ± 0.80§	9.79 ± 4.55§	5.22 ± 0.69§	3.59 ± 0.63§	1.44 ± 1.04
Muscle	2.09 ± 0.38$^{‡,‖}$	0.81 ± 0.17$^{‡,§,‖}$	0.54 ± 0.03$^{‡,§,‖}$	0.40 ± 0.12‡,§	0.54 ± 0.11$^{‡,§,‖}$
Neck†	3.04 ± 0.50$^{‡,‖}$	5.91 ± 1.96$^{‡,§,‖}$	8.73 ± 1.14$^{‡,§,‖}$	6.20 ± 1.41$^{‡,§,‖}$	3.58 ± 0.71$^{‖}$

*Tissue radioactivity is expressed as %ID/g for each group (n=4); results are reported as mean ± SD. †Expressed as %ID. $^{‡,§,‖}$Statistical significances were determined by Tukey's test; $p < 0.05$ compared with [^{125}I]BHIN (‡), [^{211}At]BHAN (§) and [^{125}I]MIBAN ($^{‖}$).

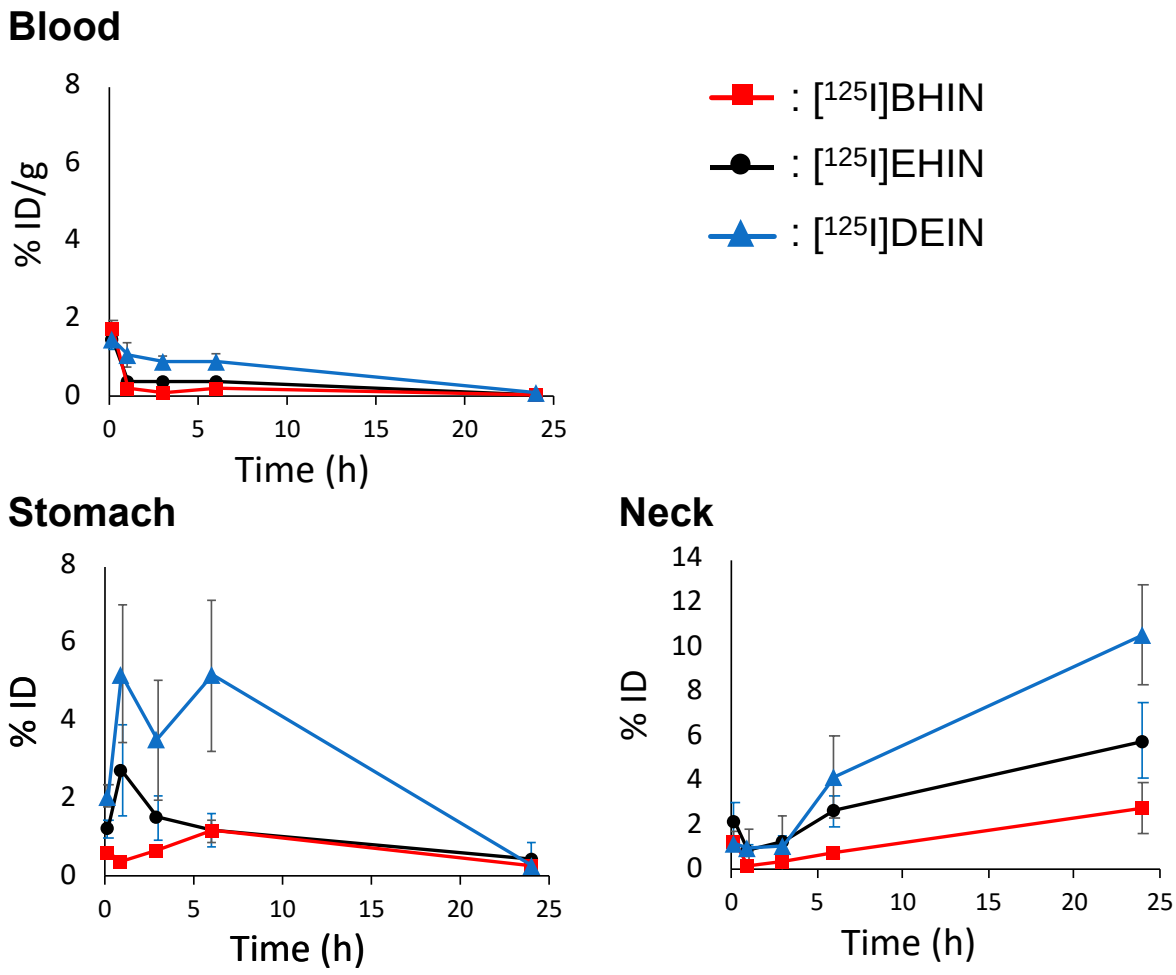

Figure 11. Pharmacokinetics of ^{125}I-labeled neopentyl derivatives. Red line: [^{125}I]BHIN, black line: [^{125}I]EHIN, blue line: [^{125}I]DEIN. The data points represent the radioactivity levels in blood, stomach, and neck (including the thyroid) at 10 minutes, 1 hour, 3 hours, 6 hours, and 24 hours post-administration.

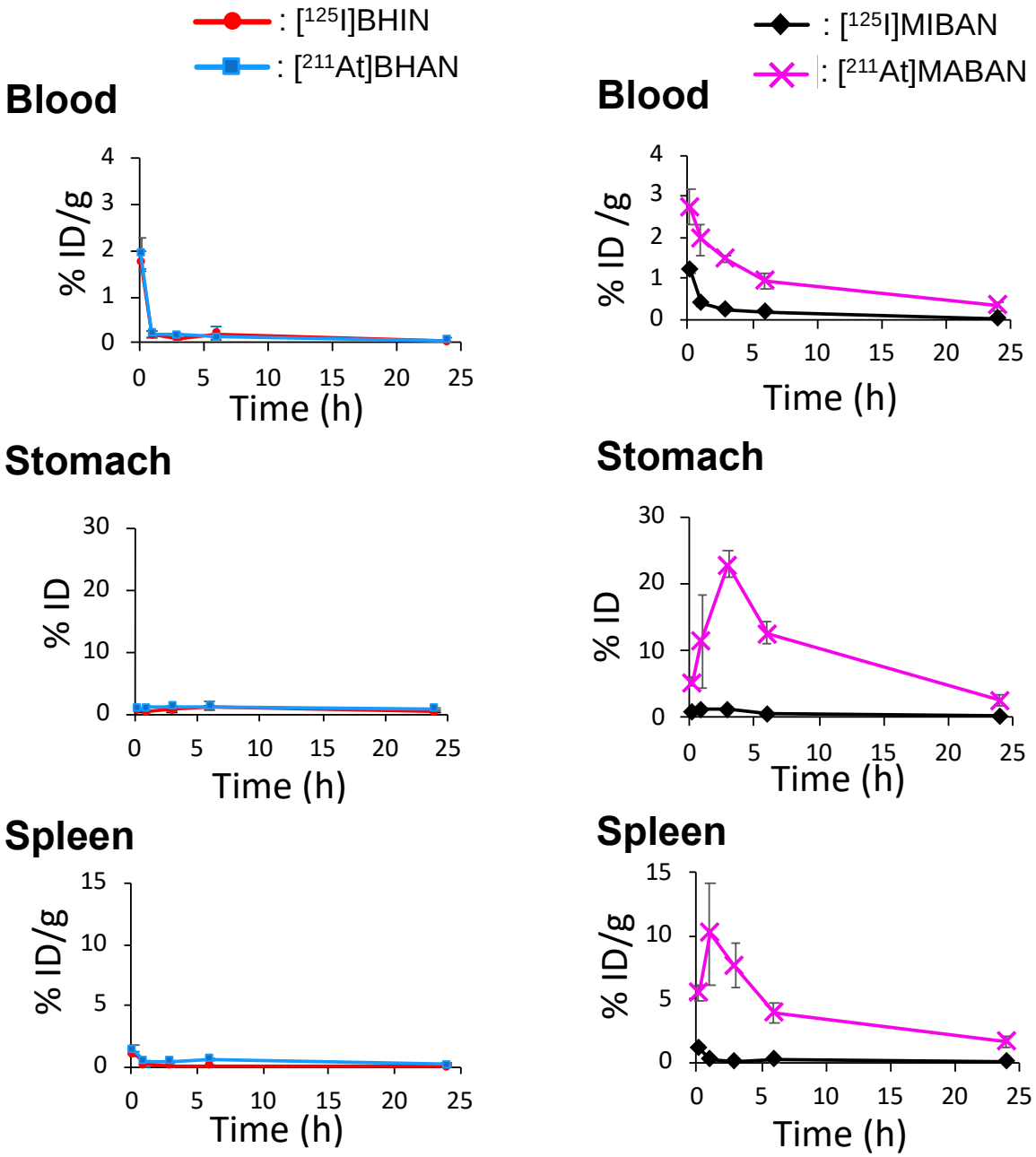

Figure 12. Comparison of biodistribution between neopentyl derivatives ([^{125}I]BHIN (red line) and [^{211}At]BHAN (blue line)) and benzoate derivatives([^{125}I]MIBAN (black line) and [^{211}At]MABAN (pink line)). The data points represent the radioactivity levels in blood, stomach, and spleen at 10 minutes, 1 hour, 3 hours, 6 hours, and 24 hours post-administration.

Analysis of urinary metabolites.

The results of the analysis of urinary metabolites by RP-HPLC are shown in Figure 13. [^{125}I]BHIN was mainly excreted as a glucuronide conjugate, and there were almost no peak in the void volume. From [^{125}I]EHIN samples, peaks of glucuronide conjugates and void volume were observed. Most of the radioactivity in the urine of the [^{125}I]DEIN administration group was observed in the void volume. When the void volume peaks observed in the analysis of [^{125}I]EHIN and [^{125}I]DEIN were reanalyzed by HILIC-HPLC, the peaks matched the retention time of [^{125}I]NaI (Figure 14). [^{211}At]BHAN, like [^{125}I]BHIN, was mainly excreted as a glucuronide conjugate (Figure 15). On the other hand, when the urine sample of the [^{211}At]MABAN administration group was analyzed, most of the radioactivity was observed in the void volume. When $^{211}At^{-}$ was analyzed in the same system, it was also observed in the void volume.

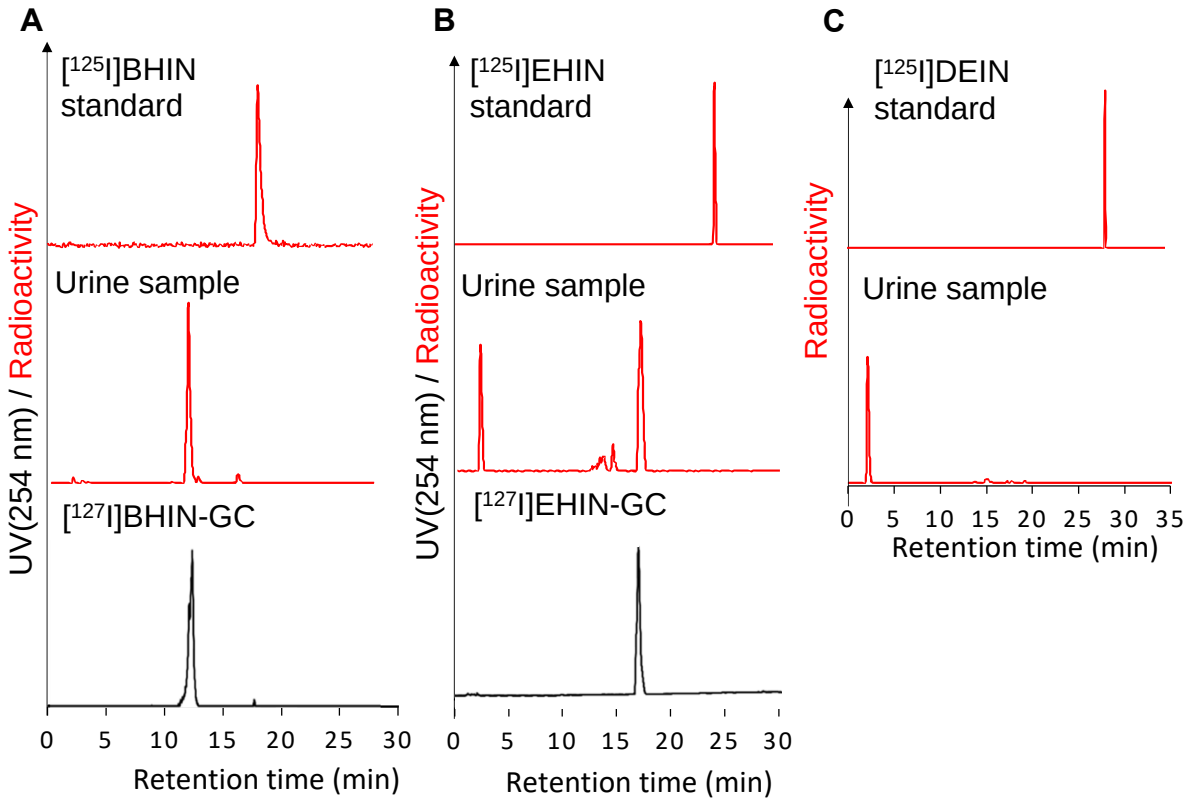

Figure 13. Urinary analysis of ^{125}I-labeled neopentyl derivatives. (A) shows the RP-HPLC charts in the following order from top to bottom: [^{125}I]BHIN standard, urine from mice administered [^{125}I]BHIN, and [^{127}I]BHIN -GC. (B) shows the RP-HPLC charts in the following order from top to bottom: [^{125}I]EHIN standard, urine from mice administered [^{125}I]EHIN, and [^{127}I]EHIN -GC. (C) shows the RP-HPLC charts in the following order from top to bottom: [^{125}I]DEIN standard and urine from mice administered [^{125}I]DEIN

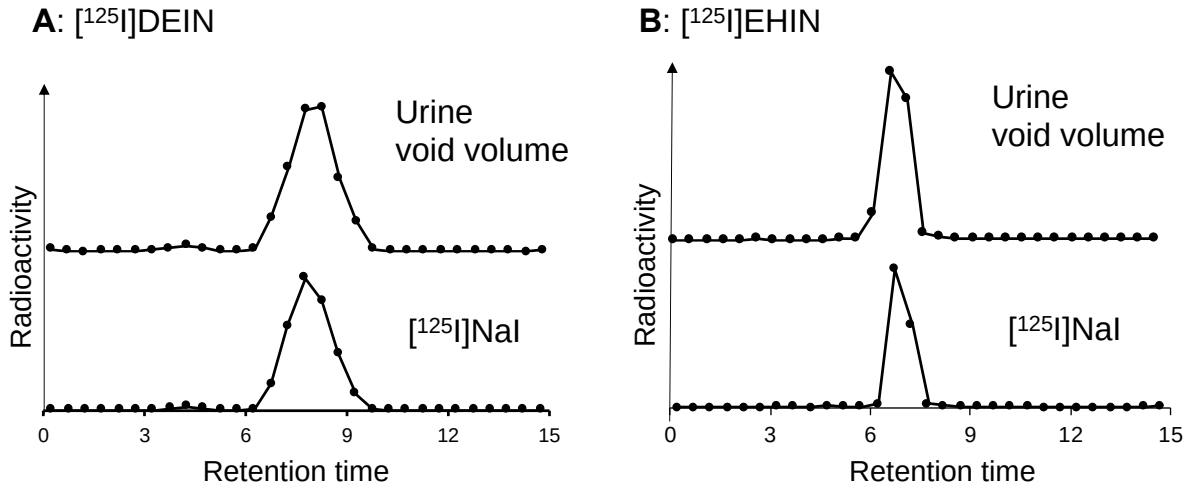

Figure 14. HILIC-HPLC reanalysis of metabolites eluted in the void volume of RP-HPLC analysis of urine.

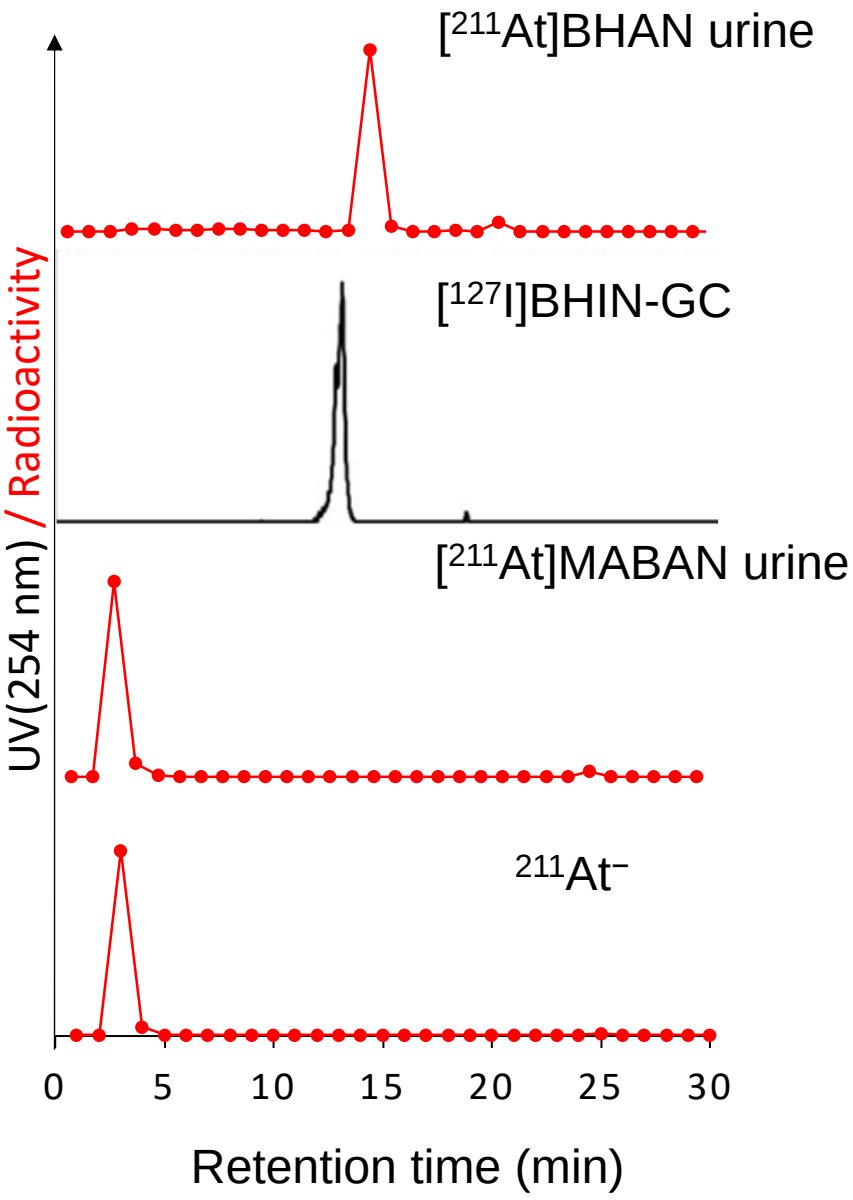

Figure 15. HPLC radiochromatograms of urine samples collected for 6 h postinjection of [^{211}At]BHAN and [^{211}At]MABAN, and their comparison with [^{127}I]BHIN-GC and ^{211}At^{-}

Discussion

The neopentyl structure has low reactivity to nucleophilic attack due to steric hindrance[57]. This characteristic affects the labeling yield of neopentyl derivatives, resulting in low labeling yields (<20%) for [^{125}I]EHIN and [^{125}I]DEIN. In contrast, [^{125}I]BHIN showed a good labeling yield (about 70%) due to introducing an acetal-protecting group, which limited the steric hindrance of the substituents. When a compound with a tosyl group was used as a labeling precursor for [^{125}I]BHIN, the synthesis yield was low even at high temperatures (110 °C), leaving unreacted precursors (data not shown). On the other hand, the presence of organic bases contributed to improved yields in ^{125}I labeling. This is likely due to their ability to neutralize the acidic conditions that arise from the decomposition of the triflate group on the precursor during the reaction. Indeed, TLC analysis suggested the presence of iodine species other than I^- when no base was added (data not shown).

Because thiol groups have high nucleophilic reactivity, GSH, a thiol-containing low-molecular-weight compound in many biological systems, is a major nucleophilic biomolecule [58,59]. GSH exists in cells at concentrations of 0.5 to 10 mM, mainly in the reduced form. Therefore, the stability of ^{125}I-labeled neopentyl derivatives against nucleophilic attack was evaluated by incubating them in a 10 mM GSH solution. As expected from the labeling reaction, all three compounds, [^{125}I]BHIN, [^{125}I]EHIN, and [^{125}I]DEIN were stable against nucleophilic substitution reactions. However, significant differences were observed in their stability against CYP-mediated metabolism. While [^{125}I]BHIN mainly remained intact after incubation, [^{125}I]DEIN was almost completely metabolized. [^{125}I]EHIN showed intermediate stability. The primary metabolites of [^{125}I]EHIN and [^{125}I]DEIN via CYP metabolism were I^-, indicating deiodination via CYP metabolism. Deiodination occurred more readily in mouse liver microsomes than in human liver microsomes. The CYP content in this study's mouse and human liver microsomes was equivalent (final concentration: mouse 0.233 nmol/mL, human 0.257 nmol/mL), suggesting the difference of species may cause these reactivities.

Due to the expression of the Na/I symporter, free [^{125}I]I^- accumulates in the stomach and thyroid[60,61]. Therefore, accumulation in these tissues serves as an indicator of *in vivo* deiodination. The radioactivity accumulation of [^{125}I]EHIN in these organs was lower than that of [^{125}I]DEIN, and [^{125}I]BHIN showed the lowest accumulation. This result is consistent with *in vitro* stability studies. All three ^{125}I-labeled neopentyl derivatives were primarily excreted in the urine. Analysis of urine samples by RP-HPLC showed that the [^{125}I]DEIN was unstable *in vivo*, with most of it being metabolized to release [^{125}I]I^- and excreted in the urine. [^{125}I]EHIN showed moderate stability, with partially released [^{125}I]I^- and another metabolite observed as the main peak. However, almost no radioactivity of [^{125}I]I^- was observed from the [^{125}I]BHIN samples, suggesting that the C-I bond of

[^{125}I]BHIN is stable *in vivo*.

Another *in vitro* test was conducted to identify the primary radioactive metabolites observed in the urine analysis of [^{125}I]BHIN and [^{125}I]EHIN. Since several nitroimidazole derivatives, such as pimonidazole and FMISO, are reported to undergo glucuronidation, [62,63] it was predicted that the metabolites of [^{125}I]BHIN and [^{125}I]EHIN would be glucuronidated compounds. *In vitro* metabolism studies using microsomes can also be applied to evaluate UGT-mediated glucuronidation in the presence of uridine 5'-diphosphate-glucuronic acid (UDPGA) as a glucuronic acid donor. As a result, glucuronidation was investigated using microsomes, and the glucuronide conjugates were obtained in all tests of [^{nat}I]BHIN, [^{125}I]BHIN, [^{nat}I]EHIN, and [^{125}I]EHIN. The isolated glucuronidated compounds of [^{125}I]BHIN and [^{125}I]EHIN were stable against CYP-mediated metabolism. This result suggests that independent of glucuronide conjugates, the C-I bond of [^{125}I]BHIN is stable against CYP-mediated dehalogenation, while [^{125}I]EHIN acquires resistance to CYP-mediated deiodination through glucuronidation. The tendency of dehalogenation reactions of neopentyl derivatives suggests that the number of hydroxyl groups in the labeling scaffold plays a vital role in the stability of CYP-mediated metabolism. This result is consistent with the high *in vivo* stability of [^{18}F]DiFA. [64] Although the role of hydroxyl groups in stability against CYP-mediated dehalogenation is still unclear, considering that CYP-mediated deiodination involves the introduction of a hydroxyl group to the carbon bonded to iodine, hydroxyl groups in the scaffold might inhibit this process. [42]

Based on the evaluation of the *in vivo* stability of neopentyl derivatives, [^{211}At]BHAN was designed. [^{125}I]NaI is supplied as NaOH solution, and adding an aqueous solution is undesirable for the labeling reaction, resulting in moderate to low radiochemical yields. However, ^{211}At purified by dry distillation can be eluted in various solvents suitable for the labeling reaction. Therefore, ^{211}At was eluted with acetonitrile and reacted under anhydrous conditions, yielding [^{211}At]BHAN in high yield (>90%) under mild conditions (37 °C).

Similar to [^{125}I]BHIN, [^{211}At]BHAN was stable in all *in vitro* stability tests, including incubation with GSH and CYP-mediated metabolism. This result was reflected in the *in vivo* distribution test. Free astatide, like iodide, accumulates in the stomach and thyroid via the Na/I symporter, making accumulation in these tissues an indicator of *in vivo* deastatination.[65] In addition to these tissues, unlike iodine, accumulation in the spleen and lungs is also observed.[27] This seems to reflect the metallic characteristics of ^{211}At. [^{211}At]BHAN showed low radioactivity levels in the stomach, neck (including the thyroid), spleen, and lungs, comparable to those of [^{125}I]BHIN. In addition to these results, the analysis of urine metabolites confirmed the high stability of [^{211}At]BHAN against *in vivo* dehalogenation, as no [^{211}At]At^{-} was detected. Furthermore, analysis of urine samples showed

metabolites with retention times close to [^{125}I]BHIN-GC. This metabolite was confirmed to be the glucuronidated compound of [^{211}At]BHAN by glucuronidation tests using liver microsomes. The similarity confirmed by *in vitro* and *in vivo* glucuronidation studies indicates that the UGT recognition of [^{125}I]BHIN and [^{211}At]BHAN is biologically equivalent. The similarity in pharmacokinetics, including metabolic recognition of [^{125}I]BHIN and [^{211}At]BHAN, suggests that the neopentyl glycol labeling scaffold with two hydroxyl groups is helpful for radiotheranostics with radioiodine and ^{211}At. On the other hand, [^{125}I]MIBAN and [^{211}At]MABAN, which are benzoate derivatives, showed different pharmacokinetics, with significantly higher radioactivity levels of [^{211}At]MABAN in the stomach, neck, spleen, and lungs. Analysis of urine metabolites of [^{211}At]MABAN confirmed the release of At^-. Thus, the *in vivo* stability of radioiodine and ^{211}At-labeled compounds via the benzoate derivatives differed significantly. Such different *in vivo* distribution profiles have been observed in previous reports and are considered to result from differences in the stability of radioiodinated and astatinated compounds.[26]

The neopentyl glycol structure with two hydroxyl groups provides radioiodine- and ^{211}At-labeled compounds with high stability *in vivo*. Considering that this structure has also been used as a labeling scaffold for ^{18}F, the structure could be used as a common labeling scaffold for ^{18}F, radioiodine, and ^{211}At. [66,67]

Summary

The neopentyl structure exhibited the intended stability against nucleophilic attack but was insufficient for *in vivo* stability. The addition of two hydroxyl groups in the neopentyl structure improved against CYP-mediated dehalogenation. Neopentyl glycol (NpG) with two hydroxyl groups provided radioiodine and ^{211}At labeled compounds with high stability against two dehalogenation mechanisms and high *in vivo* stability. Considering that the NpG structure also provides *in vivo* stable ^{18}F-labeled compounds, the NpG structure would be a useful labeling scaffold for stable radiohalogen-labeled compounds.

Chapter 2. Development of radiotheranostic agents using the neopentyl-based labeling scaffold

Introduction

Due to their active cellular activities, cancer cells increase the expression of several types of amino acid transporters more than normal cells to enhance the uptake of amino acids.[68,69] Among the amino acid transporters overexpressed in cancer cells, L-type amino acid transporter 1 (LAT1) has been confirmed to be overexpressed in various cancer cells. This transporter exchanges large neutral amino acids with bulky side chains in a sodium-independent manner.[69,70] Moreover, LAT1 exhibits a relatively broad substrate recognition profile. Considering this characteristic, it is anticipated that radiohalogen-labeled agents would receive similar recognition regardless of radiohalogen type. Consequently, LAT1 is a promising target for radiotheranostics using ^{18}F and ^{211}At.

To date, several radiopharmaceuticals recognized by LAT1, such as [^{18}F]fluoroethyl-tyrosine ([^{18}F]FET), [^{18}F]fluoro-$_{L}$-DOPA ([^{18}F]FDOPA), and [^{123}I]iodomethyl-tyrosine ([^{123}I]IMT), have been developed for diagnostics (Figure 16). The usefulness of these compounds has been demonstrated through preclinical and clinical studies.[71-75]

Recently, alpha-emitting therapeutic agents such as [^{211}At]astato-phenylalanine ([^{211}At]AtPA) have been reported.[76] However, while [^{211}At]AtPA demonstrated tumor growth inhibition effects, its low *in vivo* stability still needs to be solved, as with many other ^{211}At-labeled compounds. In Chapter 1, I demonstrated that the neopentyl glycol (NpG) scaffold provides *in vivo* stable ^{211}At-labeled compounds. Therefore, I expected that incorporating this scaffold could improve the stability of ^{211}At-labeled amino acid derivatives against deastatination.

Chapter 2 aims to develop radiohalogen-labeled amino acid derivatives using the NpG scaffold and evaluate their utility as radiotheranostics agents. Based on the structure of [^{18}F]FET, I hypothesized that substitutional modification to the phenolic hydroxyl group of the tyrosine side chain is tolerant to the substrate recognition by LAT1. Therefore, three radiohalogenated amino acid derivatives ([^{211}At]At-NpGT, [^{125}I]I-NpGT, and [^{18}F]F-NpGT, Figure 17) were designed by introducing the NpG structure to the hydroxyl group of the tyrosine side chain. These derivatives' properties as substrates of LAT1 and biodistribution were evaluated and compared. Additionally, the therapeutic efficacy of [^{211}At]At-NpGT was assessed in tumor-bearing mouse models.

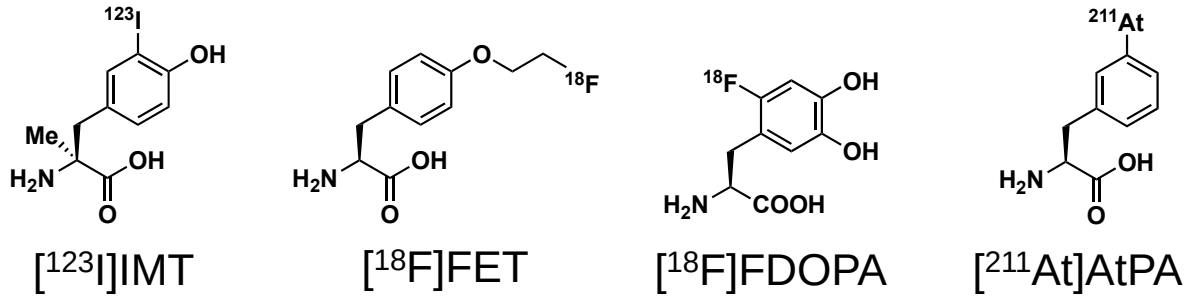

Figure 16. Chemical structures of radiohalogen-labeled amino acid derivatives

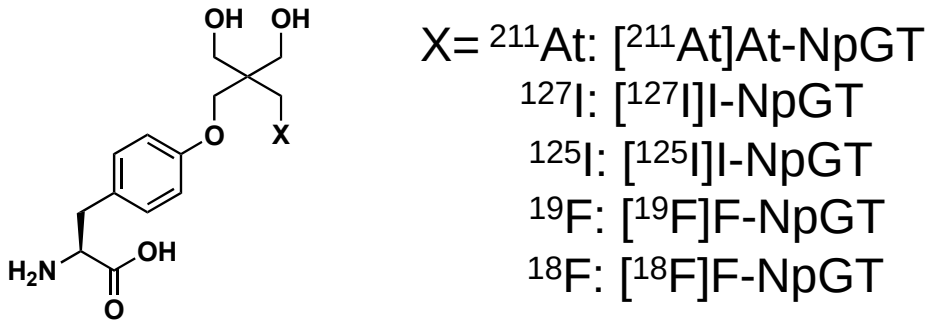

Figure 17. Chemical structures of NpGT derivatives evaluated in this study

Results

Synthesis and Radiolabeling

The non-radioactive [^{127}I]I-NpGT and [19F]F-NpGT were synthesized according to the following scheme (Scheme 5).

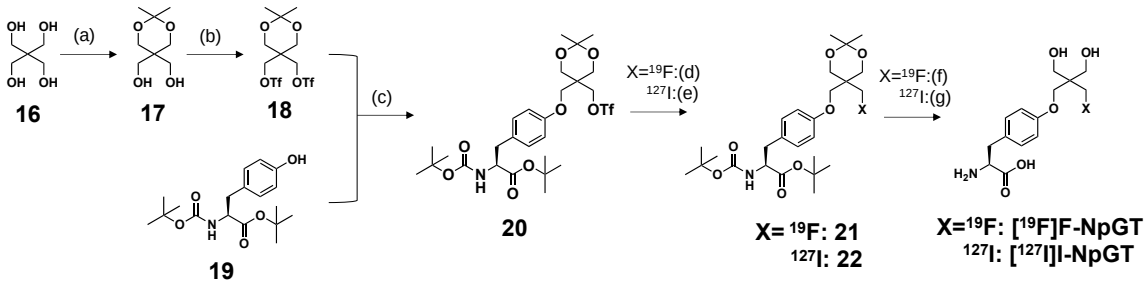

Reagent(s): (a) 2,2-dimethoxypropane, (+)-10-camphorsulfonic acid, DMF; (b) trifluoromethanesulfonic anhydride, 2,6-lutidine, CH_2Cl_2; (c) sodium hydride, THF; (d) tetrabutylammonium fluoride,THF; (e) sodium iodide, MeCN; (f) TFA ,H_2O; (g) TFA, H_2O

Scheme 5. Synthesis scheme of [^{19}F]F-NpTyr and [^{127}I]I-NpTyr

[^{211}At]At-NpGT, [^{125}I]I-NpGT, and [^{18}F]F-NpGT were synthesized from compound 20 through a two-step reaction involving halogen labeling and deprotection reactions (Scheme 6). The preparation of [^{211}At]At-NpGT and [^{125}I]I-NpGT were conducted at 37° C, yielding radiochemical yields of 44.3% (two steps) and 40.9% (two steps), respectively. The reaction rate for ^{211}At labeling improved in the presence of reducing agents, with most compound 20 converting to compound 23 after 30 minutes (Table 11). In contrast, [^{18}F]F-NpGT was obtained through an ^{18}F labeling reaction at 100° C, achieving a radiochemical yield of 35.4% (two steps). When analyzed by RP-HPLC, both [^{125}I]I-NpGT and [^{18}F]F-NpGT showed a single peak with the same retention time as the non-radioactive compounds. For ^{211}At, since there is no non-radioactive astatine isotope, a non-radioactive iodine-labeled amino acid derivative ([^{127}I]I-NpGT) was used as a standard. [^{211}At]At-NpGT exhibited a single peak with a retention time similar to that of [^{127}I]I-NpGT. To evaluate tumor uptake, I synthesized [^{125}I]IMT, an existing cancer diagnostic agent, as a control compound.

The radiochemical purity of all compounds, determined by RP-HPLC, was over 99%, and these radiolabeled compounds were used in subsequent experiments (Figure 18).

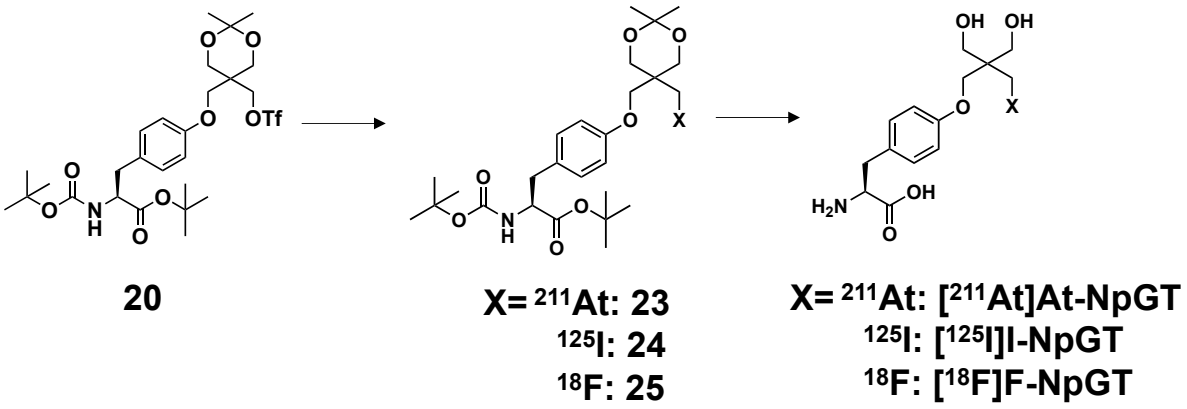

Scheme 6. Radiohalogen labeling of NpGT derivatives

Table 11. ^{211}At-labeling conversion rates in the absence or the presence of reductants.

	Radiochemical conversion (%)	
	10 min	30 min
Control	43.4±12.2	80.8±5.4
Sodium ascorbate	82.3±3.1	90.7±0.3
Glutathione	85.8±5.5	91.2±1.6
Sodium sulfite	81.5±3.4	96.5±1.4
Cysteine	80±6.3	92.9±2.7

*The data was performed by TLC

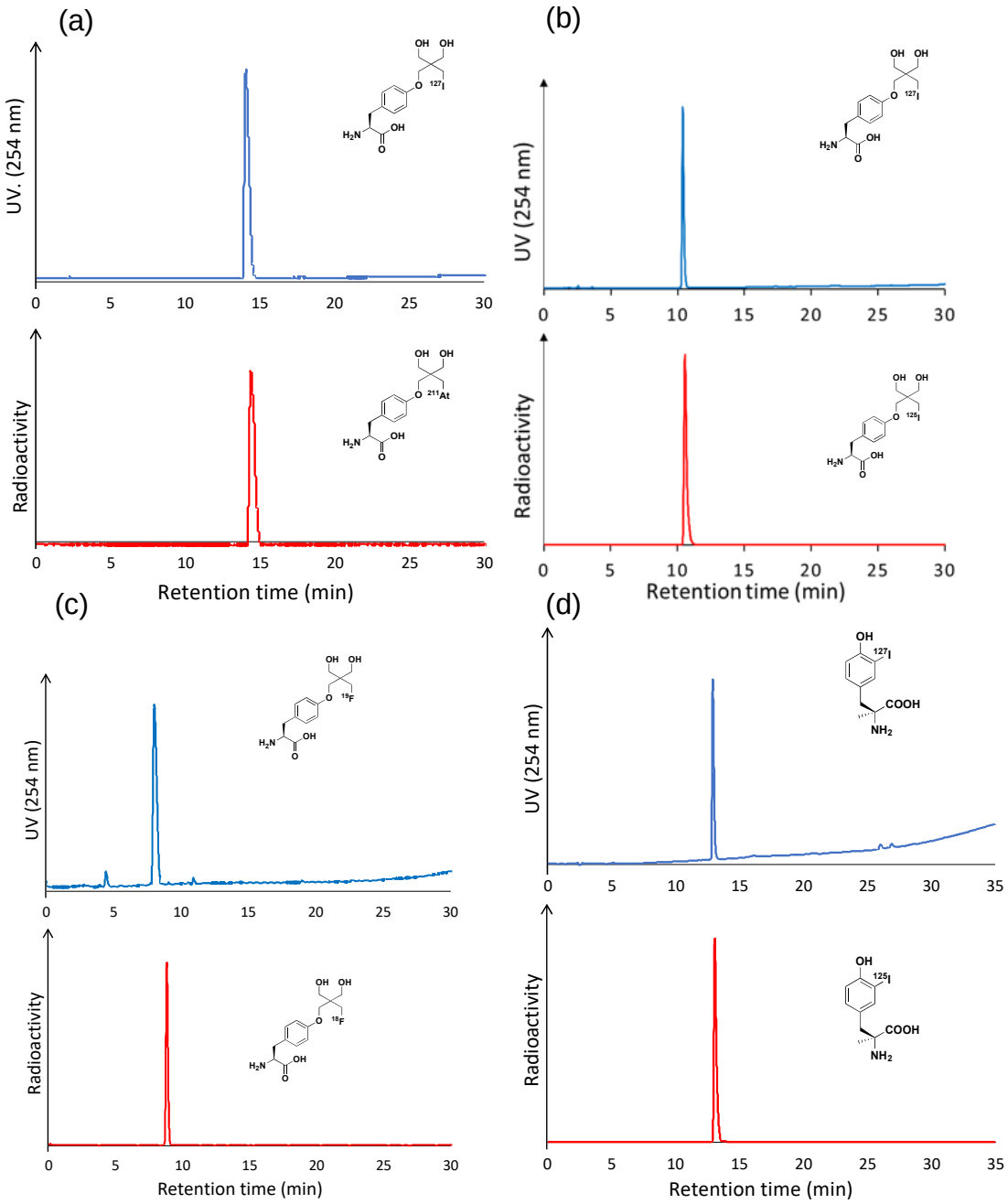

Figure 18. Identifications of [^{211}At]At-NpGT (A), [^{125}I]I-NpGT (B), [^{18}F]F-NpGT (C), and [^{125}I]-IMT (D) using RP-HPLC.

In vitro stability

[^{211}At]At-NpGT, [^{125}I]I-NpGT, and [^{18}F]F-NpGT exhibited high stability in PBS and FBS, with less than 1% halogen dissociation observed (Table 12).

Table 12. Stability of NpGT derivatives in PBS and FBS.

	% of free halogen		
In PBS*	1 h	3 h	6 h
[^{211}At]At-NpGT	< 1%	< 1%	N/A
[^{125}I]I-NpGT	< 1%	< 1%	< 1%
[^{18}F]F-NpGT	< 1%	< 1%	N/A
In FBS**	1 h	3 h	6 h
[^{211}At]At-NpGT	< 1%	< 1%	N/A
[^{125}I]I-NpGT	< 1%	< 1%	< 1%
[^{18}F]F-NpGT	< 1%	< 1%	N/A

*The data was performed by TLC

**The data was performed by RP-HPLC

In vitro experiments

The intracellular uptake of [^{211}At]At-NpGT, [^{125}I]I-NpGT, and [^{18}F]F-NpGT by C6 glioma cells increased over time (Figure 19). Additionally, these radiolabeled compounds were gradually excreted from the cells. RP-HPLC analysis revealed that intact [^{125}I]I-NpGT was excreted from the cells (Figure 20). The uptake of these radiolabeled compounds was significantly inhibited in the presence of BCH, an inhibitor of the L-type amino acid transporter AMT, amino acids recognized by LAT1, and L-tyrosine (Figure 21). In contrast, MeAIB, an inhibitor of the A-type amino acid transporter, did not inhibit their intracellular uptakes.

In the extracellular release study of [^{125}I]I-NpGT, the supernatant was analyzed by RP-HPLC (System A). The presence of intact [^{125}I]I-NpGT indicates the involvement of LAT1, a co-transported amino acid transporter.

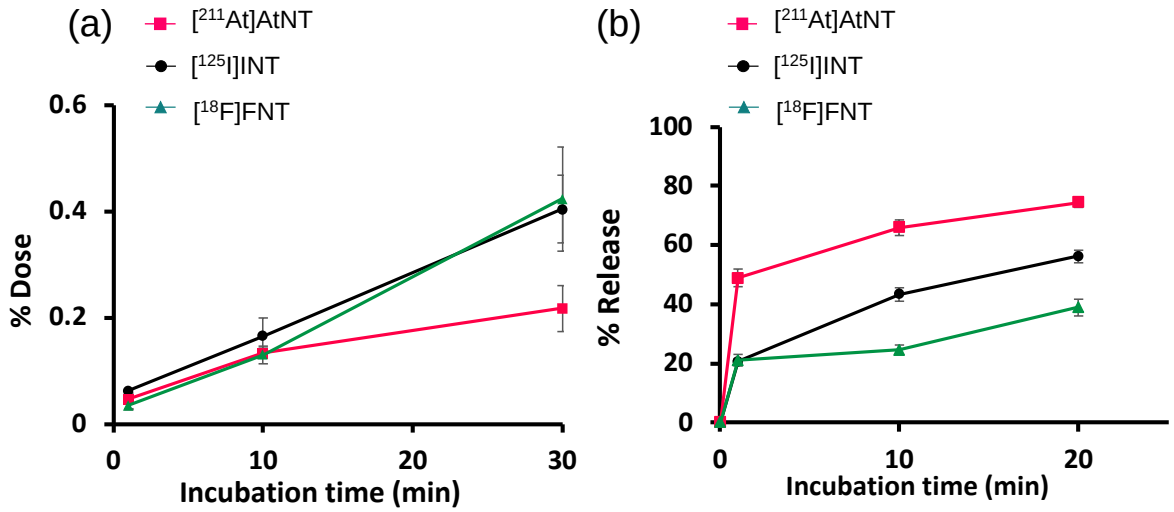

Figure 19. Cellular uptake and release of [^{211}At]At-NpGT, [^{125}I]I-NpGT and [^{18}F]F-NpGT from C6 cells. (a) Time-course study of uptake. (b) Time-course study of extracellular release. The Y-axis shows the percentage release of each agent.

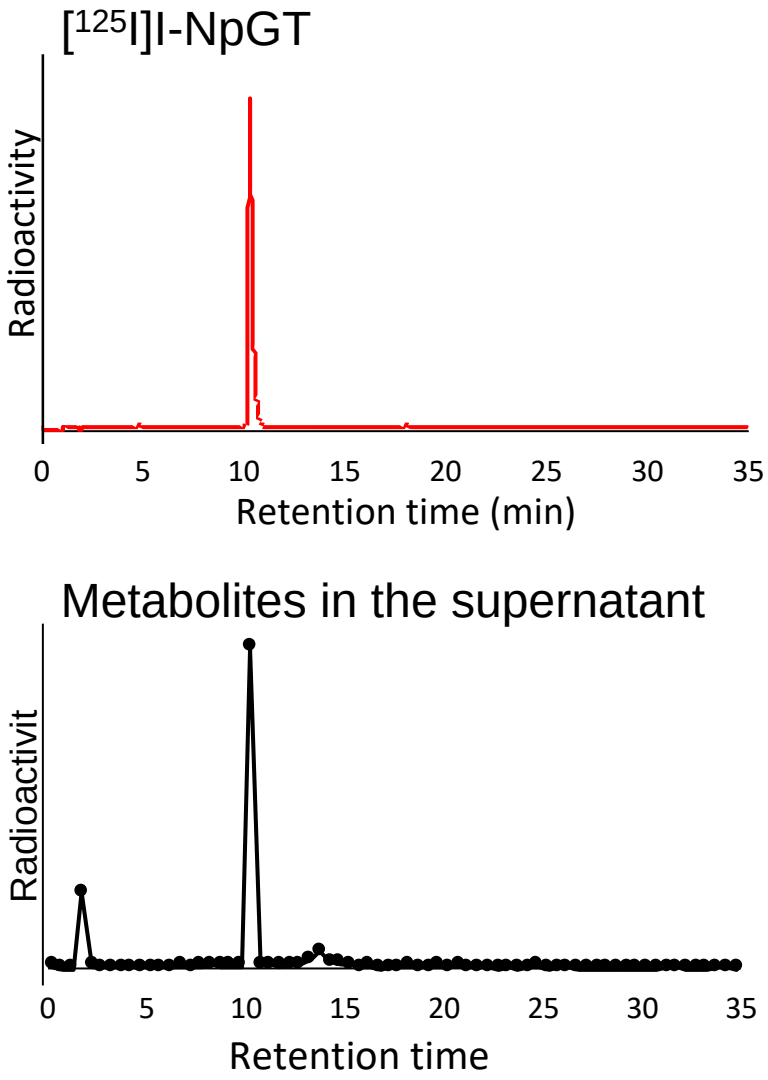

Figure 20. RP-HPLC radiochromatograms of [^{125}I]I-NpGT standard (upper) and radiometabolites of [^{125}I]I-NpGT released from C6 cells (bottom).

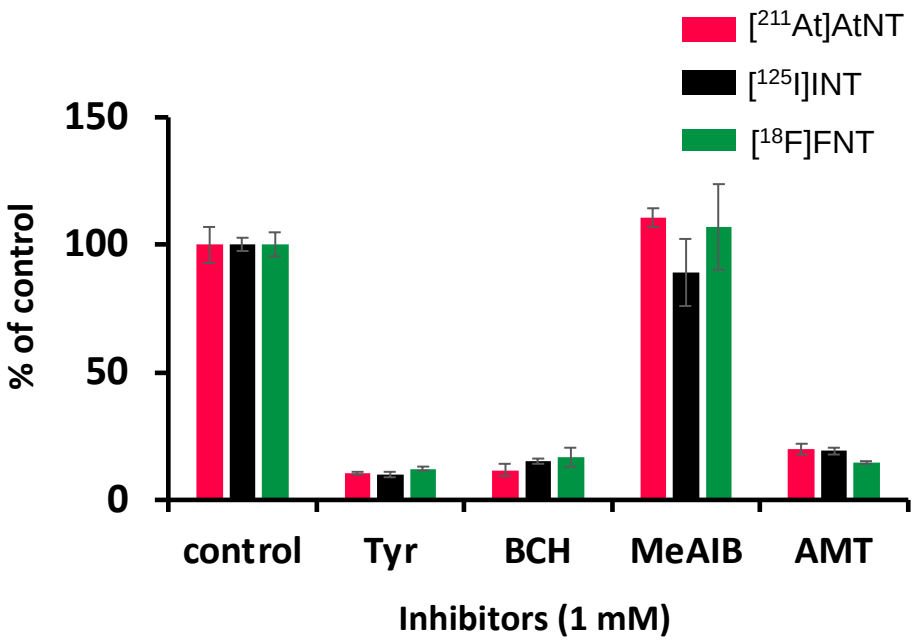

Figure 21. Inhibition of each agent's uptake with amino acids and a LAT1-selective inhibitor (1 mM). The Y-axis shows the percentage of the control. The inhibitors were as follows Tyr = L-tyrosine; BCH = 2-aminobicyclo-(2,2,1)-heptane-2-carboxylic acid; MeAIB = α-methyl-aminoisobutyric acid; AMT = α-methyl-L-tyrosine

In vivo evaluations

Biodistribution in normal mice

I administered [^{211}At]At-NpGT, [^{125}I]I-NpGT, and [^{18}F]F-NpGT to normal ICR mice and compared their biodistribution. All three compounds showed rapid clearance from the bloodstream(Table 13, Figure 22). Both [^{211}At]At-NpGT and [^{125}I]I-NpGT exhibited minimal accumulation in the stomach and thyroid, in which free astatide and iodide accumulate. [^{18}F]F-NpGT showed minimal accumulation in the bones, in which free fluoride accumulates. At both 1 hour and 3 hours post-injection, [^{211}At]At-NpGT, [^{125}I]I-NpGT, and [^{18}F]F-NpGT displayed similar biodistribution across almost all tissues.

Table 13. Biodistribution of NpGT derivatives in normal mice.

	Time after administration							
	[^{211}At]At-NpGT		[^{125}I]I-NpGT				[^{18}F]F-NpGT	
	1 h	3 h	10 min	1 h	3 h	6 h	1 h	3 h
Blood	1.37±0.10	0.33±0.06	3.13±0.13	1.39±0.25	0.30±0.02	0.18±0.03	1.54±0.25	0.19±0.01
Liver	6.60±1.18	1.73±0.44	17.29±1.91	9.89±2.62	1.92±0.22	1.18±0.16	6.59±0.80	0.68±0.04
Spleen	1.53±0.37	0.61±0.07	2.14±0.63	1.28±0.37	0.29±0.04	0.14±0.03	1.34±0.13	0.34±0.06
Kidney	14.95±5.75	3.80±1.51	25.26±3.03	12.82±1.69	4.28±1.18	2.73±0.66	11.35±1.19	1.45±0.20
Pancreas	10.26±2.62	1.94±0.62	17.85±6.68	10.87±2.41	1.73±0.19	0.76±0.24	10.97±1.54	2.30±0.16
Heart	1.30±0.20	0.58±0.17	1.20±0.17	0.94±0.15	0.30±0.04	0.13±0.04	0.86±0.08	0.30±0.03
Lung	1.75±0.19	1.04±0.90	1.92±0.15	1.32±0.22	0.32±0.02	0.14±0.05	1.32±0.16	0.31±0.03
Stomach[b]	0.81±0.20	0.65±0.13	0.76±0.12	0.72±0.17	0.67±0.30	0.40±0.04	0.62±0.03	0.18±0.02
Intestine[b]	4.97±0.54	7.50±1.86	3.90±0.47	5.75±1.27	9.33±1.88	16.88±3.18	3.84±0.39	1.62±0.12
Muscle	0.86±0.19	0.76±0.12	0.73±0.08	0.49±0.08	0.38±0.03	0.27±0.04	0.58±0.05	0.27±0.03
Bone	1.01±0.10	0.65±0.22	1.01±0.10	0.64±0.16	0.22±0.02	0.14±0.02	0.68±0.07	0.30±0.04
Neck[b]	0.06±0.00	0.07±0.03	0.04±0.01	0.09±0.02	0.17±0.04	0.32±0.03	0.03±0.00	0.01±0.00
Brain	0.18±0.03	0.12±0.02	0.22±0.22	0.18±0.18	0.11±0.11	0.09±0.09	0.10±0.01	0.06±0.01

Activity uptake in distinct organs is expressed as percentage of injected dose per organ mass (%ID/g) or as [b]percentage of injected dose (%ID)

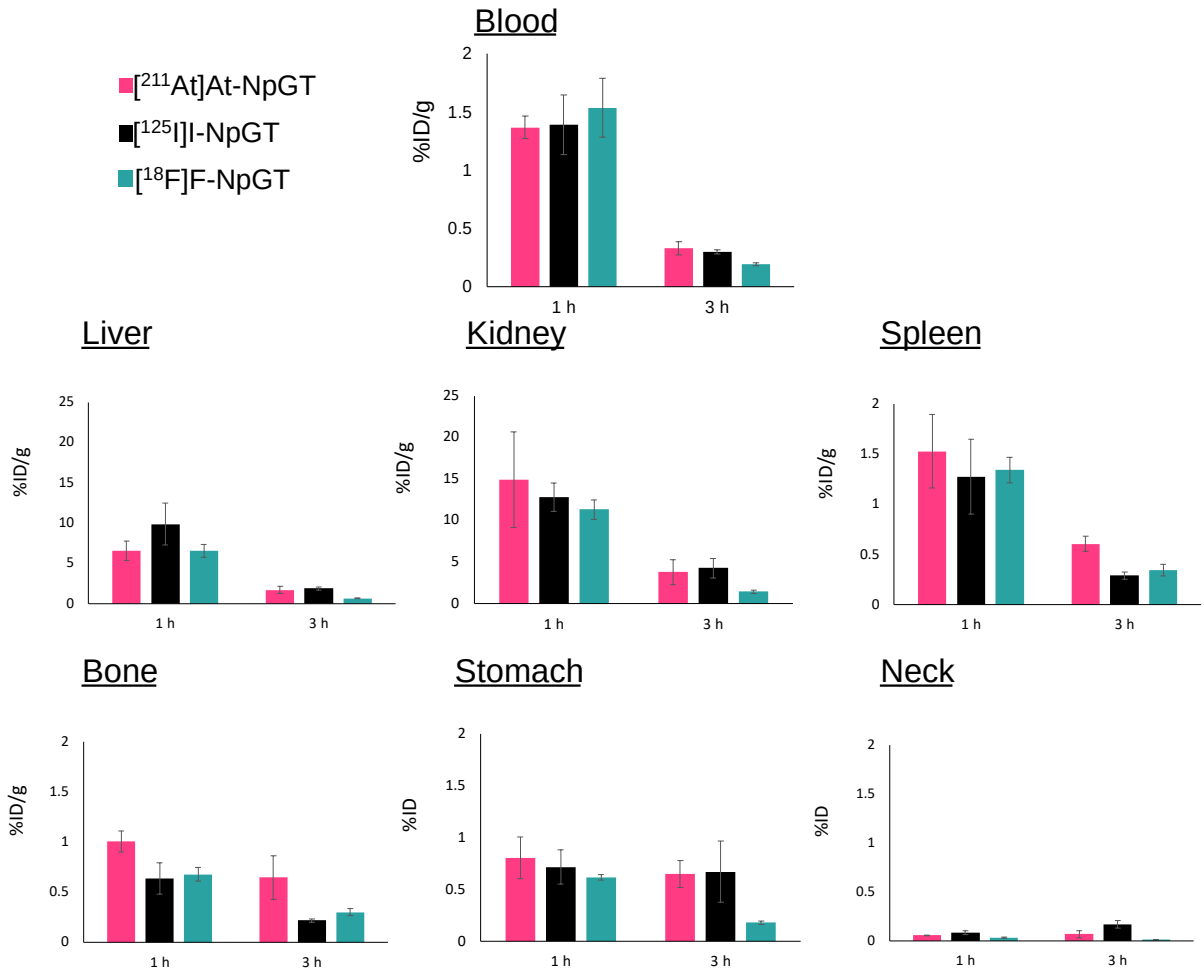

Figure 22. Comparison of radioactivity levels of NpGT derivatives in blood, liver, kidney, spleen, bone, stomach, and neck (including thyroid) at 1 hour or 3 hours post-administration. The pink line represents [^{211}At]At-NpGT, the black line represents [^{125}I]I-NpGT, and the blue-green line represents [^{18}F]F-NpGT.

Tumor uptake

C6 glioma-bearing mice were administered [^{211}At]At-NpGT, [^{125}I]I-NpGT, and [^{18}F]F-NpGT to evaluate their biodistribution and tumor uptake *in vivo*. As a control, [^{125}I]IMT, a conventional cancer diagnostic agent, was used for comparison. [^{211}At]At-NpGT, [^{125}I]I-NpGT, and [^{18}F]F-NpGT exhibited similar biodistribution patterns (Table 14). Furthermore, [^{211}At]At-NpGT, [^{125}I]I-NpGT, and [^{18}F]F-NpGT showed higher tumor uptake than [^{125}I]IMT at 1 and 3 hours post-injection (Figure 23). The tumor-to-blood ratios of these radiolabeled compounds were equal or superior to that of [^{125}I]IMT.

Table 14. Biodistribution at 1 h and 3 h Post-injection in Tumor-Bearing Mice

	[^{211}At]At-NpGT		[^{125}I]I-NpGT		[^{18}F]F-NpGT		[^{125}I]I-IMT	
Time after Injection	1 h	3 h	1 h	3 h	1 h	3 h	1 h	3 h
	%ID/g							
Blood	1.39±0.33 [c]	0.49±0.09	1.86±0.09	0.54±0.27	1.91±0.35	0.37±0.10	1.22±0.24 [f,g]	0.22±004 [e,f]
Liver	8.09±1.34	2.25±0.55	8.09±1.22	2.94±1.63	7.28±1.30	1.40±0.53	0.80±0.20 [f,g]	0.14±0.04 [e,f]
Spleen	2.22±0.58	0.94±0.17 [b]	2.30±0.58	0.56±0.24	2.36±0.68	0.63±0.20	1.01±0.22 [f,e,g]	0.16±0.05 [e,f,g]
Kidney	32.8±5.23 [c]	14.8±3.41 [c]	25.0±4.25 [d]	10.4±4.42 [d]	13.5±3.58	4.06±1.53	19.6±3.37	2.34±0.31 [e,f]
Pancreas	16.6±1.03 [b]	3.33±1.17	30.1±3.05	7.36±4.07	20.3±4.20	8.54±2.55	11.9±4.48 [f]	0.56±0.21 [f,g]
Heart	1.09±0.20	0.74±0.73	1.36±0.20	0.43±0.18	1.16±0.30	0.56±0.11	1.12±0.29	0.11±0.03
Lung	2.46±0.41 [c]	1.59±1.10	2.14±0.37 [d]	0.58±0.22	1.89±0.35	0.65±0.17	1.00±0.39 [e,f]	0.17±0.03 [e]
Muscle	0.95±0.53	0.42±0.07	0.96±0.14	0.59±0.27	0.48±0.08	0.62±0.48	1.10±0.28	0.27±0.09
Bone	0.81±0.23	0.44±0.12	1.14±0.01	0.42±0.16	0.83±0.22	0.58±0.42	0.87±0.06	0.14±0.02
Tumor	2.72±0.63	0.86±0.23 [c]	2.97±0.58	0.99±0.37	2.95±0.40	1.46±0.33	2.07±0.23 [g]	0.25±0.03 [e,f,g]
	%ID							
Intestine*	5.56±0.77 [c]	5.88±0.98 [c]	5.12±1.23	7.89±3.22 [d]	4.07±0.25	2.60±0.21	1.67±0.49 [e,f,g]	0.85±0.21 [f]
Stomach*	1.03±0.20	0.88±0.28 [c]	1.22 0.62	0.65±0.43	1.03±0.52	0.19±0.07	0.94±0.36	0.61±0.38
Neck*	0.09±0.02	0.11±0.03	0.03±0.01	0.09±0.03	0.02±0.01	0.01±0.00	0.35±0.06 [e,f,g]	0.54±0.11 [e,f,g]
	Ratio							
Tumor/Blood	2.02±0.51	1.73±0.26 [c]	1.59±0.28	1.98±0.39 [d]	1.56±0.15	3.96±0.26	1.74±0.35	1.17±0.31 [e,f,g]

aTissue radioactivity was expressed as %ID/g ± SD for each group (n = 5)

*Tissue radioactivity was expressed as %ID. Statistical analysis was performed using on-way ANOVA followed by Tukey's test between [^{211}At]At-NpGT and [^{125}I]I-NpGT (b), [^{211}At]At-NpGT and [^{18}F]F-NpGT (c), [^{125}I]I-NpGT and [^{18}F]F-NpGT (d), [^{211}At]At-NpGT and [^{125}I]I-IMT (e), [^{125}I]I-NpGT and [^{125}I]-IMT (f), and [^{18}F]F-NpGT and [^{125}I]I-IMT (g)

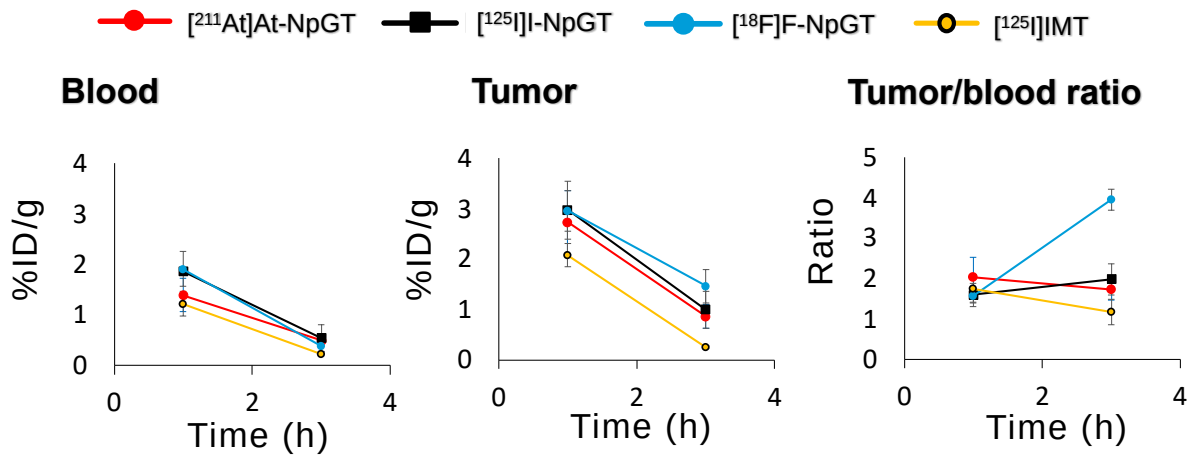

Figure 23. Comparisons of blood clearance, tumor uptake, and tumor/blood ratio of [^{211}At]At-NpGT (red), [^{125}I]I-NpGT (black), [^{18}F]F-NpGT (blue), and [^{125}I]IMT (yellow) at 1 hour or 3 hours post-administration.

Analysis of Urinary Metabolites

A urine sample (100 μL) was filtered using a 10 kDa cutoff ultrafiltration membrane, achieving a recovery rate of 73%. RP-HPLC analysis revealed the presence of intact [^{125}I]I-NpGT and unidentified metabolites in the urine (Figure 24). Minimal radioactivity was observed in the void volume fraction where free I^- elutes.

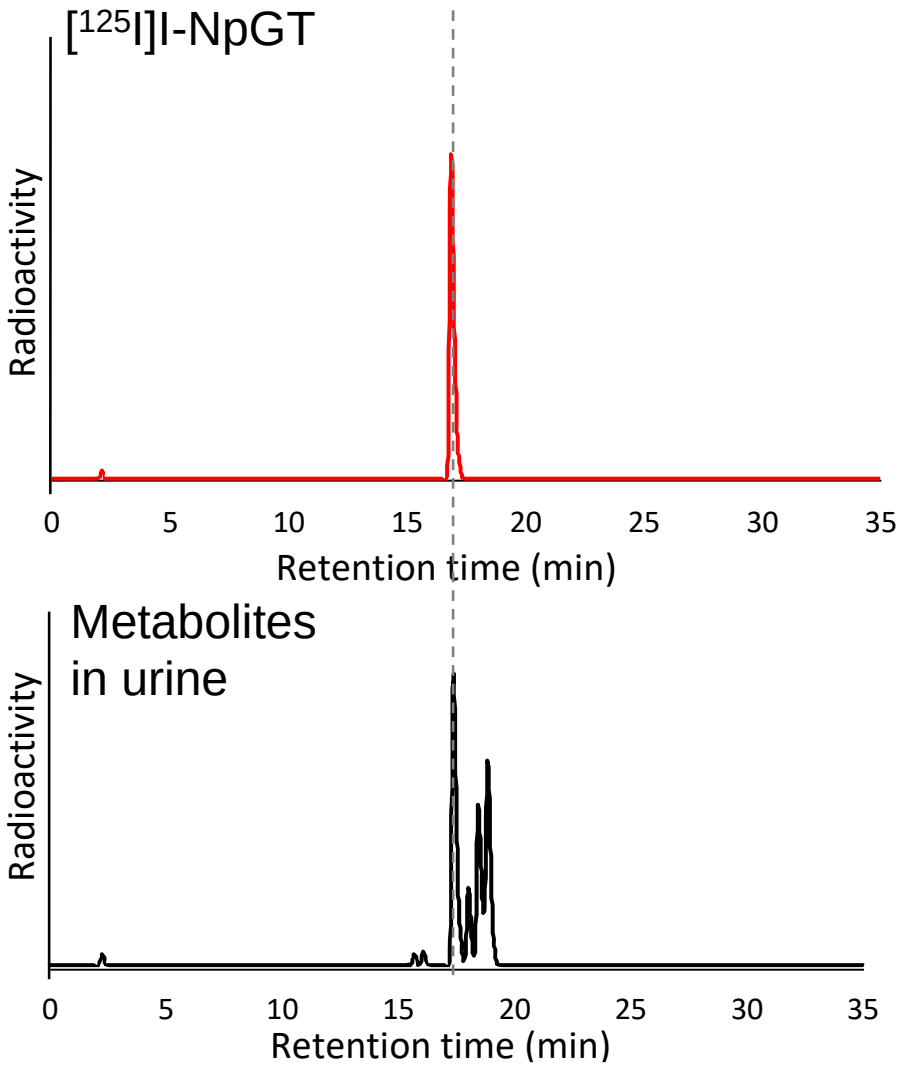

Figure 24. RP-HPLC radiochromatograms of [^{125}I]I-NpGT standard and radiometabolites of [^{125}I]I-NpGT in the urine.

Treatment study

C6 glioma-bearing mice were administered [^{211}At]At-NpGT (0.1 MBq/mouse or 0.3 MBq/mouse) or PBS (control). Compared to the control mice, [^{211}At]At-NpGT significantly inhibited the growth of C6 glioma tumors in a dose-dependent manner (Figure 25). Even in the group that received 0.3 MBq/mouse of [^{211}At]At-NpGT, there was no significant difference in body weight compared to the control mice.

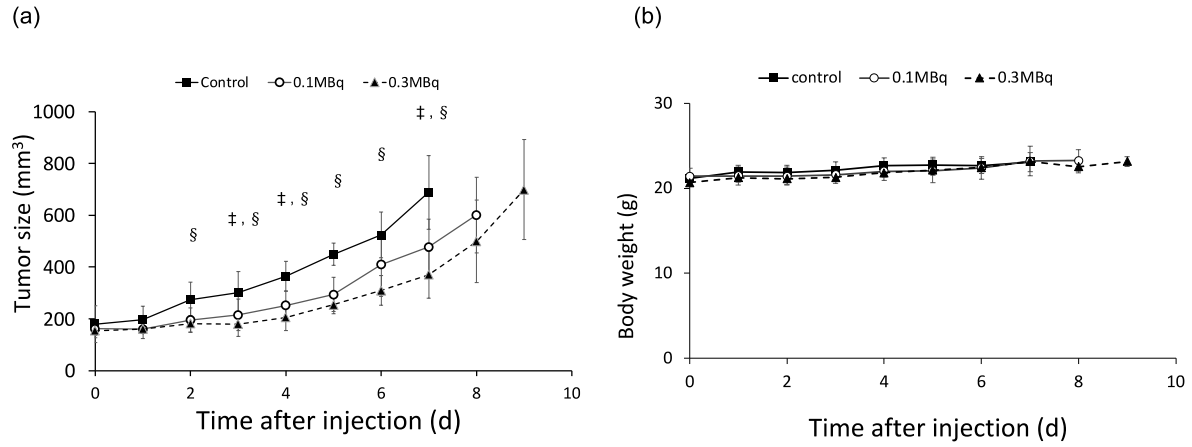

Figure 25. Tumor growth inhibition (a) and body weight change (b) by [^{211}At]At-NpGT. Statistical significances were determined by Tukey's test; $p < 0.05$ compared with 0.1 MBq (‡), 0.3 MBq(§)

Discussion

The relatively short half-life of ^{211}At (7.2 hours) necessitates rapid labeling reactions. Since the labeling of benzoate derivatives with ^{211}At typically takes about 10 minutes, it is desirable for the labeling of NpG-type scaffolds with ^{211}At to be completed within a comparable reaction time.[77] The ^{211}At labeling of NpG structures is a nucleophilic substitution reaction, which exclusively involves At^-. However, the manufactured ^{211}At exists in multiple oxidation states.[27] Therefore, I hypothesized that increasing the proportion of At^- in the ^{211}At solution would enable rapid ^{211}At labeling of NpG structures. Several reducing agents are reported to prepare At^- from solutions containing different chemical forms of astatine.[65] Therefore, I evaluated the labeling reactivity of ^{211}At in the presence of reducing agents. As a result, I observed the acceleration of the ^{211}At-labeling reaction in the presence of reducing agents. This allowed us to achieve satisfactory ^{211}At labeling in a comparable time with preparing astatobenzoate derivatives. Because of the resistance to radiolysis and tolerance to the human body, sodium ascorbate is considered the most suitable reductant for ^{211}At labeling among evaluated reductants.

As expected, the ^{18}F labeling conditions were more severe than those for radioiodine or ^{211}At labeling. The reason is that ^{18}F is recovered as an aqueous solution, and nucleophilic reactivity of ^{18}F is highly reduced by the presence of small amounts of water, more so than for radioiodine and ^{211}At. To facilitate the ^{18}F-labeling reaction, multiple azeotropic distillation steps using anhydrous acetonitrile were necessary. This process ensured the removal of residual water, which is critical for the ^{18}F-labeling reaction. Although the reaction time was not optimized, this study's reaction temperature for ^{18}F labeling was similar to that of other ^{18}F-labeled agents.[78-80] Since no precursor 20 was present after the 100 ° C labeling reaction, the extended reaction time is unlikely to improve the labeling yield.

Excellent radiochemical conversion rates >80% were achieved for all reaction steps of [^{211}At]At-NpGT, [^{125}I]I-NpGT, and [^{18}F]F-NpGT, but overall yields ranged from 30-40%. The loss of radioactivity due to purification by Sep-Pak and HPLC resulted in these lower radiochemical yields. The labeling and deprotection reactions were conducted consecutively in a single pot to eliminate the need for purification steps. However, only for [^{211}At]At-NpGT did this approach result in the unintended dissociation of ^{211}At during the deprotection process (data not shown). It is worth noting that the decomposition of ^{211}At-labeled compounds during deprotection has also been reported in other studies.[81] The Resin-Assisted Purification and Deprotection (RAPD) system, which performs purification and deprotection reactions consecutively on a solid phase, may offer a solution to reduce radioactivity loss while preventing the degradation of labeled compounds.[82]

Results of the *in vitro* studies demonstrate that these radiohalogen-labeled NpGT derivatives would be transported bidirectionally in cancer cells, which was consistent with the properties of the LAT1 transport system. In addition, the intracellular uptake of [^{211}At]At-NpGT, [^{125}I]I-NpGT, and [^{18}F]F-NpGT were all inhibited by BCH, AMT, or L-Tyr, respectively. Interestingly, the degree of inhibition rates was similar for each amino acid derivative. These results indicated that LAT1 recognized these amino acid derivatives as similar substrates. Taking account of these differences in molecular weight ([^{211}At]At-NpGT: 493, [^{125}I]I-NpGT: 407, [^{18}F]F-NpGT: 300), the present result is intriguing. This similarity supports my expectation that modifying the tyrosine's phenolic hydroxyl group has a limited impact on LAT1 recognition.

Matching the pharmacokinetics of diagnostic and therapeutic agents is a prerequisite for their use in radiotheranostics. Especially the instability of most ^{211}At-labeled agents has caused discrepancies in the pharmacokinetic properties when comparing ^{211}At-labeled agents with radioiodine-labeled counterparts[39,83]. Notably, low molecular weight ^{211}At-labeled compounds undergo significant deastatination even at 1 hour post-administration.[84,85] Therefore, it is essential

to verify the stability against dehalogenation and the biodistribution match of radiohalogen-labeled amino acid derivatives at early time points. Considering that PET imaging with ^{18}F-labeled agents is typically performed between 1 and 2 hours post-administration, the biodistribution studies of [^{18}F]F-NpGT and [^{211}At]At-NpGT were evaluated at 1 hour and 3 hours post-injection. In biodistribution studies, [^{211}At]At-NpGT exhibited very low uptake in the spleen, lungs, stomach, and neck (including thyroid), which is consistent with the findings observed in Chapter 1 and suggests it to be stable against *in vivo* deastatination. Furthermore, low radioactivity levels in the stomach and neck of [^{125}I]I-NpGT and the bone of [^{18}F]F-NpGT indicated stability against general dehalogenation mechanisms. The biodistribution beyond 3 hours post-administration was evaluated using [^{125}I]I-NpGT, which has a longer half-life. There was minimal radioactivity accumulation in tissues other than the excretory organs, namely the liver, kidneys, and intestines. Analysis of the urinary samples after [^{125}I]I-NpGT administration showed almost no radioactivity in the free iodine fraction (void volume), supporting high resistance to *in vivo* dehalogenation. [^{211}At]At-NpGT, [^{125}I]I-NpGT, and [^{18}F]F-NpGT had rapid blood clearance, and all displayed similar kinetics in almost every tissue. Moreover, these agents showed comparable tumor uptake. Given these similarities, these amino acid derivatives are promising for radiotheranostics. **In particular, this is the first time in the world that the possibility of combining ^{18}F- and ^{211}At-labeled compounds in radiotheraostics has been demonstrated.**

After intravenous injection, [^{211}At]At-NpGT, [^{125}I]I-NpGT, and [^{18}F]F-NpGT showed rapid uptake in the kidneys and pancreas followed by very rapid excretion from these organs. These biodistribution patterns appear to be analogous to other radiolabeled amino acid derivatives.[86,87] Radiohalogen-labeled amino acid derivatives (e.g., [^{18}F]FET and [^{123}I]IMT) accumulate in the pancreas in mouse studies but not in humans. [88,89] The differences in LAT1 expression distribution in the pancreas of mice and humans could contribute to this discrepancy, but the causes remain unknown. [90,91]

[^{211}At]At-NpGT, [^{125}I]I-NpGT, and [^{18}F]F-NpGT showed moderate washout from the tumor. This is in accordance with what is observed for other radiolabeled amino acid derivatives that have been reported to be radiotracers targeting LAT1.[86] LAT1 is a bidirectional amino acid transporter, and radiolabeled amino acid tracers such as [^{18}F]FET and [^{123}I]IMT are not included in protein synthesis[92,93]. Therefore, the uptake of these radiolabeled compounds in tumors gradually decreases along with blood clearance. Although the radioactive metabolites within tumor cells were not evaluated in this study, considering that most of the radioactivity excreted from cancer cells was intact [^{125}I]I-NpGT, it is likely that [^{211}At]At-NpGT, [^{125}I]I-NpGT, and [^{18}F]F-NpGT were not used for protein synthesis. However, the rapid clearance of each radiohalogen-labeled derivative resulted in a high tumor-to-blood ratio at 3 hours postinjection.

Due to the unavailability of small animal PET equipment, this study did not provide PET images of [^{18}F]F-NpGT. However, the tumor-to-blood ratio of [^{18}F]F-NpGT was equal to or greater than that of [^{125}I]IMT at the evaluated time points. Furthermore, considering that the reported tumor-to-blood ratio of [^{18}F]FET is comparable,[86] it can be inferred that the diagnostic performance of [^{18}F]F-NpGT is equivalent to conventional amino acid tracers.

The radioactivity in the liver and intestines of [^{211}At]At-NpGT, [^{125}I]I-NpGT, and [^{18}F]F-NpGT were similarly higher than that of [^{125}I]IMT. This undesirable accumulation is hypothesized to be associated with the increased lipophilicity of the NpGT derivatives. Although liver uptake of [^{18}F]FMT has been demonstrated in murine models, nonspecific abdominal uptake has not been seen in clinical trials.[94] Accordingly, radiohalogen-labeled NpGT derivatives might not be subject to accumulation in the liver and intestine in clinical.

For the evaluation of therapeutic efficacy, the tumor size change in the mouse model was observed. Without any treatment, the tumor grew to more than 800 mm^3 by day 8. In contrast, treatment of mice with 0.1 MBq/mouse of [^{211}At]At-NpGT significantly slowed the expansion of the tumors. Moreover, the 0.3 MBq/mouse group showed more suppressed tumor growth with no significant weight reduction. These results indicate the usefulness of [^{211}At]At-NpGT as a therapeutic agent.

Summary

Radiohalogen-labeled amino acid derivatives with the NpG structure ([^{211}At]At-NpGT, [^{125}I]I-NpGT, [^{18}F]F-NpGT) exhibited similar characteristics, including LAT1 recognition, pharmacokinetics, and tumor uptake. Furthermore, [^{211}At]At-NpGT demonstrated a dose-dependent therapeutic effect. These findings suggested that radiohalogen-labeled NpG derivatives, particularly the pair of [^{18}F]F-NpGT (PET) and [^{211}At]At-NpGT (α-particle therapy), would have potential applications in cancer radiotheranostics.

Conclusions

The present study showed that the NpG structure as a labeling scaffold for radiohalogens allows for the labeling of all radiohalogens under acceptable reaction conditions and can stably retain all

radiohalogens, including ^{211}At *in vivo*. ^{18}F, ^{125}I, and ^{211}At –labeled amino acid derivatives with NpG structure showed similar pharmacological properties, including LAT1 recognition, pharmacokinetics, and tumor uptake, suggesting that they were promising as radiotheranostic agents. This is the first time in the world that the possibility of the combination of ^{18}F– and ^{211}At–labeled compounds in radiotheranostics has been demonstrated. Since ^{18}F, ^{123}I, and ^{211}At are domestically produced radionuclides, the NpG scaffold would be useful for these radiohalogens and accelerate the development of radiotheranostic agents in Japan.

Methods

Chapter 1.

General

[^{125}I]NaI (≃3.7 MBq/ μ L) was purchased from Perkin Elmer (Waltham, MA, USA). CD1 mouse liver microsomes (CYP content: 1.166 nmol/mg protein) and human liver microsomes (CYP content: 0.428 nmol/mg protein) were purchased from Sekisui Xenotech (Kansas, KS, USA). Alamethicin and UDPGA trisodium salt were purchased from Sigma-Aldrich Japan (Tokyo, Japan). Glucose 6-phosphate (G6P) and β-nicotinamide-adenine dinucleotide phosphate oxidized form (β-NADP$^+$) were purchased from Oriental Yeast (Tokyo, Japan). Glucose 6-phosphate dehydrogenase (G6PDH) was purchased from FUJIFILM Wako Pure Chemical Industries (Osaka, Japan). *N*-[5-(Hydroxymethyl)-2,2-dimethyl-1,3-dioxan-5-yl]methyl-2-nitroimidazole (**1**), *meta*-tributylstannylbenzoic acid (**13**), and *N*-(2-aminoethyl)-2-nitroimidazole HCl salt (**14**) were prepared by the same procedure described previously.[95-97] The other chemicals purchased from commercial sources were of reagent grade or higher and used without further purification. ^{1}H-NMR/^{13}C-NMR spectra were obtained by a JEOL ECS-400 spectrometer (JEOL, Tokyo, Japan). Mass spectrometry was obtained on an AccuTOF LC-plus (JMS-T100LP, JEOL). The melting points were measured using an MP-500D (Yanako, Kyoto, Japan) and were reported uncorrected. The chemical purity of non-radioactive compounds was found to be >95%, as determined by RP-HPLC analyses. Radiochemical purities were determined by TLC and RP-HPLC and were >98% for both analyses.

Analytical Methods

Analytical RP-HPLC was performed with a Unison US-C18 column (4.6 × 150 mm, Imtakt, Kyoto, Japan) at a flow rate of 1 mL/min with a linear gradient starting from 95% A (0.01 M acetate buffer, pH 6.0) and 5% B (acetonitrile) for 5 min, to 30% B at 20 min, to 100% B at 30 min, and then 100 %B for 5 min (system A for the analyses of [^{125}I]BHIN and [^{211}At]BHAN), or from 95% A (0.01 M acetate buffer, pH 6.0) and 5% B (acetonitrile) for 5 min, to 40% B at 20 min, to 100% B at 30 min, and then 100 %B for 5 min (system B for the analyses of [^{125}I]EHIN, [^{125}I]DEIN, [^{125}I]MIBAN, [^{211}At]MABAN, and [^{211}At]At$^-$), or from 60% A (water) and 40% B (acetonitrile) to 100% B at 30 min, (system C for the purification of [^{125}I]DEIN and [^{125}I]3), or from 90% A (water) and 10% B (acetonitrile) to 40% B at 30 min, to 100%B at 35 min (system D for the purification of [^{211}At]BHAN) or from 60% A (water) and 40% B (acetonitrile) to 50% B at 30 min, to 100%B at 40 min, and then 100 %B for 5 min (system E for the purification of [^{125}I]8) or from 80% A (water) and 20% B

(acetonitrile) to 100% B at 20 min and then 100 %B for 5 min (system F for the purification of [^{125}I]EHIN) or from 80% A (water) and 20% B (acetonitrile) to 60% B at 20 min, to 100%B at 30 min, and then 100 %B for 5 min (system G for the purification of [^{125}I]MIBAN and [^{211}At]MABAN), and from 40% A (water) and 60% B (acetonitrile) to 100% B at 20 min, and then 100 %B for 5 min (system H for the purity check of 15). HILIC-HPLC was performed with a cosmosil HILIC packed column (4.6 × 250 mm, Nacalai tesque, Kyoto, Japan) at a flow rate of 1.0 mL/min with an isocratic solvent mixture of 5% A (0.05 M aqueous solution of $HCOONH_4$) and 95% B (acetonitrile). The effluent was monitored by detection at 254 nm with a UV detector (L-7405, Hitachi, Tokyo, Japan) coupled to a NaI(Tl) radioactivity detector (Gabi star, Raytest, Strubenhardt, Germany), or collected with a fraction collector (Frac-920, GE Healthcare Japan, Tokyo) at 1.0 min intervals, and the radioactivity counts in each fraction were determined with an automated gamma well counter (Wizard 3, PerkinElmer Japan, Yokohama, Japan). TLC (Silica gel 60 F_{254}, Merck, Tokyo, Japan) was developed with a mixture of hexane and ethyl acetate (1:10 for [^{125}I]BHIN, 1:5 for [^{211}At]BHAN, [^{125}I]MIBAN and [^{211}At]MABAN, 2:3 for [^{125}I]EHIN and 1:1 for [^{125}I]DEIN [^{125}I]3 and [^{125}I]8, v/v). RP-TLC (Silica gel 60 RP-18 F_{254S}, Merck) was developed with a mixture of 0.1% aqueous solution of TFA and acetonitrile containing 0.1%TFA (1:1, v/v). The TLC developed for radioiodinated compounds was cut into 5 mm fractions, and the radioactivity of each fraction was measured with an automated gamma well counter. The TLC developed for astatinated compounds was visualized and quantified using an imaging scanner (Typhoon FLA7000, GE Healthcare Japan, Tokyo).

Syntheses

N-[5-(Trifluoromethanesulfonyloxymethyl)-2,2-dimethyl-1,3-dioxan-5-yl]methyl-2-nitroimidazole (2)

Trifluoromethanesulfonic anhydride (139 μL, 0.848 mmol) was added to a mixture of compound **1** (153 mg, 0.565 mmol) and 2,6-lutidine (330 μL, 2.83 mmol) in dichloromethane (7.0 mL) at −78 °C under an Ar atmosphere. After the addition, the temperature of the reaction mixture was gradually raised to room temperature and then stirred for 1 h at the same temperature. To the reaction mixture was added water (20 mL), and it was extracted with ethyl acetate (15 mL × 3). The combined organic phase was dried over $MgSO_4$, and the solvent was removed *in vacuo*. The residue was subjected to flash column chromatography using hexane/ethyl acetate (100/0 to 40/60) as an eluent to provide **2** as a brown solid (122 mg, 0.303 mmol, 53.6%). Mp: 88-90 °C. ^{1}H NMR (400 MHz, $CDCl_3$): δ 1.42 [6H, s, C*H*$_3$], 3.70 [2H, d, *J* = 12.4 Hz, C*H*$_2$], 3.80 [2H, d, *J* = 12.4 Hz, C*H*$_2$], 4.50 [2H, s, C*H*$_2$], 4.75 [2H, s, C*H*$_2$], 7.20 [1H, s, C*H*],

7.21 [1H, s, C*H*]. ^{13}C NMR (100 MHz, $CDCl_3$): δ 22.63, 24.20, 29.65, 39.23, 48.74, 61.76, 75.27, 99.34, 113.65, 116.84, 120.02, 123.21, 127.15, 128.93, 145.28. HRMS(ESI) calcd for $C_{12}H_{16}F_3N_3NaO_7S$ [M + Na]$^+$: *m/z* 426.0559, found 426.0577. HPLC purity >99%, retention time 9.8 min (system C).

N-[5-(Iodomethyl)-2,2-dimethyl-1,3-dioxan-5-yl]methyl-2-nitroimidazole (3)

NaI (77 mg, 0.513 mmol) was added to a solution of compound **2** (104 mg, 0.257 mmol) in acetonitrile (2.0 mL) at room temperature and stirred for 0.5 h. To the reaction mixture was added water (10 mL), and it was extracted with ethyl acetate (5 mL × 3). The combined organic phase was dried over $MgSO_4$, and the solvent was removed *in vacuo* to provide **3** as a pale yellow oil (85 mg, 0.224 mmol, 87.1%). ^{1}H NMR (400 MHz, $CDCl_3$): δ 1.40 [3H, s, C*H*$_3$], 1.42 [3H, s, C*H*$_3$], 3.07 [2H, s, C*H*$_2$], 3.55 [2H, d, *J* = 12.4 Hz, C*H*$_2$], 3.80 [2H, d, *J* = 12.4 Hz, C*H*$_2$], 4.82 [2H, s, C*H*$_2$], 7.17 [1H, s, C*H*], 7.68 [1H, s, C*H*]. ^{13}C NMR (100 MHz, $CDCl_3$): δ 8.10, 20.57, 26.35, 36.85, 50.40, 65.53, 99.07, 126.65, 128.43, 145.84. HRMS(ESI) calcd for $C_{11}H_{17}IN_3O_4$ [M + H]$^+$: *m/z* 382.0264, found 382.0268. HPLC purity 98.0%, retention time 7.8 min (system C).

N-[2,2-Bis(hydroxymethyl)-2-(iodomethyl)ethyl]-2-nitroimidazole ([^{127}I]BHIN)

p-Toluenesulfonic acid (3.5 mg, 0.184 mmol) was added to a solution of compound **3** (43 mg, 0.112 mmol) in methanol (1.0 mL) and stirred for 2 days at room temperature. After the solvent was removed *in vacuo*, a 5% aqueous $NaHCO_3$ solution (1.0 mL) was added to the residue, and the mixture was extracted with ethyl acetate (3.0 mL × 3). After the combined organic phase was washed with a saturated aqueous NaCl solution (1.0 mL × 1) and dried over Na_2SO_4, the solvent was removed *in vacuo*. The residue was purified by preparative TLC (PLC silica gel 60 F_{254}, 1 mm, Merck) using a mixture of hexane/ethyl acetate (1:2) as a developing solvent to provide **1a** as a white solid (32 mg, 0.0923 mmol, 82.5%). Mp: 127-128 °C. ^{1}H NMR (400 MHz, CD_3Cl): δ 3.23 [2H, s, C*H*$_2$], 3.64 [4H, dd, *J* = 16.4 and 10.8 Hz, C*H*$_2$], 4.77 [2H, s, C*H*$_2$], 7.17 [1H, s, C*H*], 7.39 [1H, s, C*H*]. ^{13}C NMR (100 MHz, CD_3OD): δ 10.17, 45.13, 51.10, 64.51, 127.93, 128.87, 147.38. HRMS(ESI) calcd for $C_8H_{12}IN_3NaO_4$ [M + Na]$^+$: *m/z* 363.9770, found 363.9788. HPLC purity 96.7%, retention time 19.8 min (system A).

2-Ethyl-2-[(methoxymethoxy)methyl]propane-1,3-diol (5)

A solution of chloromethyl methyl ether (0.423 mL, 5.61 mmol) in THF (5 mL) was added to a mixture of trimethylolpropane (1.50 g, 11.2 mmol), *N,N*-diisopropylethylamine (DIEA, 7.68 mL, 44.8 mmol), and 4-dimethylaminopyridine (0.140 g, 1.14 mmol) in THF (10 mL) at 0 °C. After the addition, the temperature of the reaction mixture was gradually raised to room temperature, and the mixture was stirred overnight at the same temperature. After removing the solvent *in*

vacuo, the residue was dissolved in ethyl acetate (10 mL). The solution was washed with a saturated aqueous NH_4Cl solution (10 mL × 1), water (10 mL × 1), and a saturated aqueous NaCl solution (10 mL × 1). The combined organic phase was dried over $MgSO_4$, and the solvent was removed *in vacuo*. The residue was subjected to flash column chromatography using hexane/ethyl acetate (50/50 to 0/100) as an eluent to provide **5** as a colorless oil (402 mg, 2.25 mmol, 40.2%). ^{1}H NMR (400 MHz, $CDCl_3$): δ 0.68 [3H, t, *J* = 7.6 Hz, C*H*$_3$], 1.16 [2H, q, *J* = 7.6 Hz, C*H*$_2$], 3.21 [2H, s, C*H*$_2$], 3.30 [2H, s, C*H*$_2$], 3.33 [4H, s, C*H*$_2$], 4.49 [2H, s, C*H*$_2$]. ^{13}C NMR (100 MHz, CD_3OD): δ 7.72, 22.94, 44.31, 55.45, 63.82, 69.12, 97.86.

O,O′ -Bis(trifluoromethanesulfonyl)-2-ethyl-2-((methoxymethoxy)methyl)propane-1,3-diol (6)

Trifluoromethanesulfonic anhydride (0.846 mL, 5.15 mmol) was added dropwise to a mixture of **5** (400 mg, 2.24 mmol) and DIEA (1.04 mL, 8.96 mmol) in dichloromethane (4 mL) at −78 °C under an Ar atmosphere. After the addition, the temperature of the reaction mixture was gradually raised to −20 °C, and the mixture was stirred for an additional 18 h at the same temperature. The temperature of the reaction mixture was then gradually raised to room temperature. The reaction mixture was washed with a saturated aqueous $NaHCO_3$ solution (10 mL × 1), a saturated aqueous NH_4Cl solution (10 mL × 2), and a saturated aqueous NaCl solution (10 mL × 1). The organic phase was dried over $MgSO_4$, and the solvent was removed *in vacuo*. The residue was used for the following reaction without further purification. ^{1}H NMR (400 MHz, $CDCl_3$): δ 0.96 [3H, t, *J* = 7.6 Hz, C*H*$_3$], 1.57 [2H, q, *J* = 7.6 Hz, C*H*$_2$], 3.35 [3H, s, C*H*$_3$], 3.46 [2H, s, C*H*$_2$], 4.46 [4H, s, C*H*$_2$], 4.60 [2H, s, C*H*$_2$]. ^{13}C NMR (100 MHz, $CDCl_3$): δ 6.77, 21.78, 42.83, 55.65, 60.16, 65.25, 75.86, 96.78, 113.78, 116.96, 120.14, 123.32.

N-[2-Ethyl-2-(methoxymethoxy)methyl-2-(trifluoromethanesulfonyloxymethyl)ethyl]-2-nitroimidazole (7)

A mixture of **6** and DIEA (821 μL, 7.05 mmol) in dichloromethane (5 mL) was added to a solution of 2-nitroimidazole (213 mg, 1.88 mmol) in dichloromethane (5 mL) at −78 °C. After the addition, the temperature of the reaction mixture was gradually raised to room temperature, and the mixture was stirred overnight at the same temperature. The reaction mixture was washed with a saturated aqueous $NaHCO_3$ solution (20 mL × 1), a saturated aqueous NH_4Cl solution (20 mL × 2), and a saturated aqueous NaCl solution (20 mL × 1). The organic phase was dried over $MgSO_4$, and the solvent was removed *in vacuo*. The residue was subjected to flash column chromatography using hexane/ethyl acetate (96/4 to 47/53) as an eluent to provide **7** as a yellow oil (276 mg, 0.680 mmol, 30.4% in 2 steps). ^{1}H NMR (400 MHz, $CDCl_3$): δ 0.94 [3H, t, *J* = 7.6 Hz, C*H*$_3$], 1.42-1.59 [2H, m, C*H*$_2$], 3.31 [3H, s, C*H*$_3$], 3.45 [2H, dd, *J* = 10.4 and 29.6 Hz, C*H*$_2$], 4.45 [2H, d, *J* = 2.8 Hz, C*H*$_2$], 4.51 [2H, s, C*H*$_2$], 4.68 [2H, dd, *J* = 14.0 and 130.0 Hz, C*H*$_2$], 7.11

[1H, s, C*H*], 7.16 [1H, s, C*H*]. ^{13}C NMR (100 MHz, $CDCl_3$): δ 7.01, 23.80, 43.43, 50.46, 55.91, 67.63, 76.41, 96.78, 113.65, 116.84, 120.02, 123.20, 126.56, 128.18, 145.52. HRMS(ESI) calcd for $C_{12}H_{19}F_3N_3O_7S$ $[M + H]^+$: *m/z* 406.0896, found 406.0880. HPLC purity >99%, retention time 13.4 min (system E).

N-[2-Ethyl-2-(methoxymethoxy)methyl-2-(iodomethyl)ethyl]-2-nitroimidazole (8)

NaI (144 mg, 0.961 mmol) was added to a solution of compound **7** (130 mg, 0.321 mmol) in acetonitrile (1.0 mL) at room temperature and stirred for 3 h. After the solvent was removed *in vacuo*, the residue was dissolved in chloroform (5 mL). The solution was washed with a saturated aqueous $NaHCO_3$ solution (5 mL × 1), water (5 mL × 1), and a saturated aqueous NaCl solution (5 mL × 1). The organic phase was dried over $MgSO_4$ before removing the solvent *in vacuo*. The residue was subjected to flash column chromatography using chloroform as an eluent to provide **8** as a yellow oil (108 mg, 0.282 mmol, 87.8%). ^{1}H NMR (400 MHz, $CDCl_3$): δ 0.86 [3H, t, *J* = 7.6 Hz, C*H*$_3$], 1.42 [2H, q, *J* = 7.6 Hz, C*H*$_2$], 3.17 [2H, dd, *J* = 8.0 and 17.6 Hz, C*H*$_2$], 3.30 [3H, s, C*H*$_3$], 3.39 [2H, s, C*H*$_2$], 4.47 [3H, t, *J* = 7.0 Hz, C*H*$_3$], 4.81 [2H, d, *J* = 14.8 Hz, C*H*$_2$],7.11 [1H, s, C*H*], 7.24 [1H, s, C*H*]. ^{13}C NMR (100 MHz, $CDCl_3$): δ 7.00, 11.85, 26.63, 41.78, 51.77, 55.86, 69.53, 96.64, 126.21, 127.82, 145.95. HRMS(ESI) calcd for $C_{11}H_{19}IN_3O_4$ $[M + H]^+$: *m/z* 384.0420, found 384.0423. HPLC purity >99%, retention time 17.3 min (system E).

N-[2-Ethyl-2-hydroxymethyl-2-(iodomethyl)ethyl]-2-nitroimidazole ([^{127}I]BHIN)

A 1 *N* aqueous HCl solution (2 mL) was added to a solution of compound **8** (98 mg, 0.256 mmol) in methanol (2.4 mL), and the mixture was stirred for 2 days at 60 °C. After neutralizing the mixture with a saturated $NaHCO_3$ solution, methanol was removed *in vacuo*. The reaction mixture was then extracted with chloroform (5 mL × 3). After washing with a saturated aqueous NaCl solution (10 mL × 1), the organic phase was dried over $MgSO_4$, and the solvent was removed *in vacuo*. The residue was subjected to flash column chromatography using hexane/ethyl acetate (58/42 to 20/80) as an eluent to provide **[^{127}I]BHIN** as a yellow oil (50 mg, 0.146 mmol, 57.0%). Mp: 108-109 °C. ^{1}H NMR (400 MHz, $CDCl_3$): δ 0.87 [3H, t, *J* = 7.4 Hz, C*H*$_3$], 1.33-1.46 [2H, m, C*H*$_2$], 3.16 [2H, dd, *J* = 8.0 and 18.8 Hz, C*H*$_2$], 3.51 [2H, s, C*H*$_2$], 4.65 [2H, dd, *J* = 14.0 and 102.8 Hz, C*H*$_2$], 7.12 [1H, s, C*H*], 7.32 [1H, s, C*H*]. ^{13}C NMR (100 MHz, $CDCl_3$): δ 7.00, 11.77, 26.09, 42.41, 51.27, 64.17, 126.91, 127.84, 145.72. HRMS(ESI) calcd for $C_9H_{15}IN_3O_3$ $[M + H]^+$: *m/z* 340.0158, found 340.0162. HPLC purity 95.6%, retention time 24.5 min (system B).

O,O′ -Bis(trifluoromethanesulfonyl)-2,2diethylpropane-1,3-diol (10)

A solution of trifluoromethanesulfonic anhydride (1.81 mL, 11.0 mmol) in dichloromethane (10 mL) was added dropwise to a mixture of 2,2-diethylpropane-1,3-diol (0.66 g, 5.00 mmol) and 2,6-

lutidine (1.16 mL, 10.0 mmol) in dichloromethane (10 mL) at −78 °C under an Ar atmosphere. After the addition, the temperature of the reaction mixture was gradually raised to room temperature, and the mixture was stirred for 1 h at the same temperature. The reaction mixture was washed with water (20 mL × 3) and saturated NaCl (20 mL × 1), and the organic phase was dried over $MgSO_4$. After removing the solvent *in vacuo*, the residue was subjected to column chromatography on silica gel using ethyl acetate as an eluent to provide **10** as a pale yellow oil (1.80 g, 4.55 mmol, 91.1%). ^{1}H NMR (400 MHz, $CDCl_3$): δ 0.90 [6H, t, J = 7.6 Hz, CH_3], 1.40 [4H, q, J = 7.5 Hz, CH_2], 4.33 [4H, s, CH_2]. ^{13}C NMR (100 MHz, $CDCl_3$): δ 6.27, 21.10, 41.39, 75.84, 113.81, 117.00, 120.17, 123.35. HRMS(ESI) calcd for $C_9H_{14}F_6N_3NaO_6S_2$ [M + Na]$^+$: m/z 419.0034, found 419.0044.

N-[2,2-Diethyl-2-(trifluoromethanesulfonyloxymethyl)ethyl]-2-nitroimidazole (11)

A solution of compound **10** (1.00 g, 2.52 mmol) in DMF (2.5 mL) was added dropwise to a chilled mixture (0 °C) of 2-nitroimidazole (0.285 g, 2.52 mmol) and potassium carbonate (1.05 g, 7.57 mmol) in DMF (7.5 mL), and the mixture was stirred at room temperature for 4 h under an Ar atmosphere. To the reaction mixture was added ethyl acetate (80 mL), and the organic phase was washed with water (40 mL × 3) and saturated NaCl (40 mL × 1). After drying over Na_2SO_4, the solvent was removed *in vacuo*. The residue was subjected to column chromatography on silica gel using hexane/ethyl acetate (3:2) as an eluent to provide **11** as a pale yellow tacky solid (0.514 g, 1.43 mmol, 56.7%). ^{1}H NMR (400 MHz, $CDCl_3$): δ 0.91 [6H, t, J = 7.6 Hz, CH_3], 1.31-1.40 [2H, m, CH_2], 1.45-1.54 [2H, m, CH_2], 4.30 [2H, s, CH_2], 4.59 [2H, s, CH_2], 7.04 [1H, s, CH], 7.18 [1H, s, CH]. ^{13}C NMR (100 MHz, $CDCl_3$): δ 6.80, 23.46, 42.19, 51.83, 78.44, 113.58, 116.76, 119.93, 123.12, 126.45, 128.40, 145.42. HRMS(ESI) calcd for $C_{11}H_{16}F_3N_3NaO_5S$ [M + Na]$^+$: m/z 382.0661, found 382.0647. HPLC purity >99%, retention time 12.4 min (system F).

N-[2,2-Diethyl-2-(iodomethyl)ethyl]-2-nitroimidazole ([^{127}I]DEIN)

NaI (125 mg, 0.835 mmol) was added to a solution of compound **11** (150 mg, 0.417 mmol) in acetonitrile (7 mL) and stirred at room temperature for 1 h. To the mixture was added water (20 mL), and it was extracted with ethyl acetate (10 mL × 3). The combined organic phase was dried over Na_2SO_4, and the solvent was removed *in vacuo* to provide **[^{127}I]DEIN** as a white solid (114 mg, 0.338 mmol, 81.1%). Mp: 61-63 °C. ^{1}H NMR (400 MHz, $CDCl_3$): δ 0.83 [6H, t, J = 7.6 Hz, CH_3], 1.23-1.32 [2H, m, CH_2], 1.42-1.51 [2H, m, CH_2], 3.11 [2H, s, CH_2], 4.55 [2H, s, CH_2], 7.14 [1H, s, CH], 7.30 [1H, s, CH]. ^{13}C NMR (100 MHz, $CDCl_3$): δ 7.55, 17.27, 25.95, 40.62, 53.08, 125.94, 128.23, 145.81. HRMS(ESI) calcd for $C_{10}H_{16}IN_3NaO_2$ [M + Na]$^+$: m/z 360.0185, found 360.0201. HPLC purity 97.9%, retention time 28.4 min (system B).

N-[*N*-(*meta*-Tributylstannylbenzoyl)-2-aminoethyl]-2-nitroimidazole (15)

A solution of **13** (31 mg, 0.199 mmol) in triethylamine (550 μL) was stirred at room temperature for 5 min. A solution of **14** (163 mg, 0.397 mmol) in acetonitrile (8 mL), 1-hydroxy-7-azabenzotriazole (HOAt, 108 mg, 0.793 mmol), and 1-[bis(dimethylamino)methyliumyl]-1*H*-1,2,3-triazolo[4,5-b]pyridine-3-oxide hexafluorophosphate (HATU, 302 mg, 0.794 mmol) were added to the mixture at 0 °C. After the addition, the temperature of the reaction mixture was raised to room temperature and then stirred overnight at the same temperature. After the solvent was removed *in vacuo*, the residue was dissolved in chloroform (10 mL). That solution was washed with a 1 *N* aqueous NaOH solution (10 mL × 1), a 10% aqueous citric acid solution (10 mL × 2), and a saturated aqueous NaCl solution (5 mL × 1). The organic phase was dried over $MgSO_4$, and the solvent was removed *in vacuo*. The residue was subjected to flash column chromatography using hexane/ethyl acetate (75/25 to 43/57) as an eluent to provide **15** as a pale yellow solid (95 mg, 0.172 mmol, 86.9%). Mp: 98-100 °C. ^{1}H NMR (400 MHz, $CDCl_3$): δ 0.83-0.87 [9H, m, C*H*$_3$], 0.95-1.12 [6H, m, C*H*$_2$], 1.24-1.33 [6H, m, C*H*$_2$], 1.41-1.53 [6H, m, C*H*$_2$], 3.89 [2H, dd, *J* = 5.6 and 11.6 Hz, C*H*$_2$], 4.72 [2H, t, *J* = 5.6 Hz, C*H*$_2$], 6.84 [1H, t, *J* = 5.6 Hz, N*H*], 6.91 [1H, s, C*H*], 7.02 [1H, s, C*H*], 7.34 [2H, t, *J* = 7.2 Hz, C*H*], 7.57-7.62 [2H, m, C*H*], 7.76-7.87 [1H, m, C*H*]. ^{13}C NMR (100 MHz, $CDCl_3$): δ 9.50, 11.21, 13.56, 26.95, 27.24, 27.52, 28.82, 28.92, 29.02, 40.01, 49.30, 126.58, 127.48, 127.74, 127.87, 132.80, 134.96, 139.90, 142.94, 144.18, 169.22. HRMS(ESI) calcd for $C_{24}H_{38}N_4NaO_3Sn$ $[M + Na]^+$: *m/z* 573.1864, found 573.1873. HPLC purity 97.3%, retention time 18.5 min (system H).

N-[*N*-(*meta*-Iodobenzoyl)-2-aminoethyl]-2-nitroimidazole ([^{127}I]MIBAN)

The compound **[^{127}I]MIBAN** was prepared according to the same procedure as **15** using *meta*-iodobenzoic acid (63 mg, 0.403 mmol). The purification by flash chromatography on silica gel using hexane/ethyl acetate (96/4 to 20/80) as an eluent provided **[^{127}I]MIBAN** as a white solid (125 mg, 0.324 mmol, 80.3%). Mp: 187-189 °C. ^{1}H NMR (400 MHz, CD_3OD): δ 3.82 [2H, t, *J* = 5.6 Hz, C*H*$_2$], 4.67 [2H, t, *J* = 5.6 Hz, C*H*$_2$], 7.09 [1H, s, C*H*], 7.21 [1H, t, *J* = 8.0 Hz, C*H*], 7.35 [1H, s, C*H*], 7.69 [1H, d, *J* = 7.6 Hz, C*H*], 7.87 [1H, d, *J* = 7.6 Hz, C*H*], 8.07 [1H, t, *J* = 1.6 Hz, C*H*]. ^{13}C NMR (100 MHz, DMSO): δ 49.10, 94.65, 126.50, 127.66, 128.51, 130.50, 135.47, 136.03, 139.81, 144.74, 165.13. HRMS(ESI) calcd for $C_{12}H_{12}IN_4O_3$ $[M + H]^+$: *m/z* 386.9957, found 386.9954. HPLC purity 98.2%, retention time 24.4 min (system B).

The Glucuronide Conjugate of [^{127}I]BHIN ([^{127}I]BHIN-GC)

Alamethicin (5 μg) was added to a solution of mouse liver microsomes. The mixture was diluted with 50 mM Tris-HCl buffer (pH 7.4) (2 mg protein/mL) and left on ice for 15 min. An equivalent

volume of a mixed solution of **[^{127}I]BHIN** (5.86 mM), UDPGA trisodium salt (10 mM), and $MgCl_2$ (10 mM) in 50 mM Tris-HCl buffer (pH 7.4) was added to 500 μL of the mixture. After incubation for 2 h at 37 °C, the mixture was mixed with ethanol (100 μL), and centrifuged (10,000 g, 5 min). After purification of the supernatant by RP-HPLC (system A), the fraction containing the product was applied to a Sep-Pak C18 cartridge (Nihon Waters, Tokyo, Japan), washed with water, and then eluted with methanol. The eluent was evaporated *in vacuo* to provide **[^{127}I]BHIN-GC** as a white solid (0.3 mg, 20.8%). ^{1}H NMR (400 MHz, D_2O): δ 3.16-3.56 [11H, m, C*H* and CH_2], 3.84 [1H, d, *J* = 10.4 Hz, C*H*], 4.29 [1H, d, *J* = 8.4 Hz, C*H*], 7.06 [1H, s, C*H*], 7.47, 7.49 [1H, s, C*H*]. HRMS(ESI) calcd for $C_{14}H_{19}IN_3O_{10}$ $[M-H]^-$: *m/z* 516.0115, found 516.0120. HPLC purity 98.7%, retention time 13.6 min (system A).

The Glucuronide Conjugate of [^{127}I]EHIN ([^{127}I]EHIN-GC)

[^{127}I]EHIN-GC was synthesized according to the procedure described above using **[^{127}I]EHIN** (5.90 mM) in place of **[^{127}I]BHIN**. Purification by RP-HPLC (system B) provided **[^{127}I]EHIN-GC** as a white solid (0.3 mg, 20.1%). ^{1}H NMR (400 MHz, D_2O): δ 0.67-0.71 [3H, m, CH_3], 1.19-1.37 [2H, m, CH_2], 3.05-3.54 [9H, m, C*H* and CH_2], 3.80 [1H, d, *J* = 10.4 Hz, C*H*], 4.24 [1H, m, C*H*], 7.03, 7.04 [1H, s, C*H*], 7.46, 7.47 [1H, s, C*H*] (This compound was prepared as a mixture of diastereomers.) HRMS(ESI) calcd for $C_{15}H_{21}IN_3O_9$ $[M-H]^-$: *m/z* 514.0323, found 514.0339. HPLC purity >99%, retention time 17.0 min (system B).

Radiosynthesis

Preparation of ^{211}At

^{211}At was supplied from the Research Center for Nuclear Physics at Osaka University and RIKEN through the Supply Platform of Short-lived Radioisotopes. ^{211}At was produced by the ^{209}Bi(α, 2n)^{211}At reaction followed by separation and purification by a dry distillation method. [98,99] Briefly, a 20 mg/cm^2 metallic bismuth target was prepared by vacuum evaporation onto an aluminum foil (approximately 20 mm × 10 mm). An irradiated target was heated on a quartz tube at 850 °C under streaming helium/oxygen mixed gas. Distilled ^{211}At was deposited in a cooled Teflon tube connected to the quartz tube, and ^{211}At was eluted with 100 μL of chloroform (10-20 MBq) or water (47 MBq). Finally, a chloroform solution of ^{211}At was evaporated by the gentle flow of N_2 gas and redissolved in acetonitrile (100 μL).

Radiosynthesis of [^{125}I]BHIN

A solution of [^{125}I]NaI (1.0 μL) was added to a solution of **2** in acetonitrile (10 mM, 100 μL), and the mixture was allowed to react for 1 h at 37 °C. The radiochemical yield was determined by TLC. After the reaction, [^{125}I]**3** was purified by RP-HPLC (system C). The fractions containing the

product were concentrated *in vacuo* to provide an aqueous solution of [^{125}I]**3**. A 2% aqueous solution of *p*-toluenesulfonic acid (10 μL) was added to a solution of [^{125}I]**3**, and the mixture was heated at 60 °C for 0.5 h. The mixture was applied to a Sep-Pak C18 cartridge, washed with water, and then eluted with methanol. The eluent was concentrated *in vacuo* to provide an aqueous solution of [^{125}I]BHIN (60.1%). This solution of [^{125}I]BHIN was diluted with D-PBS(−) (Nacalai Tesque), and used for further evaluation studies. Radiochemical purity >99%, retention time 20.0 min (system A).

Radiosynthesis of [^{125}I]EHIN

A solution of [^{125}I]NaI (1.0 μL) was added to a solution of **7** in acetonitrile or 1% diisopropylethylamine (DIEA) acetonitrile (10 mM, 100 μL), and each mixture was allowed to react for 1 h at 37 °C. The radiochemical yield was determined by TLC. After the reaction, [^{125}I]**8** was then purified by RP-HPLC (system E). The fractions containing the product were concentrated *in vacuo* to provide an aqueous solution of [^{125}I]**8**. The solution of [^{125}I]**8** was added to an equivalent volume of a 2 *N* HCl aqueous solution and reacted for 0.5 h at 60 °C. The mixture was purified by RP-HPLC (system F) to isolate [^{125}I]EHIN. The fractions containing the product were concentrated *in vacuo* to provide an aqueous solution of [^{125}I]EHIN (in acetonitrile: 7.6 %, in 1%DIEA acetonitrile: 67.0%). This solution of [^{125}I]EHIN was diluted with D-PBS(−) and used for further evaluation studies. Radiochemical purity >99%, retention time 24.6 min (system B).

Radiosynthesis of [^{125}I]DEIN

A solution of [^{125}I]NaI (1.0 μL) was added to a solution of **11** in 10% DMSO/acetonitrile (10 mM, 100 μL), and the mixture was allowed to react for 1 h at 37 °C. The radiochemical yield was determined by TLC. After heating the mixture for 5 min at 120 °C to decompose **11**, [^{125}I]DEIN was purified by RP-HPLC (system C). The fractions containing the product were concentrated *in vacuo* to provide an aqueous solution of [^{125}I]DEIN (13.2%). This solution was diluted with D-PBS(−) and used for further evaluation studies. Radiochemical purity >99%, retention time 28.5 min (system B).

Radiosynthesis of [^{125}I]MIBAN

A solution of [^{125}I]NaI (1.0 μL) was added to a solution of **15** in 1% acetic acid/methanol (0.36 mM, 100 μL) and a 4% solution of *N*-chlorosuccinimide (NCS) in methanol (5 μL) and reacted for 5 min at room temperature. The radiochemical yield was determined by TLC. After the reaction, an 8% aqueous solution of $NaHSO_3$ (5 μL) was added to the mixture, and [^{125}I]MIBAN was purified by RP-HPLC (system G). The fractions containing the product were concentrated *in vacuo* to provide an aqueous solution of [^{125}I]MIBAN (71.4%). This solution was diluted with D-PBS(−) and

used for further evaluation studies. Radiochemical purity >99%, retention time 24.6 min (system B).

Radiosynthesis of [^{211}At]BHAN

Compound **2** was added to a solution of ^{211}At in acetonitrile (4.31 and 5.12 MBq, n = 2) at a final concentration of 10 mM (100 μL). After the addition of DIEA (1.0 μL), the mixture was allowed to react for 5, 15, 30, and 60 min at 37 °C. Radiochemical yields were determined by TLC. After the reaction, an equivalent volume of a 4% aqueous solution of *p*-toluenesulfonic acid was added to the reaction solution, and the mixture was allowed to react for 5 min at 60 °C. After the mixture was neutralized with a 0.1 N aqueous NaOH solution, [^{211}At]BHAN was purified by RP-HPLC (system D). A 10% aqueous solution of ascorbic acid (10 μL) was added to the fractions containing the product, and the solvent was removed *in vacuo*. Finally, an aqueous solution of [^{211}At]BHAN (3.06 and 3.23 MBq) was diluted with D-PBS(-) (uncorrected yield: 71.0% and 63.1%, n = 2). The total synthesis time was about 1.5 h. Radiochemical purity 98.4%, retention time 20.1-21.0 min (system A).

Radiosynthesis of [^{211}At]MABAN

A solution of **15** in 1% acetic acid/methanol (1.82 mM, 100 μL) was added to an aqueous solution of ^{211}At (4.31 MBq/5 μL). A 10% solution of NCS in methanol (10 μL) was added, and the mixture was allowed to react for 15 min at room temperature. Radiochemical yields were determined by TLC. After the reaction, a 20% aqueous solution of $Na_2S_2O_5$ (10 μL) was added to the mixture, and [^{211}At]MABAN was purified by RP-HPLC (system G). A 10% aqueous solution of ascorbic acid (10 μL) was added to the fractions containing the product, and the solvent was removed *in vacuo*. Finally, an aqueous solution of [^{211}At]MABAN (1.50 MBq) was diluted with D-PBS(-) (uncorrected yield: 34.8%). The total synthesis time was about 1 h. Radiochemical purity 98.0%, retention time 24.1-25.0 min (system B).

In vitro Stability Study in GSH Solution

This study was conducted according to the procedure of Weinstock et al. with slight modifications.[100] Briefly, A solution of [^{125}I]BHIN, [^{125}I]EHIN, [^{125}I]DEIN (11.1 kBq/20 μL), or [^{211}At]BHAN (6 kBq/20 μL) was added to a mixture of 12.5 mM GSH and 1.25 mM EDTA in nitrogen-purged 0.1 M P.B. (pH 7.4) (80 μL), and the mixture was incubated at 37 °C. After incubation for 1, 3, 6, and 24 h, a 2 μL aliquot of each solution was drawn, and the percent of the intact compound was determined by TLC (n = 3).

In vitro Metabolic Study Using Microsomes

CYP-Mediated Metabolism

A solution of [^{125}I]BHIN, [^{125}I]EHIN, [^{125}I]DEIN, or [^{211}At]BHAN was added to a solution of liver microsomes from mice or humans diluted with 50 mM Tris-HCl buffer (pH 7.4) (0.4 mg protein/mL for mouse liver microsomes and 1.2 mg protein/mL for human liver microsomes, 370 kBq/mL for ^{125}I-labeled compounds and 0.3 MBq/mL for [^{211}At]BHAN). After preincubating the mixture for 5 min, 50 μL aliquots of the solution were mixed with an equivalent volume of a mixture of $MgCl_2$ (10 mM), G6P (10 mM), G6PDH (2 units/mL), and β-$NADP^+$ (2 mM) in 50 mM Tris-HCl buffer (pH 7.4). After incubation for 30 min at 37 °C, ethanol (100 μL) was added to the solution, and the mixture was centrifuged (10,000*g*, 5 min). The supernatant was analyzed by TLC and RP-HPLC (n = 3).

Similar experiments were carried out for [^{125}I]BHIN-GC and [^{125}I]EHIN-GC obtained by the methods described below. In the RP-HPLC analysis of [^{125}I]EHIN and [^{125}I]DEIN, the fractions at the void volume (retention time of 1.5-2.5 min) were collected and reanalyzed by HILIC-HPLC. The total radioactivity of all fractions eluted after the HILIC analyses was almost equal to the applied radioactivity (>95%).

Glucuronide Conjugation

Alamethicin (5 μg) was added to a solution of mouse liver microsomes. The mixture was diluted with 50 mM Tris-HCl buffer (pH 7.4) (0.4 mg protein/mL) and left on ice for 15 min. To the 50 μL aliquots of the mixture were added an equivalent volume of a mixed solution of UDPGA trisodium salt (10 mM) and $MgCl_2$ (10 mM) in 50 mM Tris-HCl buffer (pH 7.4) containing [^{125}I]BHIN (370 kBq/mL), [^{125}I]EHIN (370 kBq/mL), or [^{211}At]BHAN (0.3 MBq/mL). After incubation for 30 min at 37 °C, ethanol (100 μL) was added to the solution, and the mixture was centrifuged (10,000*g*, 5 min). The supernatant was analyzed by RP-TLC and RP-HPLC. The RP-HPLC fractions containing [^{125}I]BHIN-GC and [^{125}I]EHIN-GC were concentrated *in vacuo*, diluted with D-PBS(−), and used for the *in vitro* study described above. Radiochemical purity of [^{125}I] BHIN-GC > 99%, retention time 13.5 min (system A) and radiochemical purity of [^{125}I] EHIN-GC > 99%, retention time 17.1 min (system B).

Biodistribution Study

Animal studies were conducted in accordance with the institutional guidelines approved by the Chiba University Animal Care Committee and the Osaka University Animal Care Committee. Male ICR mice (6 weeks old, 31-35 g) were intravenously injected with ^{125}I-labeled compounds (7.4 kBq) or ^{211}At-labeled compounds (30 kBq) in D-PBS(−) (100 μL). At 10 min, 1 h, 3 h, 6 h, and 24 h postinjection, mice (n = 4-5) were sacrificed, and the organs were dissected. The organs of interest were weighed, and the radioactivity counts were measured with an auto-well γ counter. Urine and feces were collected for 6 and 24 h after injection of ^{125}I-labeled compounds, and their radioactivity

counts were also measured.

Urine Analysis

A solution (100 μL) of [^{125}I]BHIN, EHIN, DEIN (300-370 kBq), [^{211}At]BHAN, [^{211}At]4c, or [^{211}At]At^{-} (200 kBq) was injected intravenously into male ICR mice (6 weeks old, 31-35 g), and the urine samples were collected for 6 h. The urine samples (100 μL) were filtered through a 10 kDa cutoff ultrafiltration membrane before being analyzed by RP-HPLC. During the analysis of [^{125}I]BHIN and [^{125}I]EHIN, the fractions at the void volume (retention time of 1.5-2.5 min) were collected and reanalyzed by HILIC-HPLC. The total radioactivity of all fractions eluted after the HILIC analyses were almost equal to the applied radioactivity (>95%).

Statistical Analysis

All data are presented as the mean ± standard deviation (SD) of at least three independent measurements. Biodistribution studies were analyzed using one-way ANOVA followed by Tukey's test for multiple comparisons (GraphPad Prism, CA). Significance was assigned at $P < 0.05$.

Chapter 2.

General.

[^{125}I]NaI (ca. 3.7 MBq/μL) was purchased from PerkinElmer (Waltham, MA, USA). ^{211}At was supplied by the Research Center for Nuclear Physics at Osaka University through the Supply Platform of Short-lived Radioisotopes and from Fukushima Medical University. ^{211}At was produced by the ^{209}Bi(α, 2n)^{211}At reaction followed by separation and purification by a dry distillation method. ^{18}F was supplied by the Chiba University Hospital. ^{1}H-NMR, ^{13}C-NMR and ^{19}F-NMR spectra were recorded on a JEOL JNM-ECS 400 spectrometer (JEOL, Tokyo, Japan). Mass spectrometry was carried out using an AccuTOF LC-plus (JMS-T100LP, JEOL, Tokyo). HPLC purification was performed using a Hitachi L-2400 system coupled to a NaI(Tl) radioactivity detector (Gabi star, Raytest, Strubenhardt, Germany). The radioactivity counts were determined with an automated gamma well counter (Wizard 3, PerkinElmer Japan, Yokohama, Japan). N^{α}-*tert*-butoxycarbonyl-L-tyrosine *tert-butyl ester* was prepared according to a previously described method.[101] The other chemicals obtained from the commercial sources were of reagent grade or higher and were used without purification.

HPLC or TLC methods

Analytical reversed-phase HPLC (RP-HPLC) was performed with a Unison US-C18 column (4.6 × 150 mm, Imtakt, Kyoto, Japan) at a flow rate of 1 mL/min using a linear gradient mobile phase starting from 90% A (0.1% aqueous trifluoroacetic acid (TFA)) and 10% B (acetonitrile with 0.1% TFA) to 50% A and 50% B in 20 min, followed by 0% A and 100% B in 30 min (System A) or from 95% A and 5% B to 0% A and 100% B in 30 min (System B). In System C, the mobile phase was maintained 100% A and 0% B for 5 min, then changed to 70% A and 30% B, followed by a change 0% A and 100% B. In System D, the mobile phase was maintained 95% A (0.01 M acetate buffer (pH 6.0)) and 0% B (acetonitrile) for 5 min, then changed gradiently to 70% A and 30% B in 20 min, followed by a change 0% A and 100% B in 30 min. RP-TLC was performed using Silica gel 60 RP-18 F254S (Merck, Darmstadt, Germany) and was developed in a mixture of tert-butyl alcohol : acetic acid : H_2O (4:1:1, v/v). Preparative RP-HPLC was performed with a Unison US-C18 column (20 × 150 mm, Imtact, Kyoto) at a flow rate of 5 mL/min using a linear gradient mobile phase starting from 90% A and 10% B to 50% A and 50% B in 30 min (System D).

Synthesis

2,2-Dimethyl-1,3-dioxane-5,5-dimethanol (17)

Pentaerythritol (**16**) (6.00 g, 44.1 mmol) and (+)-10-camphorsulfonic acid (0.205 g, 0.881 mmol) were dissolved in *N,N*-dimethylformamide (DMF) (120 mL) and the solution was heated to 80 ° C. After completion of dissolution, the temperature was reduced to 40 ° C, and 2,2-dimethoxypropane (6.50 mL, 52.8 mmol) was added dropwise. The mixture was allowed to cool to room temperature and stirred continuously for 2 days. Triethylamine (370 μL, 2.65 mmol) was added to neutralize the reaction. After removing the solvent *in vacuo*, the residue underwent a Soxhlet extraction with hexane for 2 days. The solvent was removed *in vacuo*, then compound **17** was recrystallized from a mixture of ethyl acetate and hexane as a white solid (633 mg, 3.59 mmol, 36.1%). ^{1}H-NMR (DMSO-d_6): δ 1.29 (6H, s, CH_3), 3.35-3.36 (4H, d, CH_2), 3.59 (4H, s, CH_2), 4.48-4.51 (2H, t, OH). ^{13}C-NMR (DMSO-d_6): 23.83, 38.88, 60.50, 61.67, 91.12. HRMS(ESI) calcd. for $C_8H_{16}NaO_4$ [M + Na]+: m/z 199.0946, found 199.0940.

2,2-Dimethyl-1,3-dioxane-5,5-diyl)bis(methylene) bis(trifluoromethanesulfonate) (18)

Compound **17** (633 mg, 3.59 mmol) was dissolved in dichloromethane (40 mL), and 2,6-lutidine (4.2 mL, 35.9 mmol) was added. After cooling to -78 ° C, trifluoromethanesulfonic anhydride (Tf_2O) (2 mL, 12.2 mmol) was added dropwise, and then the solution was stirred for 1 h. The reaction temperature was subsequently raised to -20 ° C and maintained overnight. The mixture was successively washed with saturated $NaHCO_3$ solution (20 mL), 5% citric acid solution (30 mL), and saturated brine (20 mL). The organic layer was dried over magnesium sulfate, and then the solvent was evaporated *in vacuo*. The product was purified by silica gel chromatography using

hexane: ethyl acetate (10:1) as an eluent to produce compound **18** as a white solid (1.30 g, 2.94 mmol, 82.0%). ^{1}H-NMR ($CDCl_3$): δ 1.44 (6H, s, CH_3), 3.79 (4H, s, CH_2), 4.57 (4H, s, CH_2). ^{13}C-NMR ($CDCl_3$): 23.39, 39.00, 60.88, 73.54, 99.71, 113.92, 117.11, 120.29, 123.47. HRMS(ESI) calcd. for $C_{10}H_{14}F_6NaO_8S_2$ $[M + Na]^+$: m/z 462.9932, found 462.9917.

Nα-(tert-butoxycarbonyl)-O-((2,2-dimethyl-5-((((trifluoromethyl)sulfonyl)oxy)methyl)-1,3-dioxan-5-yl)methyl)-L-tyrosine tert-butyl ester (20)

NaH (10.8 mg, 0.270 mmol) was suspended in tetrahydrofuran (THF) (0.50 mL). Under an argon atmosphere, a solution of compound **19** (76.0 mg, 0.226 mmol) in THF (1.50 mL) was added dropwise to the NaH suspension under ice-cold conditions. The mixture was stirred at room temperature for 30 min. Subsequently, compound **18** (100 mg, 0.226 mmol) was added, and the reaction mixture was stirred for 40 min at room temperature. After removing the solvent, the resulting residue was redissolved in ethyl acetate (10 mL) and washed thrice with a saturated $NaHCO_3$ solution (10 mL each). The organic phase was dried over magnesium sulfate. After removing the solvent, the residue was purified by a preparative TLC plate using a mixture of hexane: ethyl acetate (2:1) as a solvent to obtain compound **20** as a colorless oil (86.2 mg, 0.137 mmol, 60.8%). ^{1}H-NMR ($CDCl_3$): δ 1.41-1.45(24H, overlapped, CH_3), 2.99-3.01 (2H, t, CH_2), 3.81-3.93 (6H, overlapped, CH_2), 4.39-4.41 (1H, multiple, CH), 4.79 (2H, s, CH_2), 4.96-4.98 (1H, d, NH), 6.80-6.82 (2H, d, aromatic), 7.08-7.10 (2H, d, aromatic). ^{13}C-NMR ($CDCl_3$): 21.58, 25.62, 28.07, 28.43, 37.71, 38.90, 55.01, 61.85, 66.22, 75.43, 79.75, 82.16, 99.19, 113.94, 114.43, 117.12, 120.30, 123.48, 129.57, 130.61, 130.75, 155.19, 157.21, 170.93, 171.07. HRMS(ESI) calcd. for $C_{27}H_{40}F_3NaNNaO_{10}S$ [M + Na]+: m/z 650.2223, found 650.2218.

Nα-(tert-butoxycarbonyl)-O-((5-(iodomethyl)-2,2-dimethyl-1,3-dioxan-5-yl)methyl)-L-tyrosine tert-butyl ester (22)

Compound **20** (64.6 mg, 0.103 mmol) was dissolved in acetonitrile (1 mL). After adding sodium iodide (46 mg, 0.309 mmol), the mixture was stirred overnight at room temperature. After removing the solvent, the resulting residue was redissolved in ethyl acetate (5 mL) and washed sequentially with a 5% $NaHCO_3$ solution (5 mL), twice with water (5 mL each), and finally with saturated brine (5 mL). The organic layer was dried over magnesium sulfate. After removing the solvent *in vacuo*, the residue was purified by a preparative TLC plate using a mixture of hexane: ethyl acetate (2:1) as an eluent to afford compound **22** as a colorless oil (51.4 mg, 0.0849 mmol, 82.4%). ^{1}H-NMR ($CDCl_3$): δ 1.42-1.44 (24H, overlapped, CH_3), 2.99-3.01(2H, t, CH_2), 3.41 (2H, s, CH_2), 3.78-3.91 (4H, multiple, CH_2), 3.98 (2H, s, CH_2), 4.40-4.41 (1H, multiple, CH), 4.95-4.97 (1H, d, NH), 6.83-6.85 (2H, d, aromatic), 7.07-7.09 (2H, d, aromatic). ^{13}C-NMR ($CDCl_3$): 10.42, 27.58, 24.74, 28.11, 28.45, 36.84, 37.63, 55.02, 64.84, 68.81, 79.73, 82.11, 98.85, 114.63,

129.00, 130.65, 155.21, 157.76, 171.11. HRMS(ESI) calcd for $C_{26}H_{40}INNaO_7$ [M + Na]+: m/z 628.1747, found 628.1778.

O-(3-hydroxy-2-(hydroxymethyl)-2-(iodomethyl)propyl)-L-tyrosine ([^{127}I]I-NpGT)

Compound **22** (10.2 mg, 16.8 nmol) was dissolved in a mixture of TFA (800 μL) and H_2O (200 μL), and the solution was stirred at room temperature for 5 h. After removing the solvent *in vacuo*, the residue was subjected to azeotropic drying with acetonitrile (1 mL × 2). The residue was purified by preparative RP-HPLC (System D) to afford **[^{127}I]I-NpGT** as a white solid (5.45 mg, 10.8 nmol, 64.1%). ^{1}H-NMR (D_2O): δ 2.95-3.14 (2H, multiple, CH_2), 3.20 (2H, s, CH_2), 3.51 (4H. s, CH_2), 3.79 (2H, s, CH_2), 4.04-4.07 (1H, q, CH), 6.86-6.88 (2H, d, aromatic), 7.07-7.09 (2H, d, aromatic). ^{13}C-NMR (D_2O): 9.39, 36.07, 44.10, 56.65, 61.77, 68.26, 115.96, 128.24, 131.19, 158.65, 174.59. HRMS(ESI) calcd. for $C_{14}H_{20}INNaO_5$ [M + Na]+: m/z 432.0284, found 432.0314.

N$^{\alpha}$-(tert-butoxycarbonyl)-O-((5-(fluoromethyl)-2,2-dimethyl-1,3-dioxan-5-yl)methyl)-L-tyrosine tert-butyl ester (21)

Compound **20** (20.0 mg, 0.0319 mmol) was dissolved in THF (0.5 mL). To this solution, tetrabutylammonium fluoride (TBAF, approximately 1 mol/L in THF) (64 μL, 0.0637 mmol) was added. The mixture was then stirred at room temperature overnight. After removing the solvent, the residue was redissolved in ethyl acetate (5 mL) and successively washed with water twice (5 mL each), saturated ammonium chloride solution (5 mL), and saturated brine (5 mL). The organic layer was dried over magnesium sulfate. After removing the solvent *in vacuo*, compound **21** was obtained as a white solid (15.0 mg, 30.1 nmol, 94.5%).^{1}H-NMR ($CDCl_3$): δ 1.40-1.48 (24H, overlapped, CH_3), 2.96-3.00(2H, t, CH_2), 3.82-3.93 (6H, overlapped, CH_2), 3.98 (2H, s, CH_2), 4.37-4.39 (1H, multiple, CH), 4.52-4.63 (2H, d, CH_2) 4.92-4.94 (1H, d, NH), 6.80-6.82 (2H, d, aromatic), 7.04-7.07 (2H, d, aromatic). ^{13}C-NMR ($CDCl_3$): 23.23, 24.05, 28.00, 28.11, 28.33, 37.49, 39.00, 39.17, 54.91, 61.45 61.52, 66.69, 79.60, 81.88 ,81.99, 83.58, 98.54, 114.39, 128.92, 130.55, 155.09, 157.67, 170.97. HRMS(ESI) calcd. for $C_{26}H_{40}FNNaO_7$ [M + Na]+: m/z 520.2687, found 520.2691.

O-(3-hydroxy-2-(hydroxymethyl)-2-(fluoromethyl)propyl)-L-tyrosine ([^{19}F]F-FNT)

Compound **21** (12.0 mg, 20.4 nmol) was dissolved in a mixture of TFA (4.0 mL) and water (1.0 mL), and the resulting solution was stirred at 60 °C for 3 h. After removing the solvent, the residue was subjected to azeotropic drying using acetonitrile (1 mL × 2). The residue was purified by preparative RP-HPLC (System D) to afford **[^{19}F]F-FNT** as a white solid (5.20 mg, 13.1 nmol, 64.0%) and was successfully isolated as a white solid. ^{1}H-NMR (D_2O): δ 2.99-3.16 (2H, multiple, CH_2), 3.59 (4H. s, CH_2), 3.91 (2H, s, CH_2), 4.02-4.04 (1H, q, CH), 4.46-4.54 (2H, d, CH_2), 6.91-

6.92 (2H, d, aromatic), 7.13-7.14 (2H, d, aromatic). ^{13}C-NMR (D_2O): δ 35.69, 46.18, 46.28, 55.62, 60.49, 60.53, 66.87, 83.37, 84.47, 115.98, 127.63, 131.27, 158.87, 173.19. ^{19}F-NMR (D_2O): -237.09, -237.03, -236.94. HRMS(ESI) calcd. for $C_{14}H_{20}FNNaO_5$ $[M + Na]^+$: m/z 324.1223, found 324.1214.

Radiosynthesis of [^{211}At]At-NpGT

^{211}At was dissolved in acetonitrile (20 μL), 10% sodium ascorbate solution (2.5 μL), and 1% *N, N*-diisopropylethylamine (DIEA)/acetonitrile solution of compound **20** (0.3 mg/50 μL) were added. The mixture was heated at 37° C for 30 min and passed through a Sep-Pak C18 cartridge using H_2O and acetonitrile as solvent. After removing the solvent, 80% trifluoroacetic acid (TFA)/H_2O was added to remove the protecting groups. The mixture was heated at 60° C for 30 min. TFA was evaporated by N_2 gas, and the solution was neutralized with a 2M sodium acetate solution. The solution was purified by RP-HPLC with system A, then desalted through a Sep-Pak C18 cartridge using H_2O and acetonitrile as solvents. The solvent was removed *in vacuo*, diluted with Phosphate-Buffered Saline (PBS), and used for further evaluation studies.

Assessment of the effect of reducing agents on ^{211}At labeling

^{211}At was dissolved in acetonitrile (1 μL), 1% *N, N*-diisopropylethylamine (DIEA)/acetonitrile solution of compound **20** (0.06 mg/10 μL) and cysteine (100 μg/1 μL), glutathione (100 μg/1 μL), sodium sulfite (100 μg/1 μL), sodium ascorbate (100 μg/1 μL) or D-PBS(-) (1μL) were added. The reaction mixture was incubated at 37° C, and the conversion rate was analyzed by RP-TLC at 10 minutes and 30 minutes (N=3).

Radiosynthesis of [^{125}I]I-NpGT

A solution of [^{125}I]NaI (0.5 μL) was added to a 1% DIEA/acetonitrile solution of compound **20** (0.3 mg/50 μL). The mixture was heated at 37° C for 60 min and passed through a Sep-Pak C18 cartridge using H_2O and acetonitrile as solvent. After removing the solvent, 80% TFA/H_2O was added to remove the protecting groups. The mixture was heated at 60° C for 30 min. TFA was evaporated by N_2 gas, and the solution was neutralized with a 2M sodium acetate solution. The solution was purified by RP-HPLC with system A, then desalted through a Sep-Pak C18 cartridge using H_2O and acetonitrile as solvents. The solvent was removed *in vacuo*, diluted with PBS, and used for further evaluation studies.

Radiosynthesis of [^{18}F]F-NpGT

To the reaction vial, an aqueous potassium carbonate solution (5.85 mg/L, 0.3 mL), a Cryptofix 222 acetonitrile solution (14 mg/0.3 mL), and a solution containing ^{18}F were added. The mixture

was concentrated using a CEV1B evaporator (BioChromato, Kanagawa, Japan) with heating to 100° C. Subsequently, super-dehydrated acetonitrile (Wako, Osaka, Japan) was added to facilitate azeotropic evaporation. An acetonitrile solution of compound **20** (1.0 mg/50 μL) was added to the reaction vial. The mixture was heated at 100° C for 30 min and passed through a Sep-Pak C18 cartridge using H_2O and acetonitrile as solvent. After removing the solvent, 80% TFA/H_2O was added to remove the protecting groups. The mixture was heated at 60° C for 30 min. TFA was evaporated by N_2 gas, and the solution was neutralized with a 2M sodium acetate solution. The solution was purified by RP-HPLC with system C, then desalted through a Sep-Pak C18 cartridge using H_2O and acetonitrile as solvents. The solvent was removed *in vacuo*, diluted with PBS, and used for further evaluation studies.

Radiosynthesis of [^{125}I]-IMT

α-Methyl L-tyrosine (0.2 ng/35 μL in 0.4 M phosphate buffer (pH 6.2)) and [^{125}I]NaI (0.5 μL, ca. 1 MBq) were mixed. A 10 μL of Chloramine-T (0.45 mg/mL in 0.05 M phosphate buffer (pH 6.2)) was added to the mixture for 2 min at room temperature. The reaction was terminated by adding a 10% Na_2SO_4 solution (20 μL). The solution was purified by RP-HPLC using system B, and [^{125}I]I-IMT was desalted through a Sep-Pak C18 cartridge using H_2O and acetonitrile as solvent. The product solution was concentrated *in vacuo*, diluted with PBS, and used for further evaluation studies.

Cellular uptake study

The rat glial cell line, C6 (RCB2854), was provided by the RIKEN BRC through the National Bio-Resource Project of the MEXT/AMED, Japan. The C6 glioma cells were trypsinized and suspended in 10% Fetal Bovine Serum (FBS) (Cosmo Bio Co., LTD., Tokyo, Japan) /RPMI1640 (Nacalai Tesque, Kyoto, Japan) medium at a density of 5×10^5 cells/tube. Each tube was centrifuged at 300 × *g* for 5 min. The supernatant was discarded, and the cells were washed with 10 mM HEPES/Hanks' balanced salt solution (HBSS) (Nacalai Tesque) (1 mL × 2). The cells were resuspended in 10 mM HEPES/HBSS (500 μL). After preincubation at 37 °C for 5 min, 20 μL of 10 mM HEPES/HBSS containing either [^{125}I]I-NpGT (3.7 kBq), [^{211}At]At-NpGT (30 kBq), or [^{18}F]F-NpGT (40 kBq) was added and incubated at 37 °C for 1, 10, and 30 min. The uptake of radiolabeled amino acid derivatives was terminated by adding 1000 μL of ice-cold PBS (Nacalai Tesque), and the mixture was allowed to stand for 2 min under ice-cold conditions. After centrifugation at 300 × *g* for 5 min, the supernatant was removed, and the cells were washed twice with ice-cold PBS (1 mL × 2). The radioactivities of the precipitate and supernatant were measured using an auto-well gamma counter (Wizard 3, PerkinElmer Japan, Yokohama, Japan).

Extracellular release study

As described above, C6 glioma cells were incubated with [^{211}At]At-NpGT (30 kBq), [^{125}I]I-NpGT (3.7 kBq), or [^{18}F]F-NpGT (67 kBq) for 10 min, then 1000 μL of ice-cold PBS was added subsequently. After centrifuging the mixture at 300 × *g* for 5 min, the supernatant was discarded, and the cells were washed twice with 1000 μL of ice-cold PBS. Cells were resuspended in 10 mM HEPES/10% FBS/RPMI1640 medium (500 μL) and incubated at 37° C for 1, 10, or 30 min. The reaction was stopped by adding 1000 μL of ice-cold PBS, and the mixture was allowed to stand for 2 min under ice-cold conditions. After centrifugation at 300 × *g* for 5 min, the supernatant was removed, and the cells were washed twice with ice-cold PBS (1 mL × 2). The radioactivities of the precipitate and supernatant were measured using an auto-well gamma counter. In the study of [^{125}I]I-NpGT, the supernatant was analyzed by RP-HPLC (System A).

Inhibition assay

C6 glioma cells were suspended in 10 mM HEPES/HBSS (500 μL) containing 1 mM various inhibitors (L-tyrosine (Tyr), 2-aminobicyclo[2.2.1]heptane-2-carboxylic acid (BCH) (Sigma-Aldrich Japan, Tokyo, Japan), α-(methylamino)isobutyric acid (MeAIB) (Tokyo Chemical Industry Co., Ltd, Tokyo, Japan), α-methyl-L-tyrosine (AMT)) (Sigma-Aldrich Japan), and preincubate at 37° C for 5 min. Subsequently, [^{211}At]At-NpGT (30 kBq), [^{125}I]I-NpGT (3.7 kBq), or [^{18}F]F-NpGT (35 kBq) dissolved in 10 mM HEPES/HBSS (20 μL) was added to the mixture and incubated for 30 min. The reaction was stopped by adding 1000 μL of ice-cold PBS. The reaction mixture was allowed to stand on ice for 2 min and centrifuged at 300 × *g* for 5 min. After centrifugation at 300 × *g* for 5 min, the supernatant was removed, and the cells were washed twice with ice-cold PBS (1 mL × 2). The radioactivities of the precipitate and supernatant were measured using an auto-well gamma counter.

Stability against dehalogenation in PBS or FBS

[^{211}At]At-NpGT (44.4 kBq), [^{125}I]I-NpGT (11.1 kBq), or [^{18}F]F-NpGT (1.0 MBq) dissolved in aqueous solution (5 μL) were added to either PBS (50 μL) or FBS, 50 μL). In the PBS stability studies, RP-TLC was performed at 1, 3, and 6 h for [^{125}I]I-NpGT, and at 1 and 3 h for [^{211}At]At-NpGT and [^{18}F]F-NpGT to evaluate the percentage of the free halogen fraction. For stability studies in FBS with [^{125}I]I-NpGT, after incubation for 24 h, acetonitrile (100 μL) was added to the reaction, and the contents were centrifuged at 13,000 rpm for 10 min. The supernatant was analyzed by RP-HPLC (System A) to determine the percentage of radioactivity corresponding to the free halogen fraction. In the other studies performed [^{211}At]At-NpGT or [^{18}F]F-NpGT, after incubation for 3 h, acetonitrile (100 μL) was added to the reaction mixture, and the procedure above for sample analysis was repeated to determine the percentage of radioactivity corresponding

to the free halogen fraction.

Preparation of animals

Animal studies were conducted in accordance with the institutional guidelines approved by the Chiba University Animal Care Committee or Osaka University Animal Care Committee. Six-week-old male ICR normal mice and five-week-old male BALB/c nude mice were purchased from Japan SLC, Inc. (Hamamatsu, Japan). C6 glioma cells (5.0×10^6 cells) were suspended in 100 μL of culture medium and Matrigel (1:1 ratio; BD Biosciences, Franklin Lakes, NJ, USA). Tumor xenograft models were prepared by subcutaneously injecting a suspension of C6 glioma cells into immunodeficient nude mice.

Biodistribution of tumor-bearing mice

The animal study was conducted according to the protocol reviewed and approved by Chiba University Animal Care Committee (Permit No. 4-183) or Osaka University Animal Care Committee (Permit No. 30-103-008). One week after C6 glioma cell transplantation, nude mice were injected intravenously with [^{211}At]At-NpGT (30 kBq/mouse), [^{125}I]I-NpGT (7.4 kBq/mouse), [^{18}F]F-NpGT(400 kBq/mouse) or [^{125}I]IMT (7.4 kBq/mouse) in PBS (100 μL). At 1 and 3 h post-injection., the mice (n = 4-5) were euthanized by cervical dislocation after isoflurane (Viatris Inc., New York) inhalation, and the organs were dissected. The organs of interest were weighed, and radioactivity counts were measured using an auto-well gamma counter.

Urine analysis

Male ICR mouse was injected intravenously with [^{125}I]I-NpGT (185 kBq/mouse) in PBS (100 μL). At 6 h post-injection, a urine sample was collected. The urine sample (100 μL) was filtered through a 10 kDa cutoff ultrafiltration membrane (Sartorius, Germany) before being analyzed by RP-HPLC (system D).

Therapeutic study

The animal study was conducted according to the protocol reviewed and approved by Chiba University Animal Care Committee (Permit No. 5-225). Tumor-bearing mice were prepared in the same manner as described in the biodistribution study. After tumor volumes had reached approximately 150-200 mm^3, [^{211}At]At-NpGT (0.1 MBq/mouse (n = 5), 0.3 MBq/mouse (n = 5)) or D-PBS(-) (control (n = 5)) was administered intravenously. Tumor size (mm^3) was measured using calipers and calculated using the following elliptical sphere model equation:

$$V = 4/3 \times \pi \times a2 \times b$$

where V is the volume of the tumor (mm^3), a is the shorter radius (mm), and b is the longer radius

(mm)).

In case of weight loss of more than 20%, the appearance of moribund state signs, or tumor size greater than 800 mm^3, the mice were euthanized humanely by isoflurane inhalation.

Statical analysis

All data are presented as the mean ± standard deviation (SD) of at least three independent measurements. Biodistribution studies were analyzed using one-way analysis of variance (ANOVA) followed by Tukey's test for multiple comparisons (GraphPad Prism; GraphPad Software, San Diego, CA, USA). Statistical significance was set at $P < 0.05$.

References

(1) Johansson, L.; Mattsson, S.; Nosslin, B.; Leide-Svegborn, S. Nuclear Medicine Effective Dose from Radiopharmaceuticals. *Eur J Nucl Med* **1992**, *19*, 933-938.

(2) Kim, Y.-S.; Brechbiel, M. W. An Overview of Targeted Alpha Therapy. *Tumor Biology* **2012**, *33* (3), 573-590. https://doi.org/10.1007/s13277-011-0286-y.

(3) Lammertsma, A. A. PET/SPECT: Functional Imaging beyond Flow. *Vision Res* **2001**, *41*, 1277-1281.

(4) Rahmim, A.; Zaidi, H. Pet versus Spect: Strengths, Limitations and Challenges. *Nucl Med Commun* **2008**, *29* (3), 193-207. https://doi.org/10.1097/MNM.0b013e3282f3a515.

(5) Crişan, G.; Moldovean-Cioroianu, N. S.; Timaru, D.-G.; Andrieş, G.; Căinap, C.; Chiş, V. Radiopharmaceuticals for PET and SPECT Imaging: A Literature Review over the Last Decade. *Int J Mol Sci* **2022**, *23* (9), 5023. https://doi.org/10.3390/ijms23095023.

(6) Eychenne, R.; Chérel, M.; Haddad, F.; Guérard, F.; Gestin, J.-F. Overview of the Most Promising Radionuclides for Targeted Alpha Therapy: The "Hopeful Eight." *Pharmaceutics* **2021**, *13* (6), 906. https://doi.org/10.3390/pharmaceutics13060906.

(7) McDevitt, M. R.; Sgouros, G.; Sofou, S. Targeted and Nontargeted α-Particle Therapies. *Annu Rev Biomed Eng* **2018**, *20* (1), 73-93. https://doi.org/10.1146/annurev-bioeng-062117-120931.

(8) Baidoo, K. E.; Yong, K.; Brechbiel, M. W. Molecular Pathways: Targeted α-Particle Radiation Therapy. *Clinical Cancer Research* **2013**, *19* (3), 530-537. https://doi.org/10.1158/1078-0432.CCR-12-0298.

(9) Borsò, E.; Boni, G.; Galli, L.; Ricci, S.; Farnesi, A.; Mazzarri, S.; Cianci, C.; Mariani, G.; Falcone, A. Radium 223 Dichloride: A Multidisciplinary Approach to Metastatic Castration-Resistant Prostate Cancer. *Future Oncology* **2015**, *11* (2), 323-331. https://doi.org/10.2217/fon.14.157.

(10) Itoh, K. 99mTc-MAG3: Review of Pharmacokinetics, Clinical Application to Renal Diseases and Quantification of Renal Function. *Ann Nucl Med* **2001**, *15* (3), 179-190.

(11) Grossman, S. A.; Trump, D. L.; Chen, D. C.; Thompson, G.; Edwaldo Camargo, P. E. Cerebrospinal Fluid Flow Abnormalities in Patients with Neoplastic Meningitis An Evaluation Using 1 ' 1 Indium-DTPA Ventriculography. *Am J Med* **1982**, *73*, 641-647.

(12) Opresko, L.; Wiley, H. S.; Wallace, R. A. Proteins Iodinated by the Chloramine-T Method Appear to Be Degraded at an Abnormally Rapid Rate after Endocytosis. *Proceedings of the National Academy of Sciences* **1980**, *77* (3), 1556-1560. https://doi.org/10.1073/pnas.77.3.1556.

(13) Rissler, K.; Cramer, H. Marked Improvement of a Substance P Radioimmunoassay by Reduction of 125I-Labelled [Tyr8]-Substance P Prepared by the Chloramine-T Method with Mercaptoethanol and Subsequent Purification by Reversed-Phase Liquid Chromatography. *J Chromatogr B Biomed Sci Appl* **1991**, *564* (1), 67-79. https://doi.org/10.1016/0378-4347(91)80070-S.

(14) Chandra Kumar, C.; Nie, H.; Armstrong, L.; Zhang, R.; Vijay-Kumar, S.; Tsarbopoulos, A. Chloramine T-induced Structural and Biochemical Changes in Echistatin. *FEBS Lett* **1998**, *429* (3), 239-248. https://doi.org/10.1016/S0014-5793(98)00587-0.

(15) Bolton, R. Radiohalogen Incorporation into Organic Systems. *J Labelled Comp Radiopharm* **2002**, *45* (6), 485-528. https://doi.org/10.1002/jlcr.575.

(16) Herrmann, K.; Schwaiger, M.; Lewis, J. S.; Solomon, S. B.; McNeil, B. J.; Baumann, M.; Gambhir, S. S.; Hricak, H.; Weissleder, R. Radiotheranostics: A Roadmap for Future Development. *Lancet Oncol* **2020**, *21* (3), e146-e156. https://doi.org/10.1016/S1470-2045(19)30821-6.

(17) Gregory A. Wiseman; Christine A. White; Michael Stabin; William L. Dunn; William Erwin; Magnus Dahlbom; Andrew Raubitschek; Kastytis Karvelis; Timothy Schultheiss; Thomas E. Witzig; Richard Belanger; Stewart Spies; Daniel H.S. Silverman; Judy R. Berlfein; Eric Ding; Antonio J. Grillo-López. Phase I/II 90Y-Zevalin (Yttrium-90 Ibritumomab Tiuxetan, IDEC-Y2B8) Radioimmunotherapy Dosimetry Results in relapsed or Refractory Non-Hodgkin's Lymphoma. *Eur J Nucl Med* **2000**, *27* (7), 766-777.

(18) Eychenne, R.; Bouvry, C.; Bourgeois, M.; Loyer, P.; Benoist, E.; Lepareur, N. Overview of Radiolabeled Somatostatin Analogs for Cancer Imaging and Therapy. *Molecules* **2020**, *25* (17), 4012. https://doi.org/10.3390/molecules25174012.

(19) Grubmüller, B.; Senn, D.; Kramer, G.; Baltzer, P.; D'Andrea, D.; Grubmüller, K. H.; Mitterhauser, M.; Eidherr, H.; Haug, A. R.; Wadsak, W.; Pfaff, S.; Shariat, S. F.; Hacker, M.; Hartenbach, M. Response Assessment Using 68Ga-PSMA Ligand PET in Patients Undergoing 177Lu-PSMA Radioligand Therapy for Metastatic Castration-Resistant Prostate Cancer. *Eur J Nucl Med Mol Imaging* **2019**, *46* (5), 1063-1072. https://doi.org/10.1007/s00259-018-4236-4.

(20) Sainz-Esteban, A.; Prasad, V.; Schuchardt, C.; Zachert, C.; Carril, J. M.; Baum, R. P. Comparison of Sequential Planar 177Lu-DOTA-TATE Dosimetry Scans with 68Ga-DOTA-TATE PET/CT Images in Patients with Metastasized Neuroendocrine Tumours Undergoing Peptide Receptor Radionuclide Therapy. *Eur J Nucl Med Mol Imaging* **2012**, *39* (3), 501-511. https://doi.org/10.1007/s00259-011-2003-x.

(21) Nock, B. A.; Kanellopoulos, P.; Joosten, L.; Mansi, R.; Maina, T. Peptide Radioligands in Cancer Theranostics: Agonists and Antagonists. *Pharmaceuticals* **2023**, *16* (5), 674. https://doi.org/10.3390/ph16050674.

(22) Kratochwil, C.; Bruchertseifer, F.; Giesel, F. L.; Weis, M.; Verburg, F. A.; Mottaghy, F.; Kopka, K.; Apostolidis, C.; Haberkorn, U.; Morgenstern, A. 225Ac-PSMA-617 for PSMA-Targeted α-Radiation Therapy of Metastatic Castration-Resistant Prostate Cancer. *Journal of Nuclear Medicine* **2016**, *57* (12), 1941-1944. https://doi.org/10.2967/jnumed.116.178673.

(23) Bidkar, A. P.; Zerefa, L.; Yadav, S.; VanBrocklin, H. F.; Flavell, R. R. Actinium-225 Targeted Alpha Particle Therapy for Prostate Cancer. *Theranostics* **2024**, *14* (7), 2969-2992. https://doi.org/10.7150/thno.96403.

(24) Higashi, T.; Nagatsu, K.; Tsuji, A. B.; Zhang, M.-R. Research and Development for Cyclotron Production of 225Ac from 226Ra—The Challenges in a Country Lacking Natural Resources for Medical Applications. *Processes* **2022**, *10* (6), 1215. https://doi.org/10.3390/pr10061215.

(25) De Kruijff, R.; Wolterbeek, H.; Denkova, A. A Critical Review of Alpha Radionuclide Therapy—How to Deal with Recoiling Daughters? *Pharmaceuticals* **2015**, *8* (2), 321-336. https://doi.org/10.3390/ph8020321.

(26) Vaidyanathan, G.; Zalutsky, M. Astatine Radiopharmaceuticals: Prospects and Problems. *Current Radiopharmaceuticalse* **2008**, *1* (3), 177-196. https://doi.org/10.2174/1874471010801030177.

(27) Guérard, F.; Gestin, J. F.; Brechbiel, M. W. Production of [211At]-Astatinated Radiopharmaceuticals and Applications in Targeted α-Particle Therapy. *Cancer Biother Radiopharm* **2013**, *28* (1), 1-20. https://doi.org/10.1089/cbr.2012.1292.

(28) Feng, Y.; Zalutsky, M. R. Production, Purification and Availability of 211At: Near Term Steps towards Global Access. *Nucl Med Biol* **2021**, *100-101*, 12-23. https://doi.org/10.1016/j.nucmedbio.2021.05.007.

(29) Conti, M.; Eriksson, L. Physics of Pure and Non-Pure Positron Emitters for PET: A Review and a Discussion. *EJNMMI Phys* **2016**, *3* (1), 8. https://doi.org/10.1186/s40658-016-0144-5.

(30) Mian M Alauddin. Positron Emission Tomography (PET) Imaging with 18F-Based Radiotracers. *Am J Nucl Med Mol Imaging* **2012**, *2* (1), 55.

(31) Varagnolo, L.; Stokkel, M. P. M.; Mazzi, U.; Pauwels, E. K. J. 18F-Labeled Radiopharmaceuticals for PET in Oncology, Excluding FDG. *Nucl Med Biol* **2000**, *27* (2), 103-112.

(32) Vallabhajosula, S. 18F-Labeled Positron Emission Tomographic Radiopharmaceuticals in Oncology: An Overview of Radiochemistry and Mechanisms of Tumor Localization. *Semin Nucl Med* **2007**, *37* (6), 400-419. https://doi.org/10.1053/j.semnuclmed.2007.08.004.

(33) Jacobson, O.; Kiesewetter, D. O.; Chen, X. Fluorine-18 Radiochemistry, Labeling Strategies and Synthetic Routes. *Bioconjug Chem* **2015**, *26* (1), 1-18. https://doi.org/10.1021/bc500475e.

(34) Tang, G.; Wang, M.; Tang, X.; Gan, M.; Luo, L. Fully Automated One-Pot Synthesis of [18F]Fluoromisonidazole. *Nucl Med Biol* **2005**, *32* (5), 553-558. https://doi.org/10.1016/j.nucmedbio.2005.03.010.

(35) Guérard, F.; Maingueneau, C.; Liu, L.; Eychenne, R.; Gestin, J.-F.; Montavon, G.; Galland, N. Advances in the Chemistry of Astatine and Implications for the Development of Radiopharmaceuticals. *Acc Chem Res* **2021**, *54* (16), 3264-3275. https://doi.org/10.1021/acs.accounts.1c00327.

(36) Hadley, S. W.; Wilbur, D. S.; Gray, M. A.; Atcher, R. W. Astatine-211 Labeling of an Antimelanoma Antibody and Its Fab Fragment Using N-Succinimidyl p-[211At]Astatobenzoate: Comparisons in Vivo with the p-[125I]Iodobenzoyl Conjugate. *Bioconjug Chem* **1991**, *2* (3), 171-179. https://doi.org/10.1021/bc00009a006.

(37) Teze, D.; Sergentu, D.-C.; Kalichuk, V.; Barbet, J.; Deniaud, D.; Galland, N.; Maurice, R.; Montavon, G. Targeted Radionuclide Therapy with Astatine-211: Oxidative Dehalogenation of Astatobenzoate Conjugates. *Sci Rep* **2017**, *7* (1), 2579. https://doi.org/10.1038/s41598-017-02614-2.

(38) J. G. Hamilton; C. W. Asling; W. M. Garrison; K. G. Scott; D. Axelrod Heller. Destructive Action of Astatine211 (Element 85) on the Thyroid Gland of the Rat. *Proceedings of the Society for Experimental Biology and Medicine* **1950**, *73* (1), 51-53.

(39) Guérard, F.; Gestin, J.-F.; Brechbiel, M. W. Production of [211At]-Astatinated Radiopharmaceuticals and Applications in Targeted α-Particle Therapy. *Cancer Biother Radiopharm* **2013**, *28* (1), 1-20. https://doi.org/10.1089/cbr.2012.1292.

(40) Wilbur, D. S.; Chyan, M.-K.; Hamlin, D. K.; Vessella, R. L.; Wedge, T. J.; Hawthorne, M. F. Reagents for Astatination of Biomolecules. 2. Conjugation of Anionic Boron Cage Pendant Groups to a Protein Provides a Method for Direct Labeling That Is Stable to in Vivo Deastatination. *Bioconjug Chem* **2007**, *18* (4), 1226-1240. https://doi.org/10.1021/bc060345s.

(41) Vaidyanathun, G.; Friedman, H. S.; Keir, S. T.; Zalutsky, M. R. Evaluation of Meta-[211At] Astatobenzylguanidine in an Athymic Mouse Human Neuroblastoma Xenograft Model. *Nucl Med Biol* **1996**, *23*, 851-856.

(42) Cavina, L.; van der Born, D.; Klaren, P. H. M.; Feiters, M. C.; Boerman, O. C.; Rutjes, F. P. J. T. Design of Radioiodinated Pharmaceuticals: Structural Features Affecting Metabolic Stability towards in Vivo Deiodination. *European J Org Chem* **2017**, *2017* (24), 3387-3414. https://doi.org/10.1002/ejoc.201601638.

(43) Aoki, M.; Zhao, S.; Takahashi, K.; Washiyama, K.; Ukon, N.; Tan, C.; Shimoyama, S.; Nishijima, K.; Ogawa, K. Preliminary Evaluation of Astatine-211-Labeled Bombesin Derivatives for Targeted Alpha Therapy. *Chem Pharm Bull (Tokyo)* **2020**, *68* (6), 538-545. https://doi.org/10.1248/cpb.c20-00077.

(44) Bo-Li, L.; Yu-Tai, J.; Zheng-Hao, L.; Cheng, L.; Masaharu, K.; Minoru, M. Halogen Exchanges Using Crown Ethers: Synthesis and Preliminary Biodistribution Of. *Int J Appl Radiat Isot* **1985**, *36* (7), 561-563. https://doi.org/10.1016/0020-708X(85)90110-3.

(45) Vaidyanathan, G.; Larsen, R. H.; Zalutsky2, M. R. *5-[211At]Astato-2'-Deoxyuridine, an a-Particle-Emitting Endoradiotherapeutic Agent Undergoing DNA Incorporation1*; 1996; Vol. 56. http://aacrjournals.org/cancerres/article-pdf/56/6/1204/2462930/cr0560061204.pdf?casa_token=KYBA5iPgeRgAAAAA:6CBhv5cr1pukuU4PqSYkvNv6HlVBThSjUw2y606-V-0NEE3CxsEsSUXSiVxTL7swxcacsov5.

(46) Yssartier, T.; Liu, L.; Pardoue, S.; Le Questel, J.-Y.; Guérard, F.; Montavon, G.; Galland, N. In Vivo Stability of 211At-Radiopharmaceuticals: On the Impact of Halogen Bond Formation. *RSC Med Chem* **2024**, *15* (1), 223-233. https://doi.org/10.1039/D3MD00579H.

(47) Vaidyanathan, G.; Affleck, D.; Zalutsky, M. R. Monoclonal Antibody f(Ab′)2 Fragment

Labeled with N-Succinimidyl 2,4-Dimethoxy-3-Halobenzoates: In Vivo Comparison of Iodinated and Astatinated Fragments. *Nucl Med Biol* **1994**, *21* (1), 105-110. https://doi.org/10.1016/0969-8051(94)90136-8.

(48) Vaidyanathan, G.; Affleck, D. J.; Bigner, D. D.; Zalutsky, M. R. N-Succinimidyl 3-[211At]Astato-4-Guanidinomethylbenzoate: An Acylation Agent for Labeling Internalizing Antibodies with α-Particle Emitting 211At. *Nucl Med Biol* **2003**, *30* (4), 351-359. https://doi.org/10.1016/S0969-8051(03)00005-2.

(49) Walsh, M. E.; Kyritsis, P.; Eady, N. A. J.; Hill, H. A. O.; Wong, L. L. Catalytic Reductive Dehalogenation of Hexachloroethane by Molecular Variants of Cytochrome P450(Cam) (CYP101). *Eur J Biochem* **2000**, *267* (18), 5815-5820. https://doi.org/10.1046/j.1432-1327.2000.01666.x.

(50) Shu, Y.-Z.; Johnson, B. M.; Yang, T. J. Role of Biotransformation Studies in Minimizing Metabolism-Related Liabilities in Drug Discovery. *AAPS J* **2008**, *10* (1), 178-192. https://doi.org/10.1208/s12248-008-9016-9.

(51) Lewis, D. F. V.; Dickins, M. Baseline Lipophilicity Relationships in Human Cytochromes P450 Associated with Drug Metabolism. *Drug Metab Rev* **2003**, *35* (1), 1-18. https://doi.org/10.1081/DMR-120018245.

(52) Lewis, D. F. V.; Jacobs, M. N.; Dickins, M. Compound Lipophilicity for Substrate Binding to Human P450s in Drug Metabolism. *Drug Discov Today* **2004**, *9* (12), 530-537. https://doi.org/10.1016/S1359-6446(04)03115-0.

(53) Zhang, Z.; Tang, W. Drug Metabolism in Drug Discovery and Development. *Acta Pharm Sin B* **2018**, *8* (5), 721-732. https://doi.org/10.1016/j.apsb.2018.04.003.

(54) Kasal, P.; Jindřich, J. Kinetics of Nucleophilic Substitution of Compounds Containing Multiple Leaving Groups Bound to a Neopentyl Skeleton. *ACS Omega* **2022**, *7* (23), 20137-20144. https://doi.org/10.1021/acsomega.2c01965.

(55) Nakata, N.; Kiriu, M.; Okumura, Y.; Zhao, S.; Nishijima, K.; Shiga, T.; Tamaki, N.; Kuge, Y.; Matsumoto, H. Comparative Evaluation of [18F]DiFA and Its Analogs as Novel Hypoxia Positron Emission Tomography and [18F]FMISO as the Standard. *Nucl Med Biol* **2019**, *70*, 39-45. https://doi.org/10.1016/j.nucmedbio.2019.01.008.

(56) Zha, Z.; Zhu, L.; Liu, Y.; Du, F.; Gan, H.; Qiao, J.; Kung, H. F. Synthesis and Evaluation of Two Novel 2-Nitroimidazole Derivatives as Potential PET Radioligands for Tumor Imaging. *Nucl Med Biol* **2011**, *38* (4), 501-508.

https://doi.org/10.1016/j.nucmedbio.2010.11.001.

(57) Bartlett, P. D.; Rosen, L. J. An Acetylenic Analog of Neopentyl Bromide; Evidence That the Hindrance to Displacement Reactions in Neopentyl Halides Is Steric in Nature. *J Am Chem Soc* **1942**, *64* (3), 543-546. https://doi.org/10.1021/ja01255a020.

(58) MacFaul, P. A.; Morley, A. D.; Crawford, J. J. A Simple in Vitro Assay for Assessing the Reactivity of Nitrile Containing Compounds. *Bioorg Med Chem Lett* **2009**, *19* (4), 1136-1138. https://doi.org/10.1016/J.BMCL.2008.12.105.

(59) Meister, A.; Anderson, M. E. GLUTATHIONE. *Annu Rev Biochem* **1983**, *52* (1), 711-760. https://doi.org/10.1146/annurev.bi.52.070183.003431.

(60) Zuckier, L. S.; Dohan, O.; Li, Y.; Chang, C. J.; Carrasco, N.; Dadachova, E. Kinetics of Perrhenate Uptake and Comparative Biodistribution of Perrhenate, Pertechnetate, and Iodide by NaI Symporter-Expressing Tissues in Vivo. *J Nucl Med* **2004**, *45* (3), 500-507.

(61) Spetz, J.; Rudqvist, N.; Forssell-Aronsson, E. Biodistribution and Dosimetry of Free ^{211}At, $^{125}I^-$ and $^{131}I^-$ in Rats. *Cancer Biother Radiopharm* **2013**, *28* (9), 657-664. https://doi.org/10.1089/cbr.2013.1483.

(62) Arteel, G. E.; Thurman, R. G.; Raleigh, J. A. Reductive Metabolism of the Hypoxia Marker Pimonidazole Is Regulated by Oxygen Tension Independent of the Pyridine Nucleotide Redox State. *Eur J Biochem* **1998**, *253* (3), 743-750. https://doi.org/10.1046/j.1432-1327.1998.2530743.x.

(63) Piert, M.; Machulla, H.-J.; Becker, G.; Stahlschmidt, A.; Patt, M.; Aldinger, P.; Dißmann, P. D.; Fischer, H.; Bares, R.; Becker, H. D.; Lauchart, W. Introducing Fluorine-18 Fluoromisonidazole Positron Emission Tomography for the Localisation and Quantification of Pig Liver Hypoxia. *Eur J Nucl Med* **1999**, *26*, 95-109.

(64) Shimizu, Y.; Zhao, S.; Yasui, H.; Nishijima, K.; Matsumoto, H.; Shiga, T.; Tamaki, N.; Ogawa, M.; Kuge, Y. A Novel PET Probe "[18F]DiFA" Accumulates in Hypoxic Region via Glutathione Conjugation Following Reductive Metabolism. *Mol Imaging Biol* **2019**, *21* (1), 122-129. https://doi.org/10.1007/s11307-018-1214-y.

(65) Watabe, T.; Kaneda-Nakashima, K.; Liu, Y.; Shirakami, Y.; Ooe, K.; Toyoshima, A.; Shimosegawa, E.; Fukuda, M.; Shinohara, A.; Hatazawa, J. Enhancement of 211At Uptake via the Sodium Iodide Symporter by the Addition of Ascorbic Acid in Targeted α-Therapy of Thyroid Cancer. *Journal of Nuclear Medicine* **2019**, *60* (9), 1301-1307. https://doi.org/10.2967/jnumed.118.222638.

(66) Watanabe, S.; Shiga, T.; Hirata, K.; Magota, K.; Okamoto, S.; Toyonaga, T.; Higashikawa, K.; Yasui, H.; Kobayashi, J.; Nishijima, K.; Iseki, K.; Matsumoto, H.; Kuge, Y.; Tamaki, N. Biodistribution and Radiation Dosimetry of the Novel Hypoxia PET Probe [18F]DiFA and Comparison with [18F]FMISO. *EJNMMI Res* **2019**, *9* (1), 60. https://doi.org/10.1186/s13550-019-0525-6.

(67) Tago, T.; Toyohara, J.; Fujimaki, R.; Tatsuta, M.; Song, R.; Hirano, K.; Iwai, K.; Tanaka, H. Effects of 18F-Fluorinated Neopentyl Glycol Side-Chain on the Biological Characteristics of Stilbene Amyloid-β PET Ligands. *Nucl Med Biol* **2021**, *94-95*, 38-45. https://doi.org/10.1016/j.nucmedbio.2020.12.008.

(68) Bhutia, Y. D.; Babu, E.; Ramachandran, S.; Ganapathy, V. Amino Acid Transporters in Cancer and Their Relevance to "Glutamine Addiction": Novel Targets for the Design of a New Class of Anticancer Drugs. *Cancer Res* **2015**, *75* (9), 1782-1788. https://doi.org/10.1158/0008-5472.CAN-14-3745.

(69) Fuchs, B. C.; Bode, B. P. Amino Acid Transporters ASCT2 and LAT1 in Cancer: Partners in Crime? *Semin Cancer Biol* **2005**, *15* (4), 254-266. https://doi.org/10.1016/j.semcancer.2005.04.005.

(70) Yanagida, O.; Kanai, Y.; Chairoungdua, A.; Kim, D. K.; Segawa, H.; Nii, T.; Cha, S. H.; Matsuo, H.; Fukushima, J.; Fukasawa, Y.; Tani, Y.; Taketani, Y.; Uchino, H.; Kim, J. Y.; Inatomi, J.; Okayasu, I.; Miyamoto, K.; Takeda, E.; Goya, T.; Endou, H. Human L-Type Amino Acid Transporter 1 (LAT1): Characterization of Function and Expression in Tumor Cell Lines. *Biochimica et Biophysica Acta (BBA) - Biomembranes* **2001**, *1514* (2), 291-302. https://doi.org/10.1016/S0005-2736(01)00384-4.

(71) Shikano, N.; Kanai, Y.; Kawai, ; Keiichi; Inatomi, J.; Do, ; Kim, K.; Nobuyoshi Ishikawa, ;; Endou, H. Isoform Selectivity of 3-125 I-Iodo-Methyl-L-Tyrosine Membrane Transport in Human L-Type Amino Acid Transporters. *J Nucl Med* **2003**, *44*, 244-246.

(72) Youland, R. S.; Kitange, G. J.; Peterson, T. E.; Pafundi, D. H.; Ramiscal, J. A.; Pokorny, J. L.; Giannini, C.; Laack, N. N.; Parney, I. F.; Lowe, V. J.; Brinkmann, D. H.; Sarkaria, J. N. The Role of LAT1 in 18F-DOPA Uptake in Malignant Gliomas. *J Neurooncol* **2013**, *111* (1), 11-18. https://doi.org/10.1007/s11060-012-0986-1.

(73) Jager, P. L.; Vaalburg, W.; Pruim, J.; De Vries, E. G. E.; Langen, K.-J.; Albertus, D. Radiolabeled Amino Acids: Basic Aspects and Clinical Applications in Oncology*. *THE JOURNAL OF NUCLEAR MEDICINE* **2001**, *42* (3), 432-445.

(74) Pöpperl, G.; Kreth, F. W.; Mehrkens, J. H.; Herms, J.; Seelos, K.; Koch, W.; Gildehaus, F. J.; Kretzschmar, H. A.; Tonn, J. C.; Tatsch, K. FET PET for the Evaluation of Untreated Gliomas: Correlation of FET Uptake and Uptake Kinetics with Tumour Grading. *Eur J Nucl Med Mol Imaging* **2007**, *34* (12), 1933-1942. https://doi.org/10.1007/s00259-007-0534-y.

(75) Habermeier, A.; Graf, J.; Sandhöfer, B. F.; Boissel, J.-P.; Roesch, F.; Closs, E. I. System l Amino Acid Transporter LAT1 Accumulates O-(2-Fluoroethyl)-l-Tyrosine (FET). *Amino Acids* **2015**, *47* (2), 335-344. https://doi.org/10.1007/s00726-014-1863-3.

(76) Watabe, T.; Kaneda-Nakashima, K.; Shirakami, Y.; Liu, Y.; Ooe, K.; Teramoto, T.; Toyoshima, A.; Shimosegawa, E.; Nakano, T.; Kanai, Y.; Shinohara, A.; Hatazawa, J. Targeted Alpha Therapy Using Astatine (211At)-Labeled Phenylalanine: A Preclinical Study in Glioma Bearing Mice. *Oncotarget* **2020**, *11* (15), 1388-1398. https://doi.org/10.18632/oncotarget.27552.

(77) Elgqvist, J.; Andersson, H.; Bäck, T.; Claesson, I.; Hultborn, R.; Jensen, H.; Johansson, B. R.; Lindegren, S.; Olsson, M.; Palm, S.; Warnhammar, E.; Jacobsson, L. Alpha-Radioimmunotherapy of Intraperitoneally Growing OVCAR-3 Tumors of Variable Dimensions: Outcome Related to Measured Tumor Size and Mean Absorbed Dose. *J Nucl Med* **2006**, *47* (8), 1342-1350.

(78) Ohkubo, T.; Kurihara, Y.; Ogawa, M.; Nengaki, N.; Fujinaga, M.; Mori, W.; Kumata, K.; Hanyu, M.; Furutsuka, K.; Hashimoto, H.; Kawamura, K.; Zhang, M.-R. Automated Radiosynthesis of Two 18F-Labeled Tracers Containing 3-Fluoro-2-Hydroxypropyl Moiety, [18F]FMISO and [18F]PM-PBB3, via [18F]Epifluorohydrin. *EJNMMI Radiopharm Chem* **2021**, *6* (1), 23. https://doi.org/10.1186/s41181-021-00138-9.

(79) Lisova, K.; Wang, J.; Hajagos, T. J.; Lu, Y.; Hsiao, A.; Elizarov, A.; van Dam, R. M. Economical Droplet-Based Microfluidic Production of [18F]FET and [18F]Florbetaben Suitable for Human Use. *Sci Rep* **2021**, *11* (1), 20636. https://doi.org/10.1038/s41598-021-99111-4.

(80) Oh, S. J.; Chi, D. Y.; Mosdzianowski, C.; Kim, J. Y.; Gil, H. S.; Kang, S. H.; Ryu, J. S.; Moon, D. H. Fully Automated Synthesis of [18F]Fluoromisonidazole Using a Conventional [18F]FDG Module. *Nucl Med Biol* **2005**, *32* (8), 899-905. https://doi.org/10.1016/j.nucmedbio.2005.06.003.

(81) Tada, M.; Kaizuka, Y.; Kannaka, K.; Suzuki, H.; Joho, T.; Takahashi, K.; Uehara, T.; Tanaka, H. Development of a Neopentyl 211At-labeled Activated Ester Providing in Vivo Stable 211At-labeled Antibodies for Targeted Alpha Therapy. *ChemMedChem* **2024**.

https://doi.org/10.1002/cmdc.202400369.

(82) Ogawa, K.; Takeda, T.; Mishiro, K.; Toyoshima, A.; Shiba, K.; Yoshimura, T.; Shinohara, A.; Kinuya, S.; Odani, A. Radiotheranostics Coupled between an At-211-Labeled RGD Peptide and the Corresponding Radioiodine-Labeled RGD Peptide. *ACS Omega* **2019**, *4* (3), 4584-4591. https://doi.org/10.1021/acsomega.8b03679.

(83) Garg, P. K.; Harrison, G. L.; Zalutsky, M. R. Comparative Tissue Distribution in Mice of the α-Emitter 211At and 131I as Labels of a Monoclonal Antibody and F(Ab')2 Fragment. *Cancer Res* **1990**, *50*, 3514-3520.

(84) Wilbur, D. S.; Chyan, M.-K.; Hamlin, D. K.; Kegley, B. B.; Risler, R.; Pathare, P. M.; Quinn, J.; Vessella, R. L.; Foulon, C.; Zalutsky, M.; Wedge, T. J.; Hawthorne, M. F. Reagents for Astatination of Biomolecules: Comparison of the in Vivo Distribution and Stability of Some Radioiodinated/Astatinated Benzamidyl and Nido-Carboranyl Compounds. *Bioconjug Chem* **2004**, *15* (1), 203-223. https://doi.org/10.1021/bc034175k.

(85) Watabe, T.; Kaneda-Nakashima, K.; Shirakami, Y.; Liu, Y.; Ooe, K.; Teramoto, T.; Toyoshima, A.; Shimosegawa, E.; Nakano, T.; Kanai, Y.; Shinohara, A.; Hatazawa, J. Targeted Alpha Therapy Using Astatine (211At)-Labeled Phenylalanine: A Preclinical Study in Glioma Bearing Mice. *Oncotarget* **2020**, *11* (15), 1388-1398. https://doi.org/10.18632/oncotarget.27552.

(86) Peter Heiss; Sabine Mayer; Michael Herz; Hans-Jurgen Wester; Markus Schwaiger; Reingard Senekowitsch-Schmidtke. Investigation of Transport Mechanism and Uptake Kinetics of O-(2- [18F]Fluoroethyl)-L-Tyrosine In Vitro and In Vivo. *THE JOURNAL OF NUCLEAR MEDICINE* **1999**, *40* (8), 1367-1373.

(87) Shikano, N.; Kawai, K.; Nakajima, S.; Nishii, R.; Flores II, L. G.; Kubodera, A.; Kubota, N.; Ishikawa, N.; Saji, H. Renal Accumulation and Excretion of Radioiodinated 3-Iodo-α-Methyl-L-Ty Rosine. *Ann Nucl Med* **2004**, *18* (3), 263-270. https://doi.org/10.1007/BF02985009.

(88) Pieter L. Jager; Eric J.F. Franssen; Walter Kool; Ben G. Szabo; Harald J. Hoekstra; Harry J.M. Groen; Elizabeth G.E. de Vries; Gustaaf W. van Imhoff; Willem Vaalburgand; D. Albertus Piers. Feasibility of Tumor Imaging Using-3-[Iodine-123]-Iodo-α-Methyl Tyrosine in Extracranial Tumors. *THE JOURNAL OF NUCLEAR MEDICIN* **1998**, *39* (10), 1736-1743.

(89) Pauleit, D.; Floeth, F.; Herzog, H.; Hamacher, K.; Tellmann, L.; Müller, H. W.; Coenen,

H. H.; Langen, K. J. Whole-Body Distribution and Dosimetry of O-(2-[18F]Fluoroethyl)-L-Tyrosine. *Eur J Nucl Med Mol Imaging* **2003**, *30* (4), 519-524. https://doi.org/10.1007/s00259-003-1118-0.

(90) Rooman, I.; Lutz, C.; Pinho, A. V.; Huggel, K.; Reding, T.; Lahoutte, T.; Verrey, F.; Graf, R.; Camargo, S. M. R. Amino Acid Transporters Expression in Acinar Cells Is Changed during Acute Pancreatitis. *Pancreatology* **2013**, *13* (5), 475-485. https://doi.org/10.1016/j.pan.2013.06.006.

(91) Norihiro Nakada; Tetuo Mikami; Kiyomi Hana; Masaaki Ichinoe; Nobuyuki Yanagisawa; Tsutomu Yoshida; Hitoshi Endou; Isao Okayasu. Unique and Selective expression of L-Amino Acid Transporter 1 in Human tissue as Well as Being an Aspect of Oncofetal Protein. *Histol Histopathol* **2014**, *29*, 217-227.

(92) Wester, H. J.; Herz, M.; Weber, W.; Heiss, P.; Senekowitsch-Schmidtke, R.; Schwaiger, M.; Stã, G. Synthesis and Radiopharmacology of O-(2-[18F]Fluoroethyl)-L-Tyrosine for Tumor Imaging. *THE JOURNAL OF NUCLEAR MEDICINE* **1999**, *40* (1), 205-212.

(93) Lahoutte, T.; Caveliers, V.; Dierickx, L.; Vekeman, M.; Everaert, H.; Mertens, J.; Bossuyt, A. In Vitro Characterization of the Influx of 3-[125I]Iodo-L-α-Methyltyrosine and 2-[125I]Iodo-L-Tyrosine into U266 Human Myeloma Cells: Evidence for System T Transport. *Nucl Med Biol* **2001**, *28* (2), 129-134. https://doi.org/10.1016/S0969-8051(00)00184-0.

(94) Kaira, K.; Oriuchi, N.; Otani, Y.; Shimizu, K.; Tanaka, S.; Imai, H.; Yanagitani, N.; Sunaga, N.; Hisada, T.; Ishizuka, T.; Dobashi, K.; Kanai, Y.; Endou, H.; Nakajima, T.; Endo, K.; Mori, M. Fluorine-18-α-Methyltyrosine Positron Emission Tomography for Diagnosis and Staging of Lung Cancer: A Clinicopathologic Study. *Clinical Cancer Research* **2007**, *13* (21), 6369-6378. https://doi.org/10.1158/1078-0432.CCR-07-1294.

(95) Nakata, N.; Kiriu, M.; Okumura, Y.; Zhao, S.; Nishijima, K. ichi; Shiga, T.; Tamaki, N.; Kuge, Y.; Matsumoto, H. Comparative Evaluation of [18F]DiFA and Its Analogs as Novel Hypoxia Positron Emission Tomography and [18F]FMISO as the Standard. *Nucl Med Biol* **2019**, *70*, 39-45. https://doi.org/10.1016/J.NUCMEDBIO.2019.01.008.

(96) Arano, Y.; Wakisaka, K.; Ohmomo, Y.; Uezono, T.; Mukai, T.; Motonari, H.; Shiono, H.; Sakahara, H.; Konishi, J. Maleimidoethyl 3-(Tri-n-Butylstannyl)Hippurate: A Useful Radioiodination Reagent for Protein Radiopharmaceuticals To Enhance Target Selective Radioactivity Localization. *J Med Chem* **1994**, *37* (16), 2609-2618. https://doi.org/10.1021/jm00042a014.

(97) Zha, Z.; Zhu, L.; Liu, Y.; Du, F.; Gan, H.; Qiao, J.; Kung, H. F. Synthesis and Evaluation of Two Novel 2-Nitroimidazole Derivatives as Potential PET Radioligands for Tumor Imaging. *Nucl Med Biol* **2011**, *38* (4), 501-508. https://doi.org/10.1016/j.nucmedbio.2010.11.001.

(98) Watabe, T.; Kaneda-Nakashima, K.; Shirakami, Y.; Liu, Y.; Ooe, K.; Teramoto, T.; Toyoshima, A.; Shimosegawa, E.; Nakano, T.; Kanai, Y.; Shinohara, A.; Hatazawa, J. Targeted Alpha Therapy Using Astatine (211At)-Labeled Phenylalanine: A Preclinical Study in Glioma Bearing Mice. *Oncotarget* **2020**, *11* (15), 1388-1398. https://doi.org/10.18632/oncotarget.27552.

(99) Ogawa, K.; Takeda, T.; Mishiro, K.; Toyoshima, A.; Shiba, K.; Yoshimura, T.; Shinohara, A.; Kinuya, S.; Odani, A. Radiotheranostics Coupled between an At-211-Labeled RGD Peptide and the Corresponding Radioiodine-Labeled RGD Peptide. *ACS Omega* **2019**, *4* (3), 4584-4591. https://doi.org/10.1021/acsomega.8b03679.

(100) Weinstock, J.; Wu, J.; Cao, P.; Kingsbury, W. D.; McDermott, J. L.; Kodrasov, M. P.; McKelvey, D. M.; Suresh Kumar, K. G.; Goldenberg, S. J.; Mattern, M. R.; Nicholson, B. Selective Dual Inhibitors of the Cancer-Related Deubiquitylating Proteases USP7 and USP47. *ACS Med Chem Lett* **2012**, *3* (10), 789-792. https://doi.org/10.1021/ml200276j.

(101) Akizawa, H.; Imajima, M.; Hanaoka, H.; Uehara, T.; Satake, S.; Arano, Y. Renal Brush Border Enzyme-Cleavable Linkages for Low Renal Radioactivity Levels of Radiolabeled Antibody Fragments. *Bioconjug Chem* **2013**, *24* (2), 291-299. https://doi.org/10.1021/bc300428b.

Associated articles

Main article

Yuta Kaizuka, Hiroyuki Suzuki, Tadashi Watabe, Kazuhiro Ooe, Atsushi Toyoshima, Kazuhiro Takahashi, Koichi Sawada, Takashi Iimori, Yoshitada Masuda, Takashi Uno, Kento Kannaka & Tomoya Uehara "Neopentyl glycol-based radiohalogen-labeled amino acid derivatives for cancer radiotheranostics." *EJNMMI Radiopharmacy and Chemistry* 9.1 (2024): 17.

Related article

Hiroyuki Suzuki, Yuta Kaizuka, Maho Tatsuta, Hiroshi Tanaka, Nana Washiya, Yoshifumi Shirakami, Kazuhiro Ooe, Atsushi Toyoshima, Tadashi Watabe, Takahiro Teramoto, Ichiro Sasaki, Shigeki Watanabe, Noriko S. Ishioka, Jun Hatazawa, Tomoya Uehara, and Yasushi Arano "Neopentyl glycol as a scaffold to provide radiohalogenated theranostic pairs of high *in vivo* stability." *Journal of Medicinal Chemistry* 64.21 (2021): 15846-15857.

Acknowledgment

I am deeply grateful to Professor Tomoya Uehara, PhD., who gave me guidance and encouragement in doing this research.

My sincere gratitude to Assistant Professor Hiroyuki Suzuki, PhD., who continuously supported and patiently guided me during my ups and downs in doing this research.

I would like to thank Assistant Professor Kento Kannaka, PhD., for supported and advice in doing this research.

I would like to express my deep gratitude to Professor Emeritus Yasushi Arano, Ph.D., who taught me the fundamentals of research during my early years as a researcher.

I would like to express my profound gratitude to Associate Professor Tadashi Watabe, MD., PhD., Professor Atsushi Toyoshima, PhD., Associate Professor Takahiro Teramoto, PhD., Associate Professor Kazuhiro Ooe, PhD., Specially Appointed Associate Professor Yoshifumi Shirakami, Ph.D., Professor Emeritus Jun Hatazawa, PhD. Professor Kazuhiro Takahashi, PhD., Senior Principal Researcher Noriko S. Ishioka, Ph.D., Principal Researcher Shigeki Watanabe PhD., Senior Engineer Mr. Ichiro Sasaki and all the staff at Osaka University, Fukushima Medical University, and National Institute for Quantum Science and Technology who have been involved in the ^{211}At research for their meticulous guidance regarding the ^{211}At experiments.

I also wish to extend my sincere appreciation to Professor Yoshitada Masuda, PhD., Professor Takashi Uno, MD., PhD., and the staff members of the Department of Radiology, Chiba University, for their continuous support of the ^{18}F experiments.

I am also profoundly grateful to Professor Hiroshi Tanaka, Ph.D., for his guidance and valuable advice on synthetic routes and reaction conditions.

I would like to express my gratitude to Assistant Professor Hiroyuki Suzuki, PhD., Ms. Fumiko Suzuki, and the staff members of the RI Research Center, Chiba University and Radioisotope Laboratory, Chiba University, who gave great cooperation and understanding for the management of radionuclides and laboratory facilities.

I would like to thank Ms. Satsuki Shimada, secretary at the Laboratory of Molecular Imaging and Radiotherapy at Chiba University, for her great assistance and understanding.

Also, I would like to express my sincere gratitude to everyone at Laboratory of Molecular Imaging and Radiotherapy Chiba University for advice and cooperation in this research.

Last but not least, I am deeply grateful to my lovely wife Satomi Kaizuka and my daughter Ray Kaizuka, to all of my family and friends who supported me and giving encouragement in doing this research.

Chiba, July 2024

Yuta Kaizuka

Dissertation committee

This dissertation was evaluated by the following committee authorized by the Graduate School of Pharmaceutical Sciences, Chiba University:

Chief examiner:

- Professor Hiroto Hatakeyama, PhD., Laboratory of Design and Drug Disposition

Associate examiner:

- Professor Yasumitsu Ogra, PhD., Laboratory of Toxicology and Environmental Health.
- Professor Muchtaridi, PhD., Department of Pharmaceutical Analysis and Medicinal Chemistry, Universitas Padjadjaran
- Lecturer Shigeki Aoki, PhD., Laboratory of Biopharmaceutics.

All affiliated to the Graduate School of Pharmaceutical Sciences, Chiba University.